



Australia's National
Science Agency

Topic 2 – Analytical methods for determination of stable operation of IBRs in a future power system

2024/25 CSIRO Research

Commonwealth Scientific and Industrial Research
Organization

Sushrut Thakar, Vishal Verma, Stavros Konstantinopoulos,
Deepak Ramasubramanian, Mobolaji Bello (EPRI)
20th May 2025



Citation

S. Thakar, V. Verma, S. Konstantinopoulos, D. Ramasubramanian and M. Bello (2025) Topic 2 – Analytical methods for determination of stable operation of IBRs in a future power system. CSIRO, Australia.

Copyright

© Commonwealth Scientific and Industrial Research Organisation 2025. To the extent permitted by law, all rights are reserved and no part of this publication covered by copyright may be reproduced or copied in any form or by any means except with the written permission of CSIRO.

Important disclaimer

CSIRO advises that the information contained in this publication comprises general statements based on scientific research. The reader is advised and needs to be aware that such information may be incomplete or unable to be used in any specific situation. No reliance or actions must therefore be made on that information without seeking prior expert professional, scientific and technical advice. To the extent permitted by law, CSIRO (including its employees and consultants) excludes all liability to any person for any consequences, including but not limited to all losses, damages, costs, expenses and any other compensation, arising directly or indirectly from using this publication (in part or in whole) and any information or material contained in it.

CSIRO is committed to providing web accessible content wherever possible. If you are having difficulties with accessing this document please contact csiro.au/contact.

Contents

Acknowledgments.....	vi
Executive summary	vii
Part I Introduction and background	1
1 Introduction	2
1.1 Relation to Research Roadmap	4
1.2 Background work	5
1.3 Summary of work effort.....	7
2 Methodology followed in the project	9
Part II Improvements to incorporating IBR models to small-signal stability studies	10
3 Incorporating Blackbox OEM IBR models to small signal stability studies.....	11
3.1 Obtaining the small-signal models of IBRs	11
3.2 Integration of blackbox models in the system-wide analysis	26
3.3 Conclusions of Blackbox model identification and integration	28
4 Utilizing positive sequence models for small signal analysis.....	29
4.1 Obtaining the small-signal models of IBRs based on positive sequence models	30
4.2 Restricting the active power setpoint	32
4.3 Validation against analytical models	36
4.4 Comparing EMT and RMS models	42
Part III Services from IBRs and small signal stability	51
5 Impact of obtaining services from IBRs on small signal stability	52
Part IV Conclusions and future work	60
6 Conclusion and future work.....	61
Appendix A IBR model parameters	63
Appendix B APM results for OEMs	69
References	79

Figures

Figure 1 Operating point dependence of frequency domain admittance characteristics for an IBR model, with variation in Pref from 0.1 to 2.0 MW and variation in Vref from 0.9pu to 1.1pu for a 2.5 MVA IBR.....	6
Figure 2 The training (blue) and test (orange) operating points selected for OEM IBR model a) P vs. Q b) P vs. V.....	12
Figure 3 Two qualitative trends in the observed impedance at a) test operating point OP-3 b) test operating point OP-7.....	14
Figure 4 Additional test training points for the OEM IBR shown in purple a) P vs. Q b) P vs. V..	16
Figure 5 Two qualitative trends in the observed admittance at a)operating point OP-3 b) operating point OP-7.....	17
Figure 6. Comparison of measured and estimated time response for different test points a)OP-3, b) OP-7.	19
Figure 7 Two qualitative trends in the observed admittance at a) operating point OP-3 b) operating point OP-7.....	21
Figure 8 Comparison of measured and estimated time response for different test points a) OP-3, b) OP-7.	23
Figure 9. Two qualitative trends in the observed impedance at a) operating point OP-3 b) operating point OP-7.....	25
Figure 10 Closed Loop Poles with Blackbox GFM Models Integrated in the Synthetic NEM (r/s represents radians per second).....	27
Figure 11 Generator Speed for System Impulse Response.....	28
Figure 12 The procedure to use positive sequence models in a small signal assessment	29
Figure 13 The training (blue) and test (orange) operating points selected for positive sequence IBR model.....	30
Figure 14 The expected frequency domain admittance characteristics (blue, solid) for a positive sequence IBR model compared with the predicted impedance characteristics (orange, dashed) at the same operating point using APM algorithm for two test operating points, OP-2 and OP-4.	31
Figure 15 Vector fitted model compared with the input data supplied to the vector fitting block for the predicted admittances for two operating points, OP-2 and OP-4	32
Figure 16 The different operating points chosen for testing the frequency domain admittance. The two colours of points indicate two distinct qualitative trends in the observed admittances	33
Figure 17 Two qualitative trends in the observed admittance at different operating points.....	33
Figure 18 Updates to the training and test points to retain all the points above 0.2 p.u. active power setpoint.....	34

Figure 19 The expected (blue, solid) and predicted (orange, dashed) admittances at two test points (OP-2 and OP-4) with the updated data – the predicted and expected curves overlap, indicating a good match.....	34
Figure 20 The open loop poles obtained for the fitted models based on the predicted and expected admittance at two test operating points, OP-2 and OP-4.....	35
Figure 21 Closed loop poles when interfacing the fitted models based on expected and predicted models with an infinite bus model, OP-2 and OP-4	36
Figure 22 A comparison of the frequency domain admittance scans with the corresponding analytical small signal model admittances for two test operating points, OP-2 and OP-4	37
Figure 23 A comparison of the frequency domain admittance scans with the vector fitted model as well as the corresponding analytical small signal model admittances for a test point $V= 0.95$ pu, $P= 0.58$ pu, $Q= 0$ pu	38
Figure 24 Open loop poles of the vector fitted model based on positive sequence IBR model and the corresponding analytical small signal model for a test point $V= 0.95$ pu, $P= 0.58$ pu, $Q= 0$ pu	39
Figure 25 Closed loop poles in a single machine infinite bus system for the vector fitted model based on positive sequence IBR model and the corresponding analytical small signal model for a test point $V= 0.95$ pu, $P= 0.58$ pu, $Q= 0$ pu.....	39
Figure 26 Comparison of the synthetic NEM network small signal models using analytical (red) or vector fitted (blue) models for 31 IBRs based on positive sequence IBR model (r/s represents radians per second).....	41
Figure 27 Comparison of the impulse response of the small signal model with all analytical models (left) and with fitted models for 31 IBRs.....	42
Figure 28 Frequency step response of Test model B_EMT and Test model B_PSeq	43
Figure 29 Voltage step response of Test model B_EMT and Test model B_PSeq.....	44
Figure 30 Comparing frequency domain admittances - Test model B_EMT (orange) and Test model B_PSeq (blue).....	45
Figure 31 Frequency domain admittance scans and the vector fitted model for Test model B_EMT – close match of the curves resulting in overlap at many frequencies shows a successful fit.....	46
Figure 32 Frequency domain admittance scans and the vector fitted model for Test model B_PSeq – close match of the curves resulting in overlap at many frequencies shows a successful fit.....	47
Figure 33 Comparing open loop poles of the models fitted based on frequency responses of Test model B_EMT and Test model B_PSeq (r/s represents radians per second)	48
Figure 34 Comparison of the poles for the closed loop model in a single machine infinite bus system for vector fitted models based on Test model B_EMT and Test model B_PSeq. This plot corresponds to network conditions of $SCR=6.0$ and $X/R=10.0$	49

Figure 35 Comparison of the poles for the closed loop model in a single machine infinite bus system for vector fitted models based on Test model B_EMT and Test model B_PSeq. This plot corresponds to network conditions of SCR=1.5 and X/R=10.0	49
Figure 36 Comparison of the voltage step response for the three IBR modes, a voltage dip of 0.05 pu applied at 8s.....	53
Figure 37 Comparison of the frequency step response for the three IBR modes, a frequency dip of 0.5 Hz is applied at 8s.	54
Figure 38 Comparison of the frequency domain admittances of the three IBR modes for the first operating point - V=0.97 pu, P=47.33 MW, Q=-0.08 MVar	55
Figure 39 Comparison of the frequency domain admittances of the three IBR modes for the second operating point - V=1.02 pu, P=50.7 MW, Q=10.0 MVar	55
Figure 40 Comparison of the frequency domain admittances of the three IBR modes for the third operating point - V=1.035 pu, P=50.7 MW, Q=-15.0 MVar	56
Figure 41 Poles of the synthetic NEM network small signal model where the GFL IBRs use the parameterization of IBR_ConstPQ mode (r/s represents radians per second).....	57
Figure 42 Poles of the synthetic NEM network small signal model where the GFL IBRs use the parameterization of IBR_slow_resp mode (r/s represents radians per second)	58
Figure 43 Poles of the synthetic NEM network small signal model where the GFL IBRs use the parameterization of IBR_fast_resp model (r/s represents radians per second).....	59

Tables

Table I Table summarizing the different tests/comparisons throughout this report 8

Table II Goodness of fit metric comparing the expected and predicted admittances at the test points 15

Table III Goodness of fit metric comparing the expected and predicted admittances at the test points 17

Table IV Goodness of fit metric comparing the expected and predicted admittances at the test points 21

Table V Goodness of fit metric comparing the expected and predicted admittances at the test points 26

Table VI Goodness of fit metric comparing the expected and predicted admittances at the test points 35

Table VII Operating points from the synthetic NEM network where GFL IBR models are replaced by the fitted models..... 40

Acknowledgments

The research presented in this report was funded by CSIRO, Australia's national science agency, and carried out as part of the initiatives under Australian Power Systems Renewables Transition (A-PSRT) research. This research supports Australia's transition to a stable, secure and affordable power system and contributes to critical research identified by the Consortium required to accelerate the decarbonisation of our electricity grid. More details can be found at <https://www.csiro.au/en/research/technology-space/energy/G-PST-Research-Roadmap>.

The team would like to acknowledge the valuable feedback and inputs from CSIRO and AEMO subject matter experts throughout the course of the project.

Executive summary

There has been a large increase in the share of inverter-based resources (IBRs) in the Australian power networks in the past, and this share is expected to continue to grow in the near future. Maintaining a stable and reliable operation of the Australian power system considering these changes to the system is important – one aspect in this, is ensuring the stable operation of IBRs and their operating point stability margin in the small signal domain. In the research roadmap submitted to CSIRO in 2021 around stability tools and methods, ‘stability margin evaluation’ and ‘small signal stability screening methods’ were identified as critical research topics, and this stage of the project aims to continue to address these two research topics.

At different times of day/year, the power system operating point differs in terms of the overall demand as well as the operational dispatch for different generation technologies; including synchronous-based and inverter-based generation. It is important to ensure that the system remains stable across these operating points – including aspects such as large signal stability (with aspects such as fault response) and small signal stability, related to aspects such as oscillatory modes. With an increase in the share of new devices such as IBRs, the modes observed may be different from those historically observed in systems with lower shares of IBRs. Traditionally, small signal stability (and stability margin) is assessed by analytically modelling the network and connected devices in detail, however, this may not be directly possible when IBRs are represented using blackbox models. In such cases, the critical topic ‘stability margin evaluation’ aims to develop/extend tools to evaluate stability margins using blackbox models and perform evaluation at multiple operating points.

Due to the different dispatches for different time of day/year as well as different potential scenarios during planning, there can be a large number in operating points in which the stability needs to be assessed. In such cases, screening methods based on small signal stability aims to screen and identify scenarios/operating points to be studied in detail. This critical topic of ‘small signal stability screening methods’ also relate to developing such screening methods that can be applied based on impedance-based methods.

Previous research has shown the frequency domain admittance characteristics of IBRs to be dependent on the operating point. Hence, in the previous stages of CSIRO funded topic 2 research, analytical prediction method (APM) was developed to estimate the frequency domain admittance of an IBR model at operating points separate from the training data. First objective of Stage 4 is to use the Analytical Prediction Method (APM), developed in the previous stage of the project, to predict the admittance/impedance characteristics of two Original Equipment Manufacturer (OEM) IBR models. In the previous stage of the project, a similar study was carried out for a generic IBR model. However, an OEM model is proprietary and has more complex control structure. In this task, APM is used to predict the impedance characteristics of an OEM model. Once a satisfactory match is obtained between the expected and predicted impedance or admittance, a small signal model of the OEM IBR model is obtained at the operating points using vector fitting.

The second objective in the stage 4 work is to assess the applicability of positive sequence IBR models to represent the small signal stability characteristics of an inverter at a particular operating

point. One of the challenges in the EMT domain in utilizing more detailed IBR models (that are traditionally utilized for impedance-based small-signal characteristics) is the required computational effort and time in performing the frequency domain scans to obtain the small-signal admittance or impedance models of IBRs. IBR models in positive sequence domain have simplified representations not considering the faster dynamics and can be simulated much faster, when compared to EMT domain models. Hence, an objective in this stage of the research is to evaluate the potential and the limits of utilizing positive sequence IBR models instead of EMT IBR models to incorporate IBRs in small-signal analysis via impedance scan-based procedures described in the previous stage 3 of the research. The APM and vector fitting are successfully applied to obtain an approximate small signal model for the positive sequence IBR at a new operating point. Since the positive sequence IBR considered is a generic white box model, the obtained vector fitted small signal models are compared with the analytical models – in a single machine infinite bus setup as well as using a small signal model of the synthetic NEM network.

With the increase in the share of IBRs in a power network, different grid services may need to be obtained from IBRs. Another objective in stage 4 work is to examine the impact of obtaining such grid services from IBRs on their own small-signal characteristics and whether obtaining such services from IBRs enhances or deteriorates the small-signal stability. Three IBR modes were selected to represent different level of responses (constant power, slow response and fast response) It was observed that the frequency domain admittances for these IBRs were different. Further, these three IBR modes or parameterizations, when applied to all IBRs in the synthetic NEM small signal model, also yielded different small signal stability characteristics.

In relation to 2021 Topic 2 Research Roadmap, the work done in this project addresses the topics listed below and advances the work by respective estimated percentage amounts:

- Stability margin evaluation (critical topic) – 85%
- Small signal stability screening methods (critical topic) – 85%

Part I Introduction and background

1 Introduction

There has been a large increase in the share of inverter-based resources (IBRs) in the Australian power networks in the past, and this share is expected to continue to grow in the near future. Maintaining a stable and reliable operation of the Australian power system considering these changes to the system is important – one aspect in this, is ensuring the stable operation of IBRs and their operating point stability margin in small signal domain. In the research roadmap submitted to CSIRO in 2021 [1] around stability tools and methods, ‘stability margin evaluation’ and ‘small signal stability screening methods’ were identified as critical research topics and this stage of the project aims to continue to address these two research topics.

With the evolving operating point characterized by different overall demand and different operational dispatch, traditional methods of repeating time domain simulations to evaluate stability of a large network are computationally intensive. Small signal stability screening methods aim to reduce the total number of scenarios that may need to be checked in detail by identifying conditions with potential for instability or scenarios that are closer to instabilities. This can be achieved by utilizing a small signal model of the network. Here, an analytical small signal model can lead to stability margin evaluation that is less computationally intensive. Such evaluation may also indicate devices interacting to form a particular dynamic mode such as oscillatory modes, aiding root cause identification.

When evaluating small signal stability of IBRs, there are two common approaches that are adopted. The first, linearization of the potentially non-linear IBR control structure and parameters, can yield information about the IBR states that participate in particular oscillatory or unstable modes and the control blocks associated with those states. This ensures an understanding and identifying pathways to ensure small signal stable operation. However, implementing this approach requires a detailed information about the control structure and parameters. Such information may not be available for IBRs installed/planned to be installed in a real network, because original equipment manufacturers (OEMs) and IBR project developers/owners may often only share blackbox models of IBRs in which the detailed control structure is not available.

In such cases, the second approach, that is frequency domain admittance-scan based methods and model fitting, may be utilized to incorporate models of such IBRs in small signal stability analysis in order to identify any potential small signal instabilities and oscillatory modes as well as the devices that may be interacting to form those modes, including the blackbox models. However, the small-signal model formed to represent the IBR behaviour is typically valid only in a small region around the operating point at which the frequency domain scans were performed. Since the frequency domain admittance scanning process is computationally intensive, estimating the frequency domain admittance of an IBR at a large number of distinct operating points may not be practical. The expected distinct operating points varies at different times of the day or year. Considering that large number of IBR devices have different controls, it is expected that the frequency domain scanning process needs to be repeated for each IBR.

In Stage 2 of the project [2], two methods to estimate IBR frequency domain admittance at a new operating point using the measurements from a set of training operating point were developed. A Synthetic NEM network dynamic cases with high IBR penetration corresponding to 24 load profiles (one for each hour of a day) were also developed in that stage, and stability analysis including system strength analysis, voltage profile optimization were applied, and an investigation into the small signal stability aspects was conducted for these models, utilizing time domain dynamic simulations. In Stage 3, a systematic procedure was developed to incorporate IBR models using frequency domain characteristics while limiting the number of operating points where one needs to obtain the frequency domain admittance characteristics of an IBR device to a pre-set number of training operating points. In this developed procedure, these data are then utilized using analytical prediction method (APM) developed and improved over stage 2 [2] and stage 3 [3] of the research to estimate the frequency domain admittance characteristics at any new operating point. A “Vector fitting” model approximation process is then applied to these characteristics at the new operating point to create a state space small signal model to be incorporated into small signal analysis of a network. The systematic procedure developed in the previous Stage 3 of the work was also applied to a large synthetic network representing the footprint served by the Australian National Electricity Market (NEM) and included a large number of IBRs, some of which were modelled as blackbox IBRs.

In the previous stage of the project [3], a trial blackbox model of a single IBR device created by the project team was used to test this developed systematic procedure designed to incorporate any blackbox IBR model within a network small signal stability assessment. This trial blackbox model was a simple generic model representing some of the elementary control functions of a typical IBR. However, blackbox models of real IBRs submitted to network operators are often very complex compared to the one used in the previous stage of the project and may require careful considerations when applying the developed procedure developed. Hence, the first aim in this stage of the research was to test and improve the developed procedure to incorporate other black box models by applying the procedure to OEM blackbox IBR models.

Another challenge (the second) identified in the previous stage of the work is the high computational burden of performing the frequency domain scans on the EMT domain IBR models due to the large number of frequencies and especially the longer simulations times necessary to capture the lower frequency dynamics. Including such lower frequencies may become impractical especially if the procedure is to be repeated over a large number of operating points and a large number of different EMT models. Typically, the operating point dependence of the IBR frequency domain admittance characteristics is also more prominent in the lower frequency region (lower than ~ 10 Hz). Hence, another aim in this stage of the project is to evaluate the extent to which and whether positive sequence models are useful in representing the IBR small signal behaviour using the procedure developed in the previous stage of the project, and the limitations in adopting this approach – considering that positive sequence models require much less computational resources to simulate.

A third objective in this stage of the research is to assess the impact of obtaining different services from IBRs on their own small-signal stability characteristics. As the share of IBRs in a network grows, it may be needed to obtain some grid services such as frequency/active power or voltage/reactive power support in different timeframes, or fault current support from the IBRs in the network in addition to the synchronous machine resources connected to the network that

traditionally provide the bulk of these services. Obtaining these services from an IBR requires (assuming the relevant hardware capabilities are present) selecting and implementing appropriate control functionality/blocks/parameters for that IBR. Since the frequency domain admittances as well as small-signal stability characteristics are expected to be changed if IBR control parameters or control structure is modified, an investigation of this aspect for some of the grid services is imperative, which is also an objective in this stage of the research.

While this research is relevant for power systems worldwide, these topics are especially relevant to the Australian power system, owing to the large share of IBRs added to the system over the past few years and those that are expected to continue to be added in near future. With this increased share of IBRs, modelling these IBRs and studying their impact on small signal stability of the network is important to ensure a stable network operation and identify any potential oscillatory interactions in the network. Due to the distinctly different control and physical device characteristics of IBRs compared to traditional synchronous machine devices connected to the grid, IBRs can have unique interactions and potential oscillatory modes that may be different from the modes observed historically in the network with low IBR penetration level. Hence accurately modelling the IBRs in small signal stability analysis for the network is important in the Australian context with the large growth of IBRs in the network.

1.1 Relation to Research Roadmap

The research carried out in this stage is related to the following open research questions raised from the Topic 2 research roadmap document:

- *Nonlinear Stability Margins*: Is it possible to evaluate non-linear stability margins using blackbox IBR models? Here, non-linear refers to the large-signal behaviour of the IBR. Blackbox EMT models more closely reflect the actual device behaviour under different conditions. A blackbox model is also expected to capture the dynamics of an IBR over a wider frequency range. However, research would need to be done to evaluate whether a non-simulation based analytical process can be used to evaluate the stability margins under varying network behaviour.
- *Balance of IBR Sources Representation*: How would stability properties of other sources in the network be represented when designing an IBR plant?
- *Black box model small signal modes*: Would it be possible to efficiently evaluate small-signal modes and stability profile with black box models?
- *Impedance-based procedures for stability screening*: Can procedures be identified, using impedance-based methods for stability screening and screening of converter driven stability risks? The methods and practices should be simple and yet reasonably accurate and aimed at reducing the total number of scenarios that need to be investigated with the use of detailed EMT time domain simulations.
- *Impedance-based IBR interaction screening*: Can the team document methods that use extracted impedances to screen for risk of converter interactions as well as risk of instability?
- *Impedance-based models for both EMT and positive sequence analysis*: Continuous development and use of impedance-based tools that can be applied in both positive sequence domains as well as EMT. Positive sequence impedance-based tools can perform accurate scans while considering

various network topological conditions with relatively minor computational effort. However, care should be taken to represent inverter interfaced resources as their impedance characteristics is not easily available and will vary with loading conditions, control models used, and so on.

- *Applicability of frequency domain methods for stability and interaction analysis:* The use of linear, frequency domain methods, such as linear models and eigenvalue analysis is another area that could benefit from additional research. It is well understood that linear methods can be used as an additional tool for the evaluation of some of the converter driven instabilities mentioned in this document. However, detailed linearized models for IBRs are not widely available in the industry at present. While some commercial applications for linear/small signal analysis exist, those mainly account for models used to study electromechanical modes, such as inter- and intra-area oscillations. To study faster control interactions, the analysis tools and models used would have to account for the faster regulators that impact a lot of those control instabilities. To what extent linearized models of IBRs can capture some of these phenomena, and how those models should be developed, is another area that would require further investigation.
- *Multiple operating point small signal models:* Development of a multi-operating point small-signal model (either impedance based or linearized state-space). Here again, there should be close synergy with Topic 1 to develop a multi-operating point model that can also be easily interfaced with existing small signal stability tools used by transmission network service providers (TNSPs) in Australia.

Specifically, the project has progressed work related to two critical topics identified in the research roadmap:

- Stability margin evaluation
- Small-signal stability screening methods

For each of these topics, the percentages of the research that have been progressed are (in relation to the initial 2021 roadmap) estimated as:

- Stability margin evaluation – 85%
- Small-signal stability screening methods – 85%

1.2 Background work

Some aspects of the background work for this report are presented in this section. Note, these all were utilized (in case of the C-code based blackbox IBR model and the small signal framework) and/or developed/improved over the previous stage of the research, and more details are available regarding all these in the report describing the previous stage research [3].

1.2.1 Inverter admittance operating point dependence

Although an IBR is a three-phase device, the (positive sequence) frequency domain admittance characteristics of IBRs are computed in dq domain, yielding four complex scalar quantities – Y_{dd} ,

Y_{dq} , Y_{qd} and Y_{qq} . These quantities correspond to inputs and outputs along the d and q axes and are defined as follows:

$$Y_{inv} = \begin{pmatrix} Y_{dd} & Y_{dq} \\ Y_{qd} & Y_{qq} \end{pmatrix} = \begin{pmatrix} \frac{\partial i_d}{\partial v_d} & \frac{\partial i_d}{\partial v_q} \\ \frac{\partial i_q}{\partial v_d} & \frac{\partial i_q}{\partial v_q} \end{pmatrix} \quad (1)$$

These quantities depend on factors such as IBR control structure and parameters, as well as on the operating point of the IBR characterized by the active power, reactive power and voltage magnitude. Figure 1 shows the four frequency domain admittance terms for an example IBR model. Different curves in this plot correspond to different operating points, and the figure illustrates the operating point dependence of IBR frequency domain admittance characteristics. This operating point dependence is more prominent in the lower frequency region – i.e. less than 10 Hz.

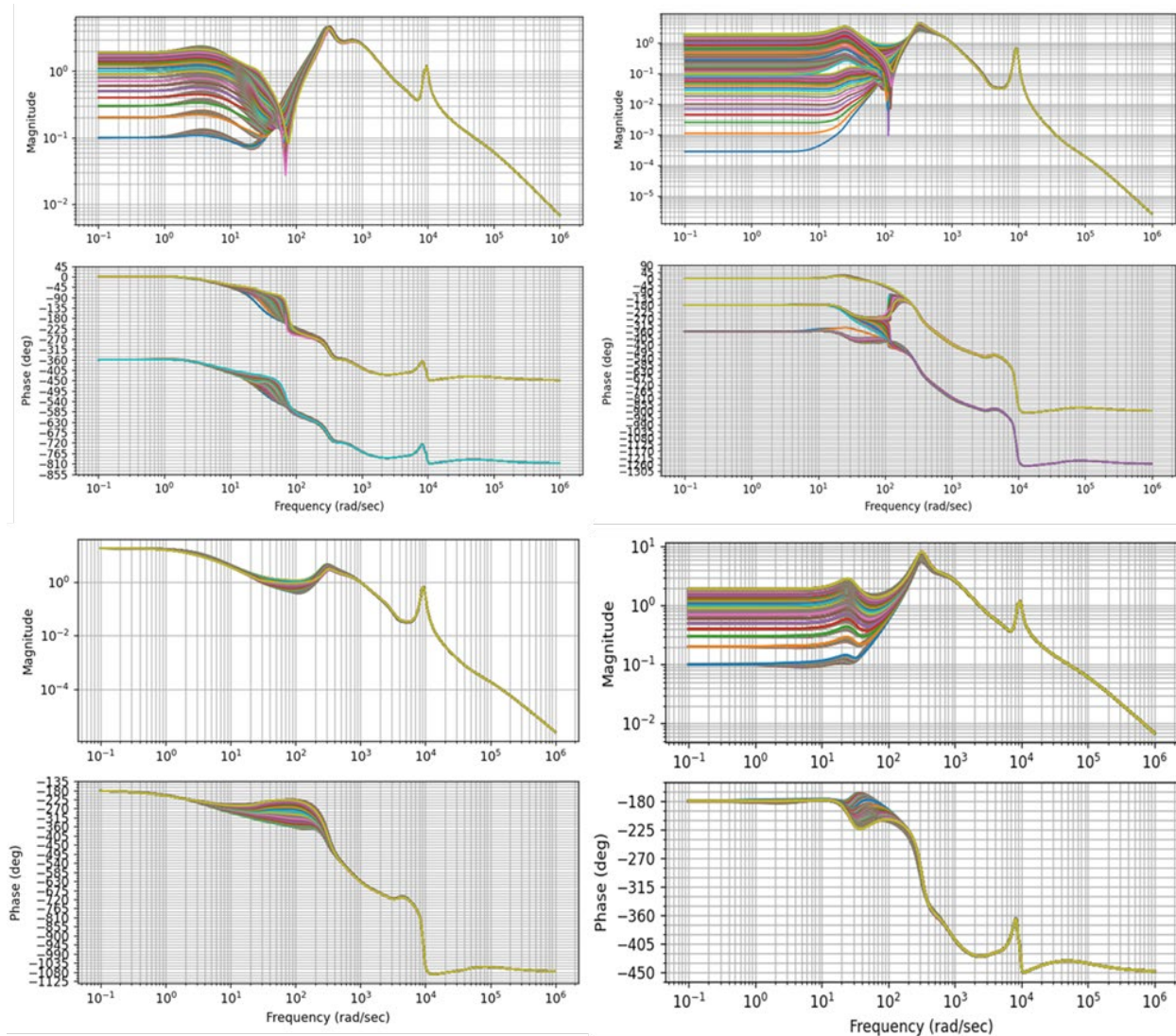


Figure 1 Operating point dependence of frequency domain admittance characteristics for an IBR model, with variation in P_{ref} from 0.1 to 2.0 MW and variation in V_{ref} from 0.9pu to 1.1pu for a 2.5 MVA IBR

1.2.2 Procedure to incorporate blackbox models in network small signal analysis

In the previous stage of the project, a systematic procedure was established to incorporate a blackbox EMT model into small-signal stability analysis of a network [3]. This procedure is used and improved throughout this stage of the research.

1.2.3 C code based blackbox IBR model

A generic C code based blackbox model was utilized in this stage of the research as a simple EMT model to compare against positive sequence IBR models. This C code based IBR model has been developed using a standardized code format being developed under the IEEE/CIGRE B4-82 working group and can be seamlessly used in different EMT domain simulation software packages. This code based model was also extensively used in the last stage of the research [3] and more testing/validation of the model can be found in [4].

1.2.4 Small-signal analysis framework

The framework utilized for the small signal analysis conducted under this project is the same as the framework utilized in the previous stage of the project. This framework was originally developed by EPRI to address control and dynamic interactions during power system restoration [5]. This previous work examined the IBR-based blackstart for bulk transmission power systems, and the small signal framework was developed and utilized to assess the network small signal stability efficiently and identify any oscillatory modes as well as the devices/control loops contributing to the oscillatory modes in the different stages of blackstart using eigen-analysis of a linearized power system model.

In the previous stage 3 of the project [3], this framework was applied for small-signal analysis of several test networks including the synthetic NEM network. The original synthetic NEM network was developed in [6], [7] and [8] and further modified in Stage 2 Topic 2 research [2]. Stage 2 research had developed 24 cases corresponding to different hours, and hour=19 case was utilized in Stage 3 Topic 2 research – the same case power flow is utilized in this stage as well.

1.3 Summary of work effort

In this stage of the project, the following work efforts were conducted:

- Obtained frequency scans of an OEM IBR EMT model at numerous training operating points and then used the analytical prediction method (APM) to predict the impedance characteristics at (different) test operating points. This process was repeated for three different OEM models (from two different OEMs), exploring the capabilities and limitations of the method when applying to OEM IBR EMT models
- Obtaining the frequency domain admittance characteristics for EMT domain IBR models is computationally burdensome. Hence, in this stage of the project, generic positive sequence IBR models that are part of the standard libraries in positive sequence software packages are studied to understand the suitability of these models for obtaining the frequency domain admittance characteristics to be used for the small signal analysis through the

procedure developed in the previous stage of the project, and to understand the nuances and limitations of such approach.

- Changes to control structure and control parameters are necessary when obtaining different grid services from IBRs. Another aim of this project is to understand the impact of some of these changes on the small signal stability characteristics of IBRs.
-

Table I Table summarizing the different tests/comparisons throughout this report

SECTION	DEVICE MODELLED	MODEL TYPE	TRAINING OPERATING POINTS	TEST OPERATING POINTS	ASSESSMENT	PURPOSE
3	OEM 1 IBR device GFM model	EMT black box	24	7	Qualitative trend of bode plots, Goodness of fit, and step response comparison	Assess the performance of admittance prediction method on EMT models
3	OEM 1 IBR device GFL model	EMT black box	24	7	Qualitative trend of bode plots, Goodness of fit, and step response comparison	Assess the performance of admittance prediction method on EMT models
3	OEM 2 IBR device GFL model	EMT black box	24	7	Qualitative trend of bode plots, Goodness of fit	Assess the performance of admittance prediction method on EMT models
4.1-4.2	Generic IBR Device A	+ve sequence RMS	19	7	Goodness of Fit, qualitative trend of Bode plots, Open loop poles and zero predictions	Assess the performance of admittance prediction method on positive sequence models
4.3	Generic IBR Device A	+ve sequence RMS and analytical small signal model	19	7+31	Qualitative trend of bode plots, open loop poles and closed loop poles for single machine infinite bus setup (7 test points) as well as synthetic NEM network small signal model, impulse response of synthetic NEM network small signal model (31 IBRs replaced)	Compare the frequency domain admittance and the small signal stability of Generic IBR device D against analytical small signal models
4.4	Generic IBR Device B_EMT, Generic IBR Device B_RMS	+ve sequence RMS and code-based EMT model	1	1	Qualitative trend of bode plots, open loop poles and closed loop poles for single machine infinite bus setup	For a positive sequence model approximating the EMT model, find similarities and differences in small signal stability
5	Three generic IBR devices	+ve sequence RMS		3	Qualitative trend of bode plots, closed loop poles of synthetic NEM network small signal model	Compare stability profiles of three IBR models with different levels of frequency and voltage controls

2 Methodology followed in the project

In the previous stage of the project, the analytical prediction method described in [2] and [3] was used to find the impedance characteristics of a blackbox generic IBR model developed by the project team. In this stage, the impedance characteristics of an OEM model is obtained using the APM. This helps in further testing and improving the robustness of the algorithm and understanding the limitations of the APM procedure.

Another aim is to assess the applicability of positive sequence IBR models to create admittance-based models for small signal stability assessment. A generic positive sequence IBR model was selected based on one of the IBRs from the synthetic NEM network. For this IBR model, the frequency domain admittance characteristics were obtained and small signal model using vector fitting (following the procedure developed in the previous stage of the research and described in Section 5.4 of [3]) was applied to understand the nuances in applying this procedure to a positive sequence model.

In addition, a generic positive sequence RMS IBR model with some of the similar controls as the EMT model utilized in the previous stage of the research was selected, and these models were tuned to be as similar as possible. The frequency domain admittance characteristics and the small signal characteristics of these models were compared, revealing the similarities and differences in these characteristics between the two models in the two simulation domains.

Lastly, for evaluating the impact of obtaining services from IBRs, three IBR parameterizations using positive sequence RMS models were utilized, and small signal stability characteristics for these with different control options corresponding to the different levels of services provided (no, slow, and fast, frequency control) were analysed.

Part II Improvements to incorporating IBR models to small- signal stability studies

3 Incorporating Blackbox OEM IBR models to small signal stability studies

Frequency scans were obtained from an OEM IBR EMT model to predict the frequency domain admittance characteristics and improve the robustness of the analytical prediction method (APM) developed in the previous stage. In the previous stage of the research, a systematic procedure was developed to form a small signal model of an IBR based on frequency domain admittance/impedance scans and incorporated into small signal analysis of a network [3]. This procedure can be summarized into the following steps (the steps are reproduced from the previous stage report):

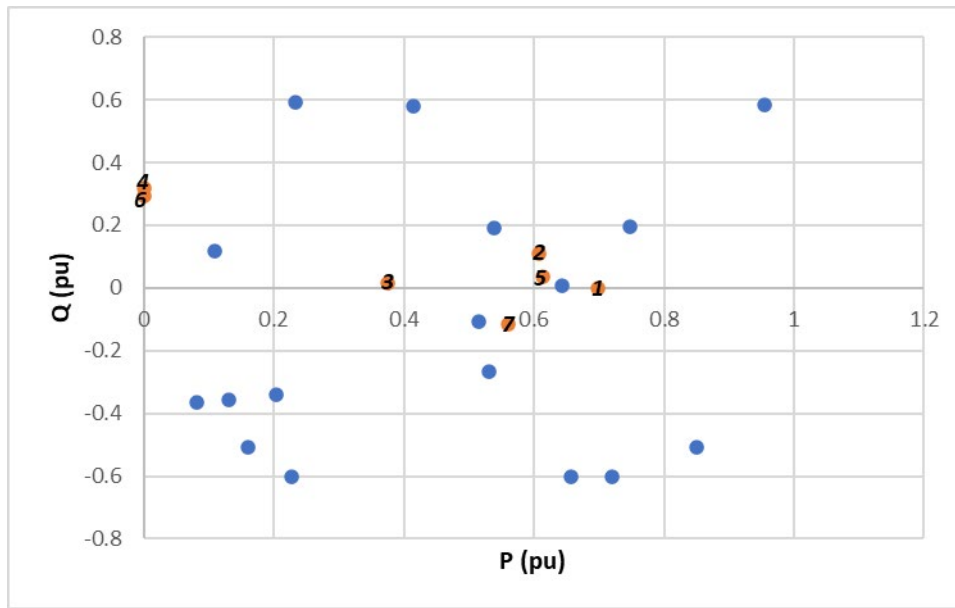
1. Obtain frequency scans for the IBR device at few select operating points.
2. Use the obtained frequency scans as the training data for the IBR admittance estimation method(s) discussed previously in [2].
3. From the network power flow solution, the required operating point(s) can be obtained where the device needs to be represented.
4. Using APM, the IBR admittance frequency characteristics at the required operating points are estimated. These are in the format of the admittance or impedance values for a pre-determined set of frequencies.
5. A system identification (addressing multiple distinct frequencies of the scalar frequency response) is then used to fit a model representing the IBR characteristics. This can be in the form of a transfer function or a state space model.
6. The state space model thus formed can be incorporated into the network model by converting/transforming the inputs and outputs into the required frame of reference or format.

Note, for the frequency scan method, readers can refer to [9] or [10], though there are several other references for other techniques for this purpose that are available on this topic, and once the frequency scans are obtained using any of the methods/tools the rest of the procedure can be followed for a device.

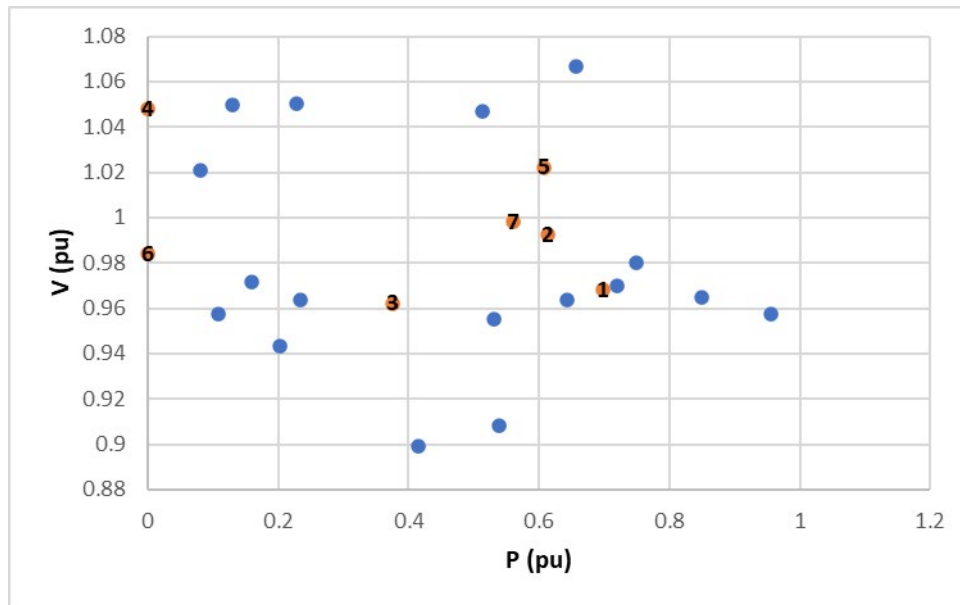
3.1 Obtaining the small-signal models of IBRs

3.1.1 Grid Forming model (GFM)

As a first step, frequency scans of an OEM GFM device shown in Figure 2, are obtained for the 17 training operating points (blue) and 7 test operating points (orange, and numbered for reference). The training and test operating points are selected such that they cover the active power, reactive power and voltage (PQV) operating space adequately.



(a)

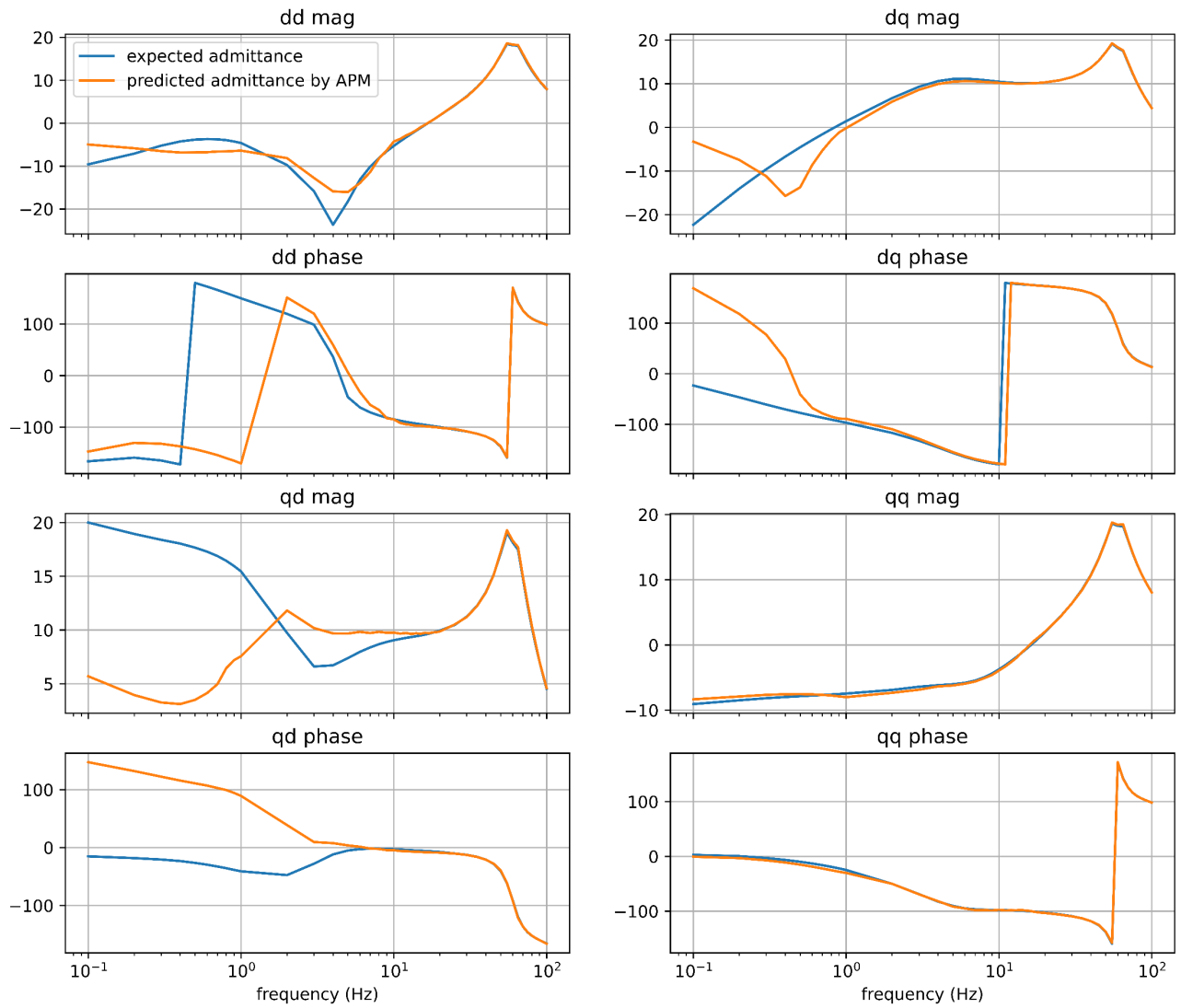


(b)

Figure 2 The training (blue) and test (orange) operating points selected for OEM IBR model a) P vs. Q b) P vs. V

The Analytical prediction method (APM), developed in the previous stage of the work, is then used with the training points to predict the admittance of the test operating points. The analytical prediction method was developed to obtain approximate frequency domain admittance of an IBR model at a new operating point using the frequency domain admittances at a given set of training operating points. More details and previous results from using this method can be found in [2] and [3]. The frequencies used in the frequency scans at the training operating points (as well as the test operating points for validation purposes) span 0.1 to 100 Hz range, with frequencies distributed in piecewise linear fashion in 0.1-1 Hz, 1-20 Hz and 20-100 Hz (with steps of 0.1 Hz, 1 Hz and 5 Hz, respectively). These are the same frequencies contained in the outputs of the APM. Output of the APM for the test operating points (denoted as the “predicted” admittances) is then compared with the frequency scans of the test operating points (denoted as the “expected”).

Figure 3 shows the comparison between the testing points as predicted by the APM for test points 3, and 7 (results for rest of the test operating points are shown in Appendix B).



(a)

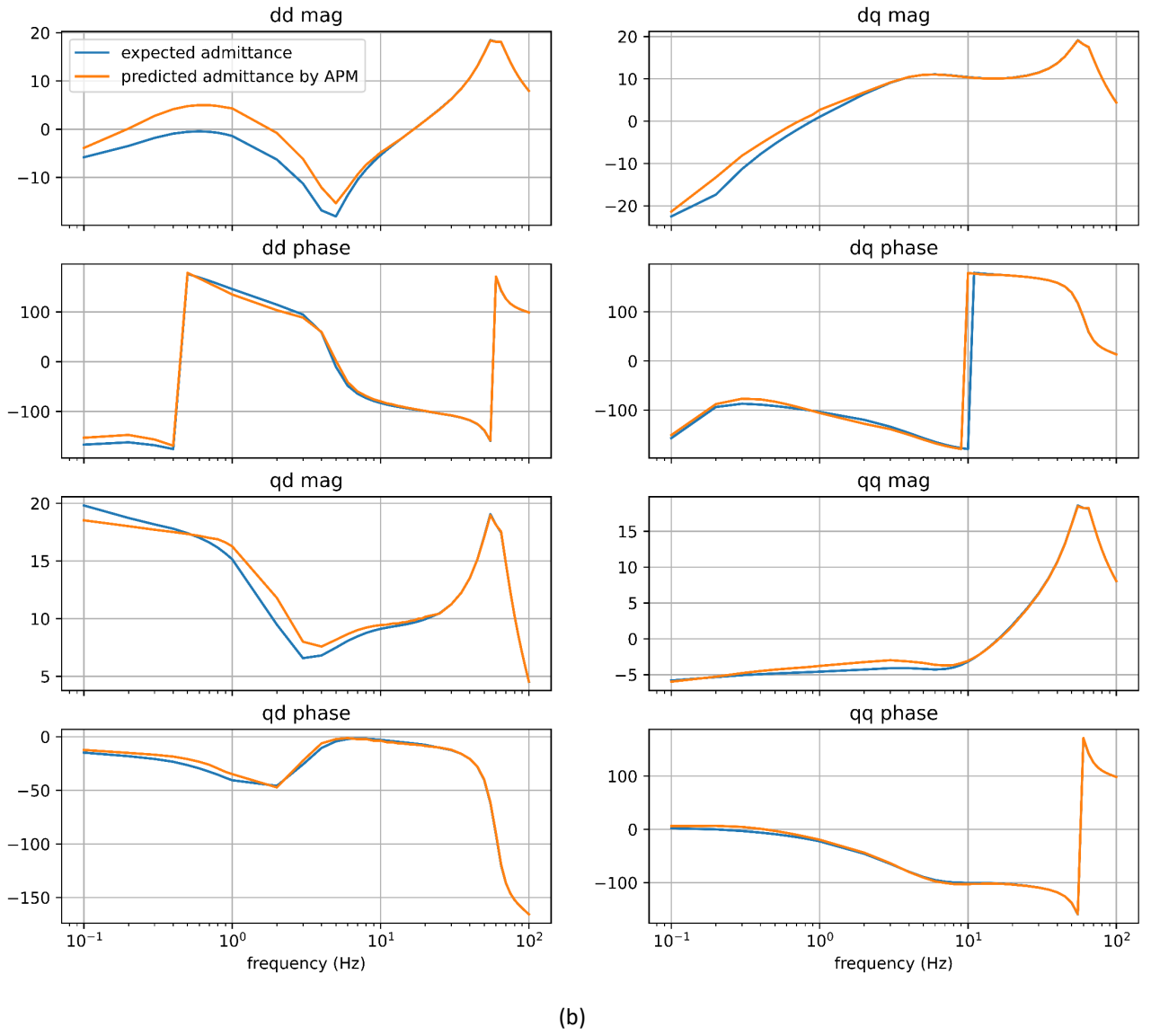


Figure 3 Two qualitative trends in the observed impedance at a) test operating point OP-3 b) test operating point OP-7

From Figure 3 it can be observed that for test point 7, the predicted admittance matches well with the expected admittance. However, for test point 3 there is a poor match for lower frequencies (less than 10 Hz). This mismatch can be due to limitations of the method, measurement errors during scanning, or due to limited training data size.

For all seven test operating points, the goodness of fit between the expected and predicted operating points was also calculated using the following formula, and is given in Table II:

$$err_{fit} = \frac{\|x_{ref} - x\|}{\|x_{ref} - \text{mean}(x_{ref})\|} \quad (2)$$

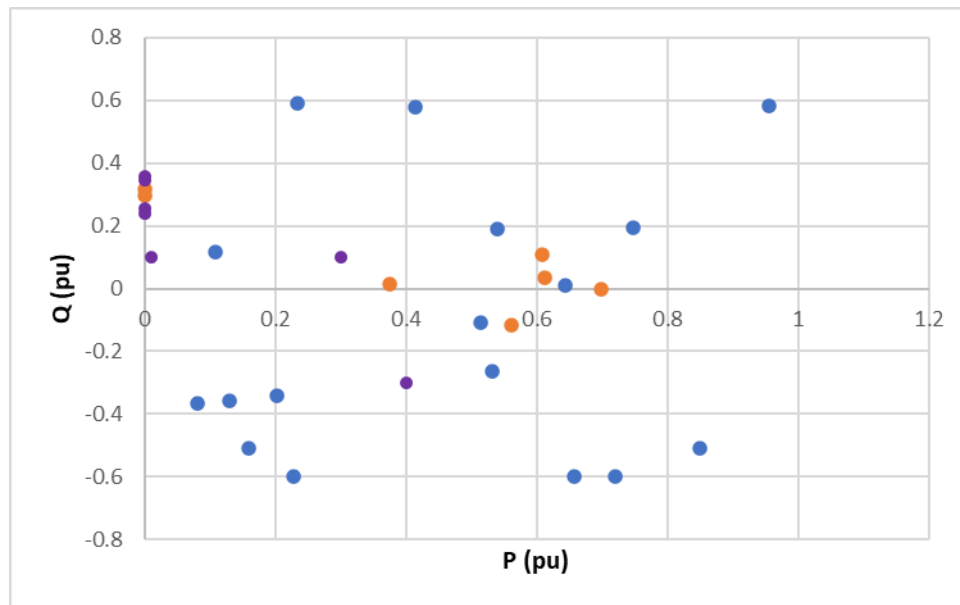
Here x is any quantity for which the goodness of fit is calculated, i.e. test data. x_{ref} is the reference data array, i.e. expected data. $\|\alpha\|$ represents the 2-norm array of α . Based on this formula, a smaller goodness of fit metric, approximately less than 10^{-3} corresponds to a very good fit result.

As seen in Table II, the goodness of fit is not small for the test operating points, this suggests that a good match is not obtained. However, a goodness of fit is just one possible candidate metric, and to confirm the goodness of match between the predicted and expected values, a comparison of dynamic response through a small signal model should be used.

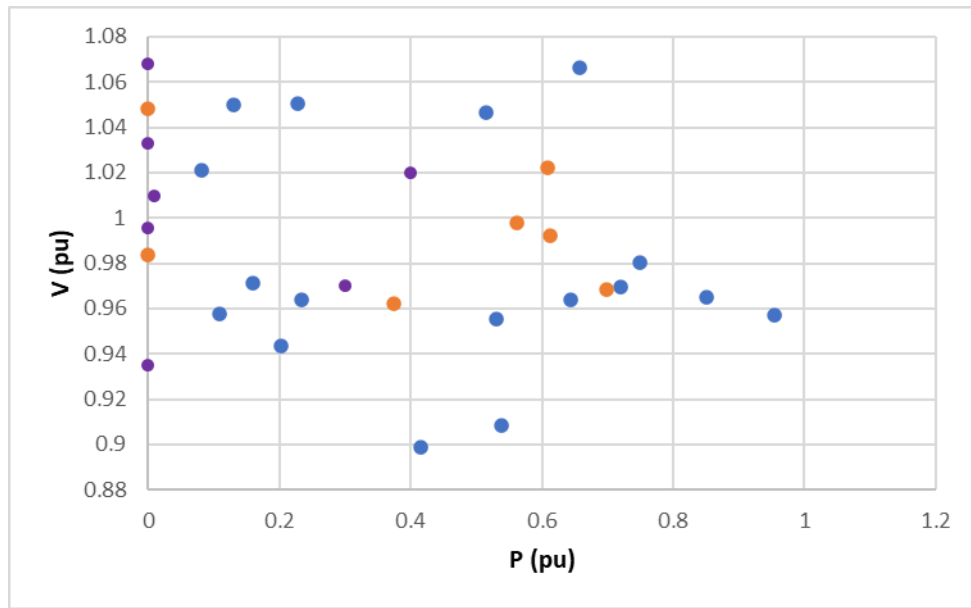
Table II Goodness of fit metric comparing the expected and predicted admittances at the test points

OPERATING POINT	GFIT_DD	GFIT_DQ	GFIT_QD	GFIT_QQ
1	0.0752	0.0750	0.3841	0.0181
2	0.0492	0.0849	1.7825	0.0220
3	0.0676	0.0736	1.1530	0.0267
4	0.0584	0.0695	0.1354	0.0440
5	0.0987	0.0787	1.0021	0.0286
6	0.0482	0.0549	0.8501	0.0263
7	0.1238	0.0366	0.1226	0.0183

For now, we increased the number of training operating set points from 17 to 24, additional training operating points are shown in Figure 4. Note, the selected frequency sample points were not changed.

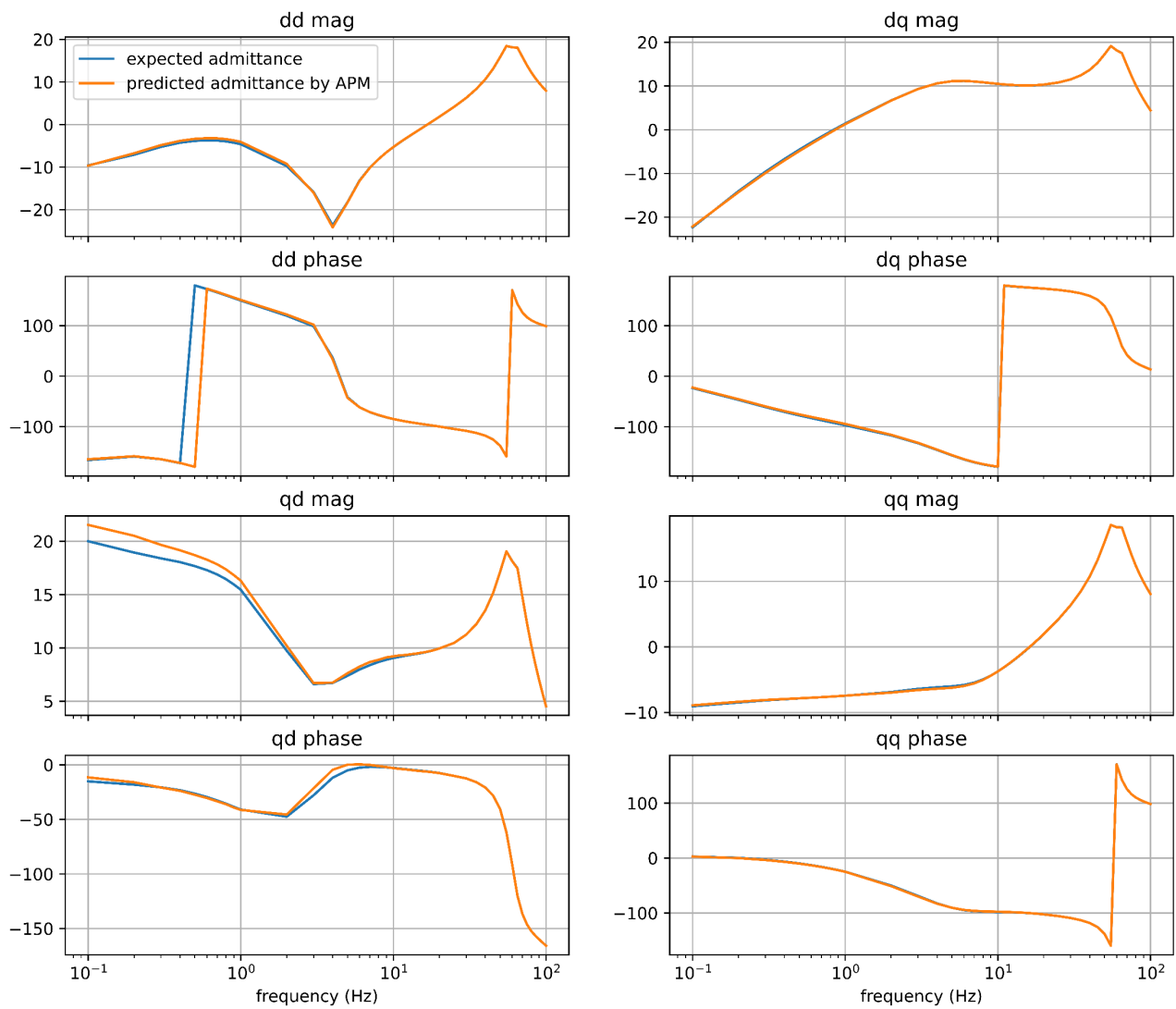


(a)



(b)

Figure 4 Additional test training points for the OEM IBR shown in purple a) P vs. Q b) P vs. V



(a)

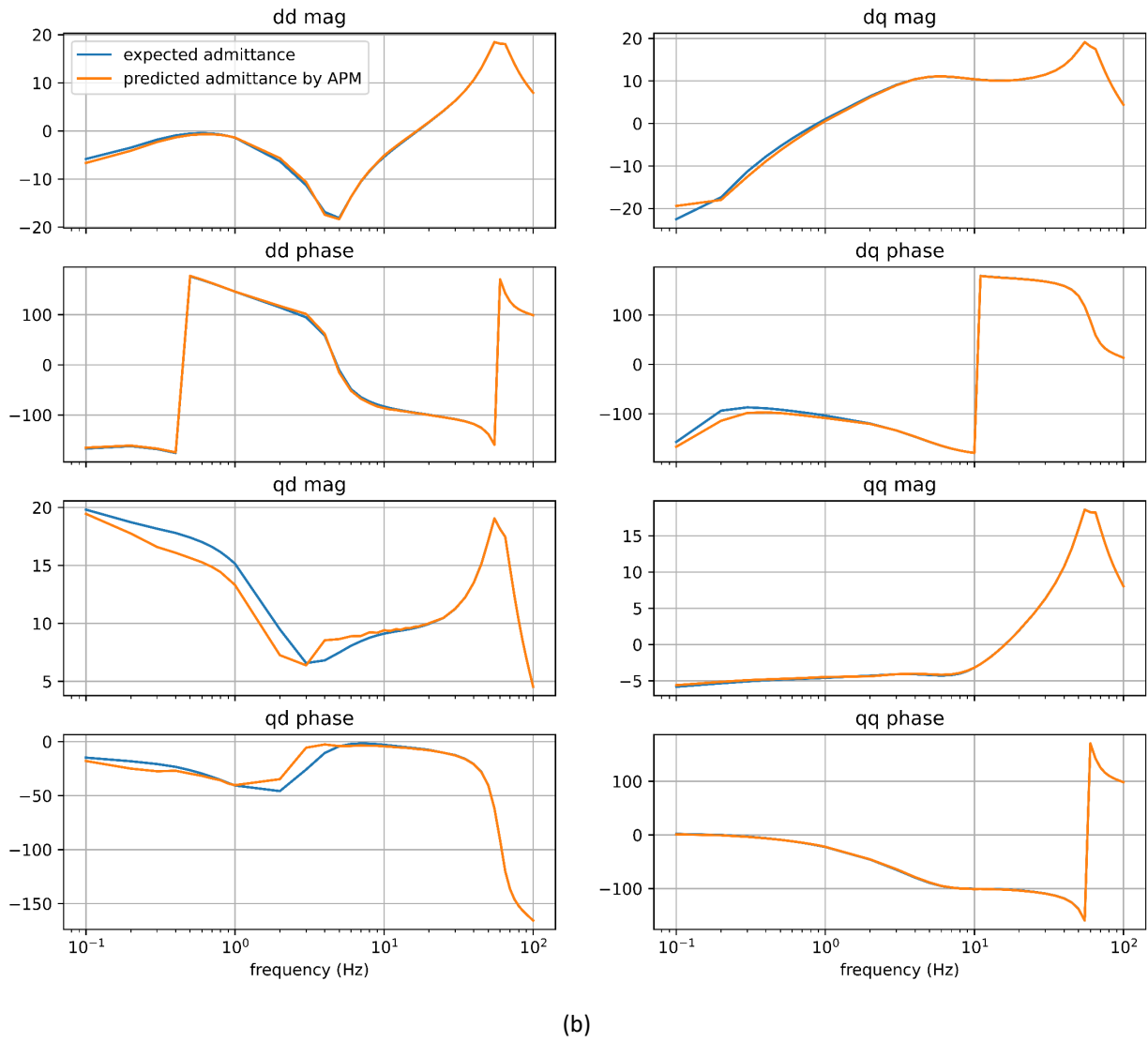


Figure 5 Two qualitative trends in the observed admittance at a) operating point OP-3 b) operating point OP-7

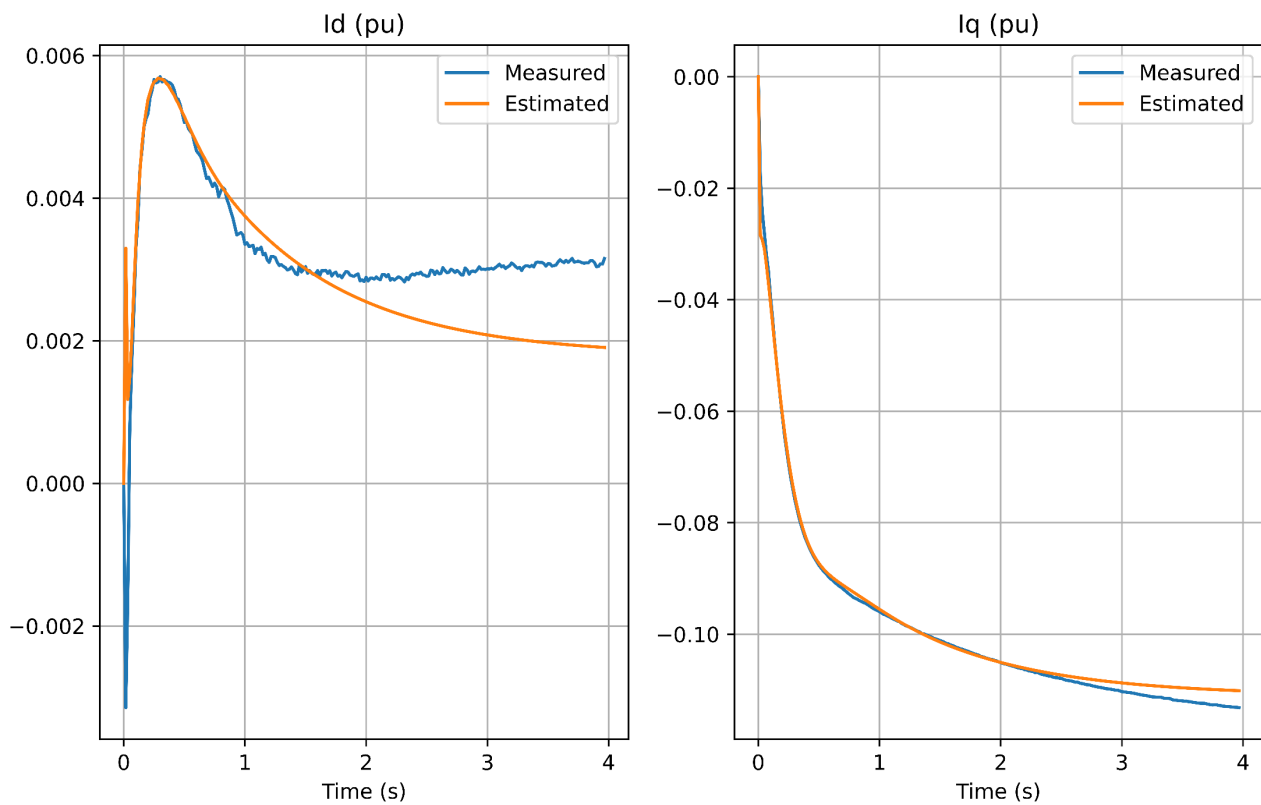
The results of the APM using the new training data [11] for test points 3, and 7 is shown in Figure 5. A better match for test point 3 is obtained, however the mismatch in the test point 5 (Appendix B) is still significant. Table III shows the goodness of fit after the addition of new training points. It is observed that the addition of new test points helps in improving the goodness of fit value compared to before, which means better prediction, but the value of goodness of fit remains high (which is unfavourable).

Table III Goodness of fit metric comparing the expected and predicted admittances at the test points

OPERATING POINT	GFIT_DD	GFIT_DQ	GFIT_QD	GFIT_QQ
1	0.0233	0.0107	0.2253	0.0046
2	0.0322	0.0254	0.3826	0.0126
3	0.0063	0.0073	0.1488	0.0030
4	0.0139	0.0009	0.5051	0.0034
5	0.0446	0.0488	0.6781	0.0288
6	0.0008	0.0010	0.0278	0.0008
7	0.0083	0.0131	0.1684	0.0038

More points can be added to get a good match; however, this may result in overfitting of the data. Therefore, as a next step, a state-space system identification step is applied to these points to check the dynamic response of the predicted and expected data for these test points. The predicted admittances are subsequently fitted to a state-space model, via the System Identification toolbox of MATLAB [11], which utilizes the predicted admittance points, as function of frequency, by the APM. As an additional verification test, the responses for a voltage step are compared between the “measured” EMT model’s dynamic response and compared with the output of the estimated state-space plant when subjected to the same input.

OP 3 Test_2



(a)

OP 7 Test_2

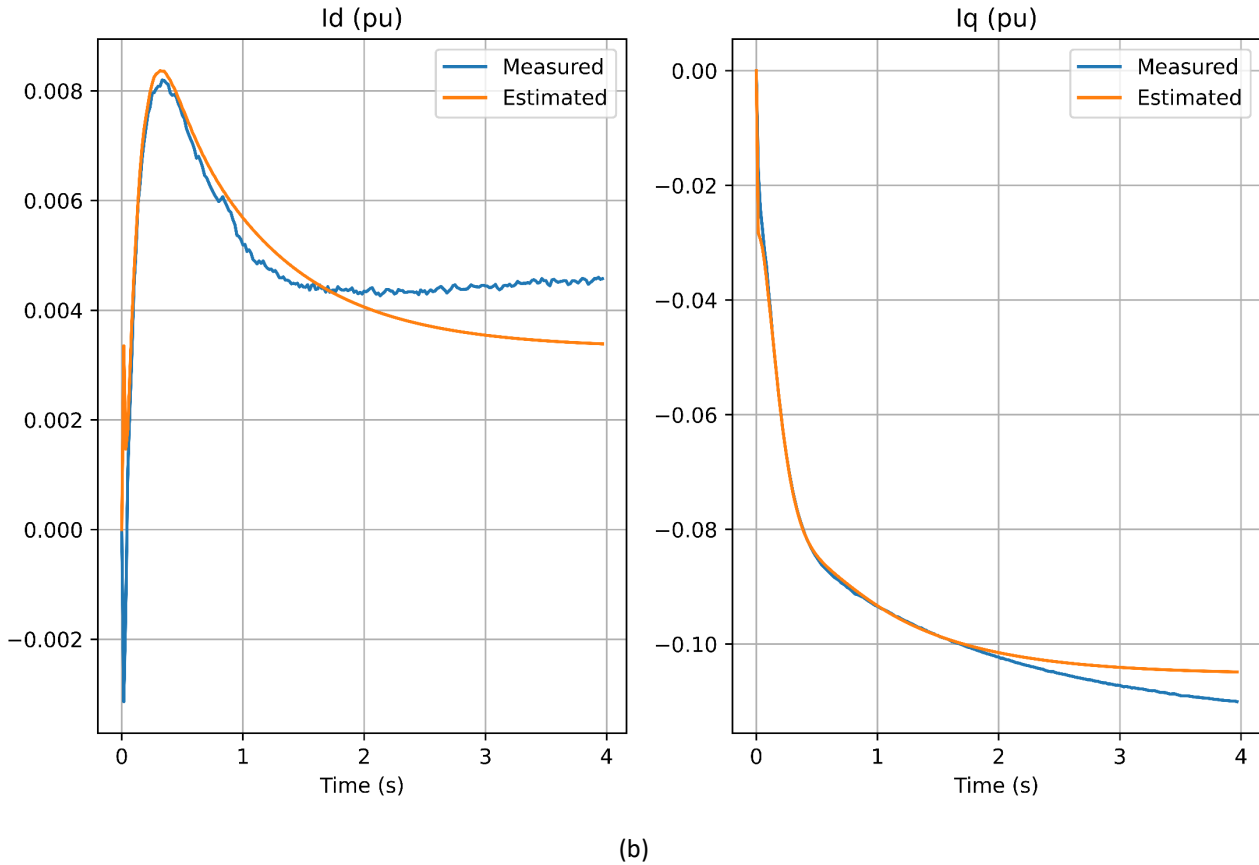


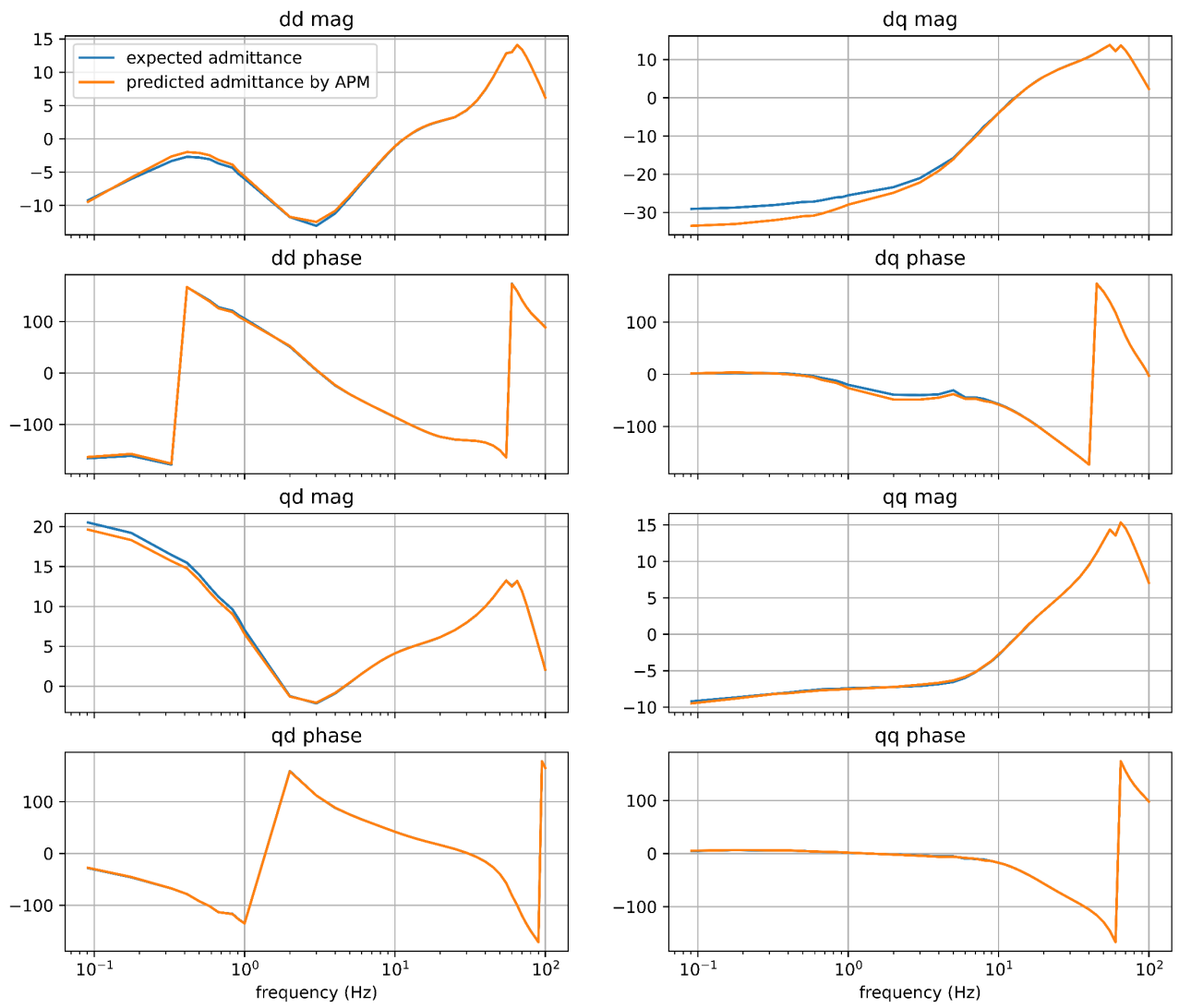
Figure 6. Comparison of measured and estimated time response for different test points a)OP-3, b) OP-7.

Figure 6 shows a comparison of the change in I_d and I_q for the measured and estimated model. Good match in the transient response is observed. Although, some errors can be observed at the steady state values, the estimated model eventually settles. This can be due to errors from the APM with respect to admittance prediction and the small fitting errors present in the identified state-space models close to the 0 Hz range.

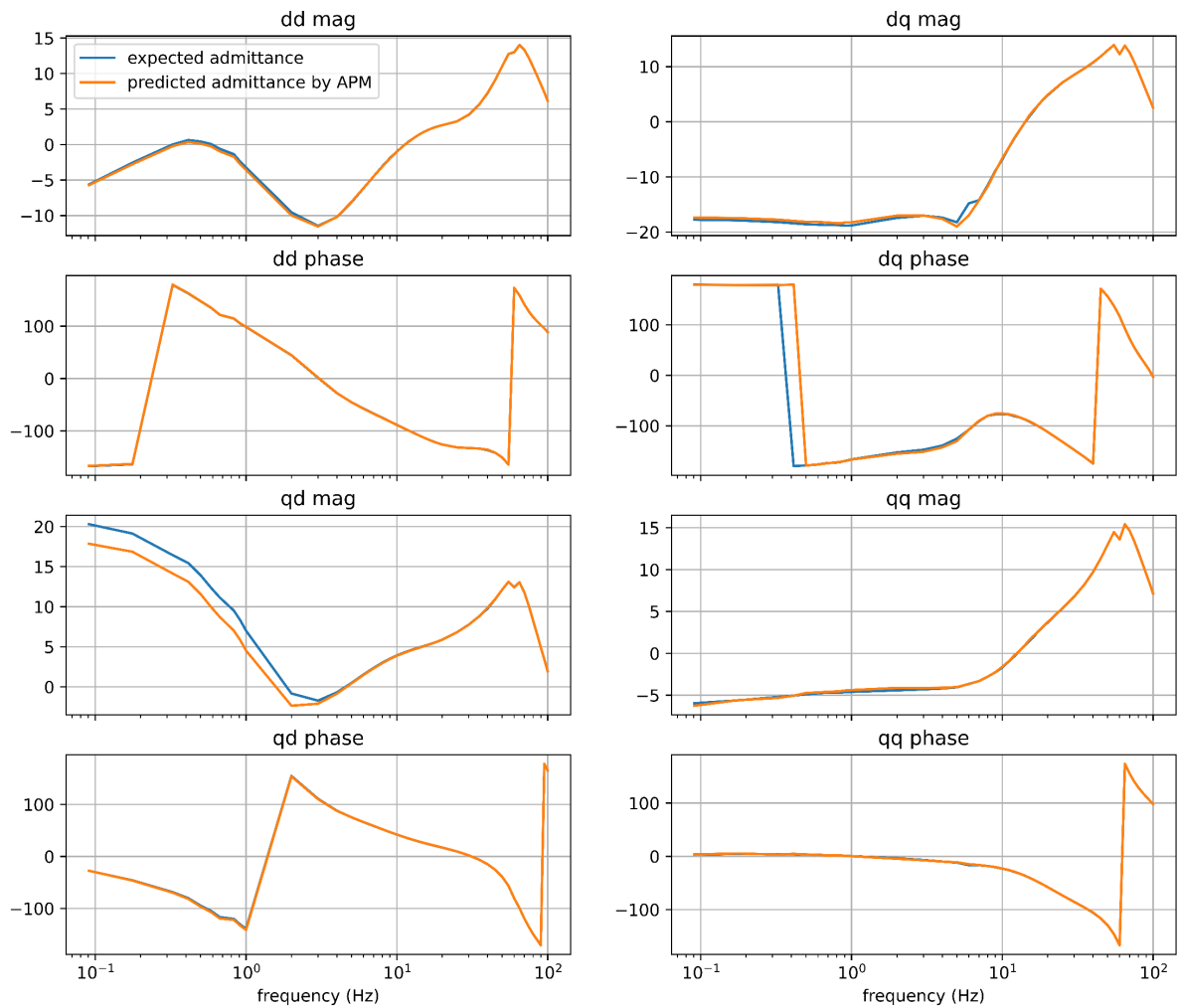
3.1.2 Grid Following Model (GFL) 1

Next, frequency scans of an OEM GFL device are obtained for the 24 training operating points (these operating points are same as GFM device) and 7 test operating points (same as before).

Analytical prediction method (APM), developed in the previous stage of the work, is then used with the training points to predict the admittance of the test operating points. The output of the APM for the test operating points (denoted as the “predicted” admittances) is then compared with the frequency scans of the test points (denoted as the “expected”). Figure 7 shows the comparison between the testing points as predicted by the APM for test points 3 and 7.



(a)



(b)

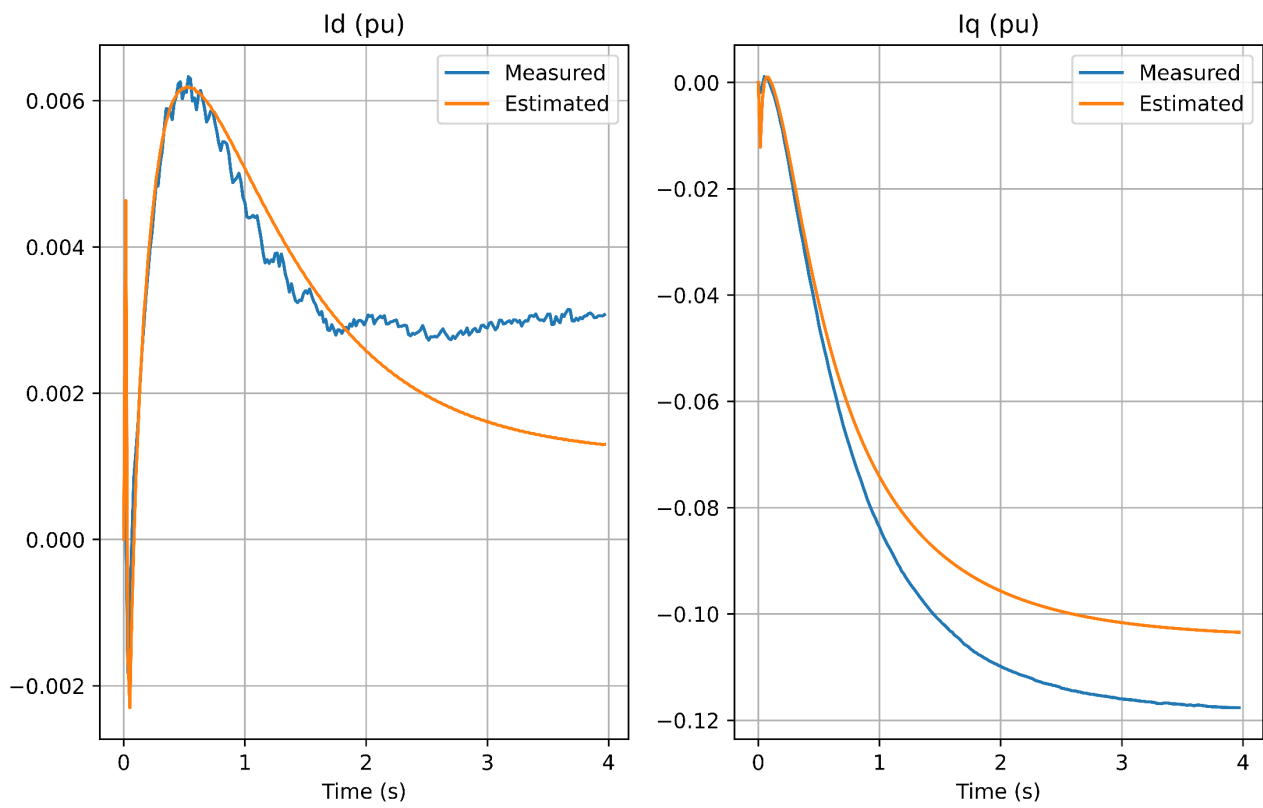
Figure 7 Two qualitative trends in the observed admittance at a) operating point OP-3 b) operating point OP-7

For all seven test operating points, the goodness of fit between the expected and predicted operating points was also calculated using (2), and is given in Table IV (goodness of fit is small for the test operating points). This suggests that a good match is obtained. However, a goodness of fit is just one possible candidate metric, and to confirm the goodness of match between the predicted and expected values, a comparison of dynamic response through a small signal model should be used.

Table IV Goodness of fit metric comparing the expected and predicted admittances at the test points

OPERATING POINT	GFIT_DD	GFIT_DQ	GFIT_QD	GFIT_QQ
1	0.0257	0.0143	0.1866	0.006
2	0.0300	0.0204	0.4668	0.0101
3	0.0125	0.0067	0.0770	0.0033
4	0.0043	0.0057	0.0160	0.0046
5	0.0610	0.0453	0.7878	0.0222
6	0.0057	0.0052	0.0047	0.0037
7	0.0090	0.0064	0.206	0.0048

OP 3 Test_2



(a)

OP 7 Test_2

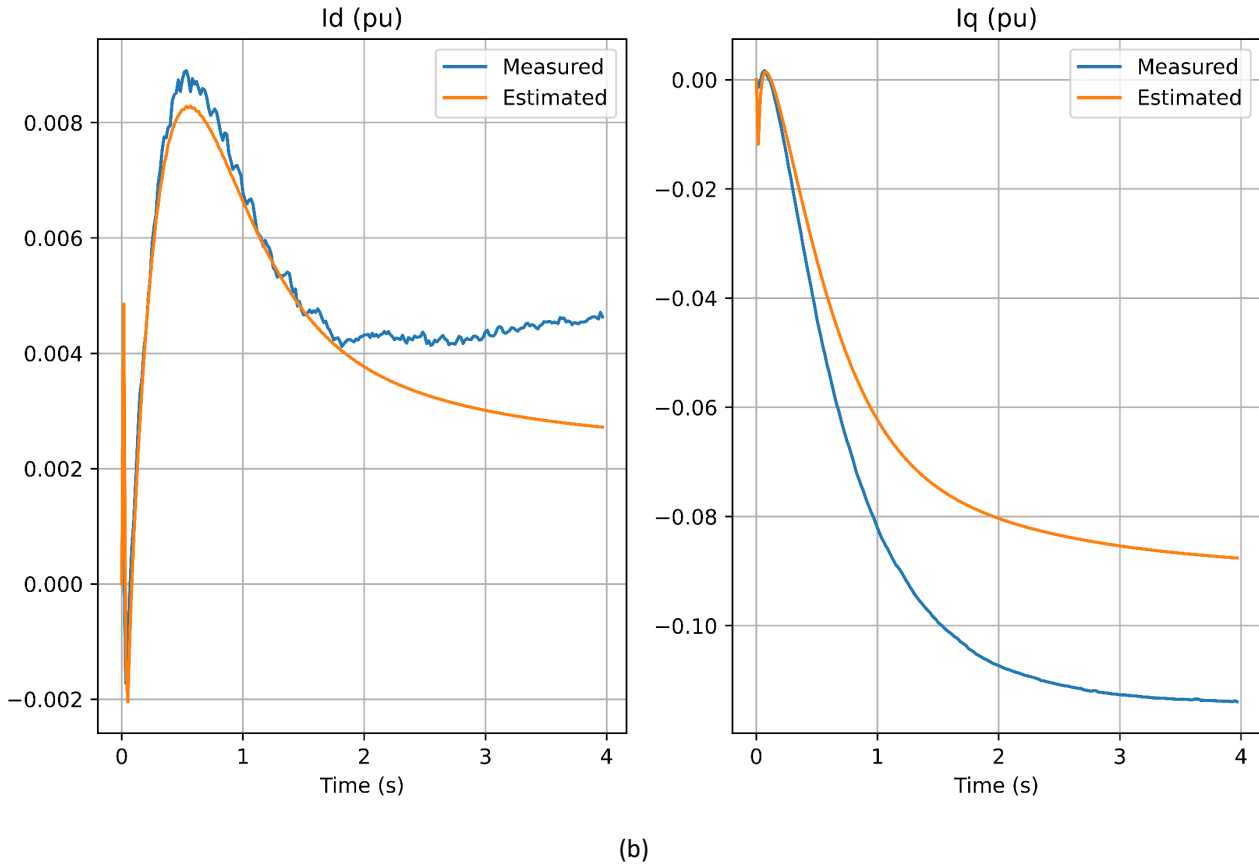
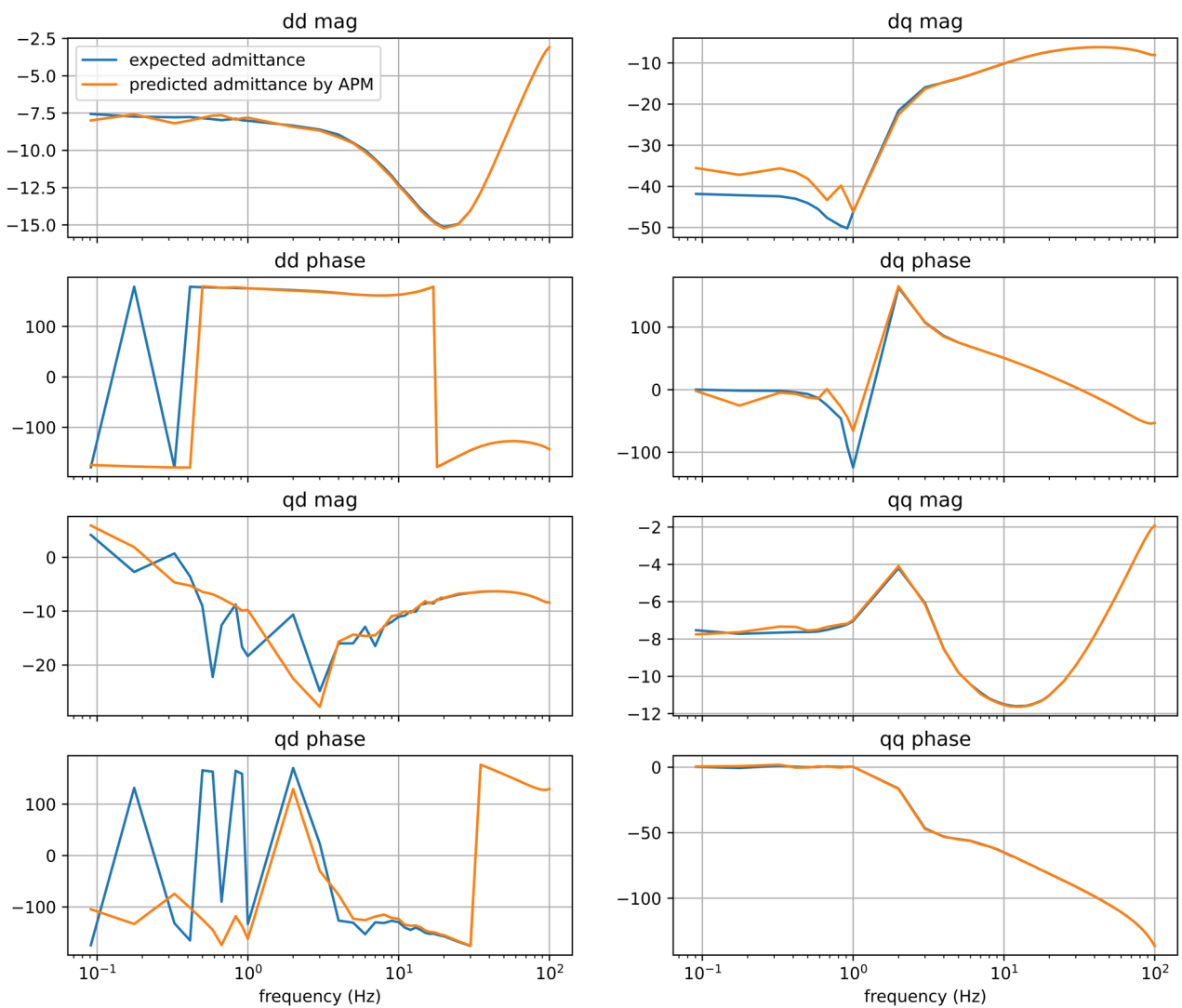


Figure 8 Comparison of measured and estimated time response for different test points a) OP-3, b) OP-7.

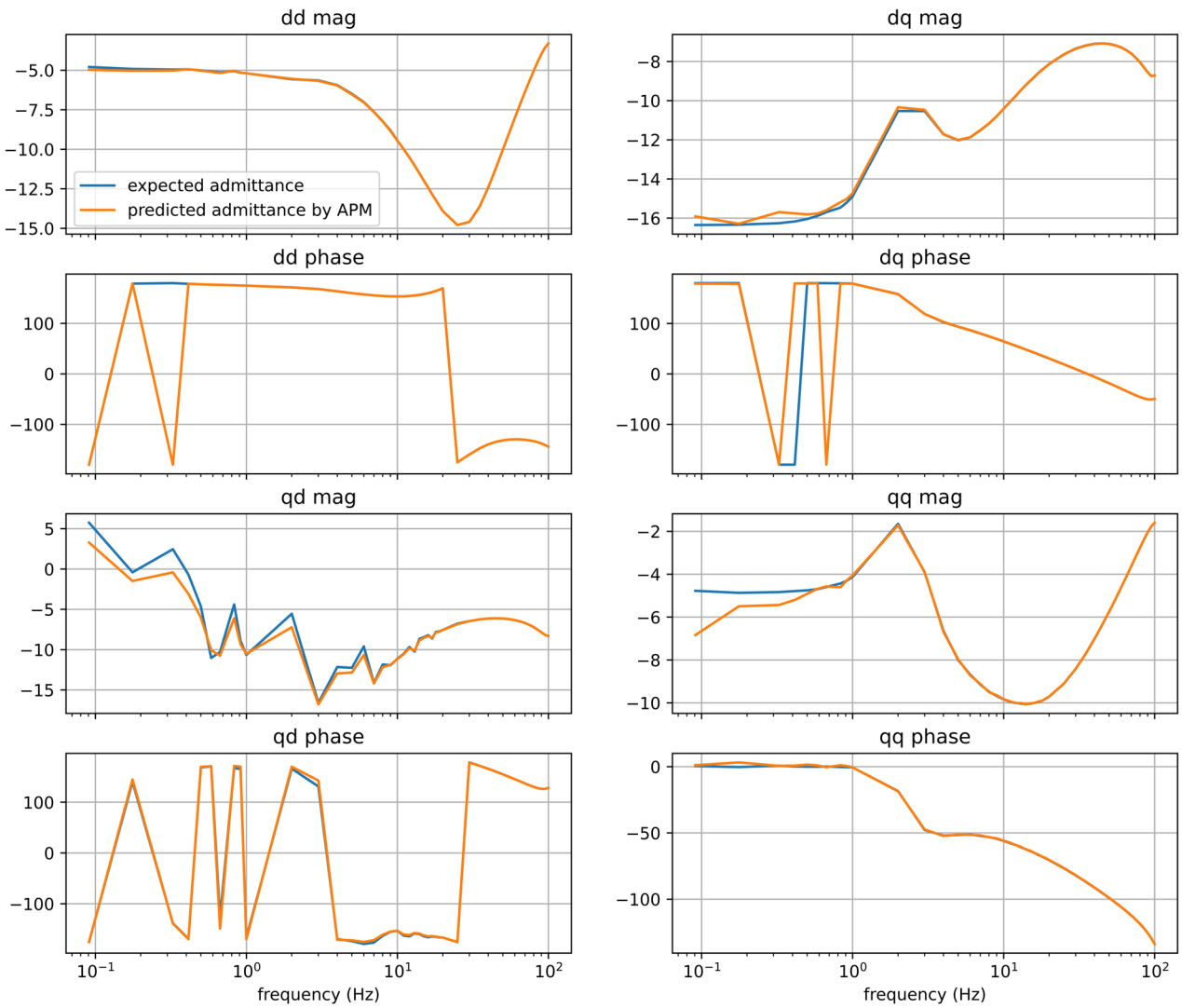
The step responses of the fitted and measured current present good match, except for the operating point (OP) 5 (Appendix B). As noted in the predicted admittance, there exist underestimation of the magnitude in the lower frequencies. This, along with any fitting errors can cause mismatch of the steady state value where the IBR device settles. Despite this issue, the initial transient response appears to follow the same trend as the measured time-domain data.

3.1.3 Grid Following Model (GFL) 2

A second GFL model examined was also put through the same procedure to predict admittances across the same varying operating points.



(a)



(b)

Figure 9. Two qualitative trends in the observed impedance at a) operating point OP-3 b) operating point OP-7

Figure 9 shows the comparison between the testing operating points as predicted by the APM for test operating set points 3 and 7. Note, each operating point the frequency samples remain same, and each operating point is characterized by a different value of active power, reactive power, and voltage. It can be observed that a good match is not obtained for test points 3. This can also be confirmed with the goodness of fit metrics shown in Table V. Fitting a state-space model directly on the predicted frequency responses yielded high fitting errors, thus the step response comparison was not carried out. Future work can look into the challenges of estimating and fitting such state-space models, before incorporating them in small-signal analysis frameworks.

Table V Goodness of fit metric comparing the expected and predicted admittances at the test points

OPERATING POINT	GFIT_DD	GFIT_DQ	GFIT_QD	GFIT_QQ
1	0.0382	0.0416	0.1355	0.0487
2	0.0918	0.0699	0.1441	0.0992
3	0.0440	0.0144	1.2958	0.0140
4	0.0258	0.0068	0.6801	0.0549
5	0.3503	0.2895	1.0125	0.2776
6	0.0164	0.0024	0.4342	0.0104
7	0.0108	0.0105	0.2813	0.0541

3.2 Integration of blackbox models in the system-wide analysis

Similarly to the previous stage of this work, the OEM models whose frequency responses were identified via frequency scans and subsequence state-space model fitting, are to be integrated in the synthetic NEM model. For this analysis, the OEM GFM models are integrated, in the network locations identified via analysis previously carried out [3]. The analysis in the previous stage identified locations with deficit of available short circuit capacity and the installation of GFM plants was tested as a potential remedy. The operating points for the GFM models were 0 active power with a small reactive power injection and variable terminal voltages depending on the voltage profile of the adjacent buses. It should be noted that in the training dataset, only 4 points were included with 0 active power output.

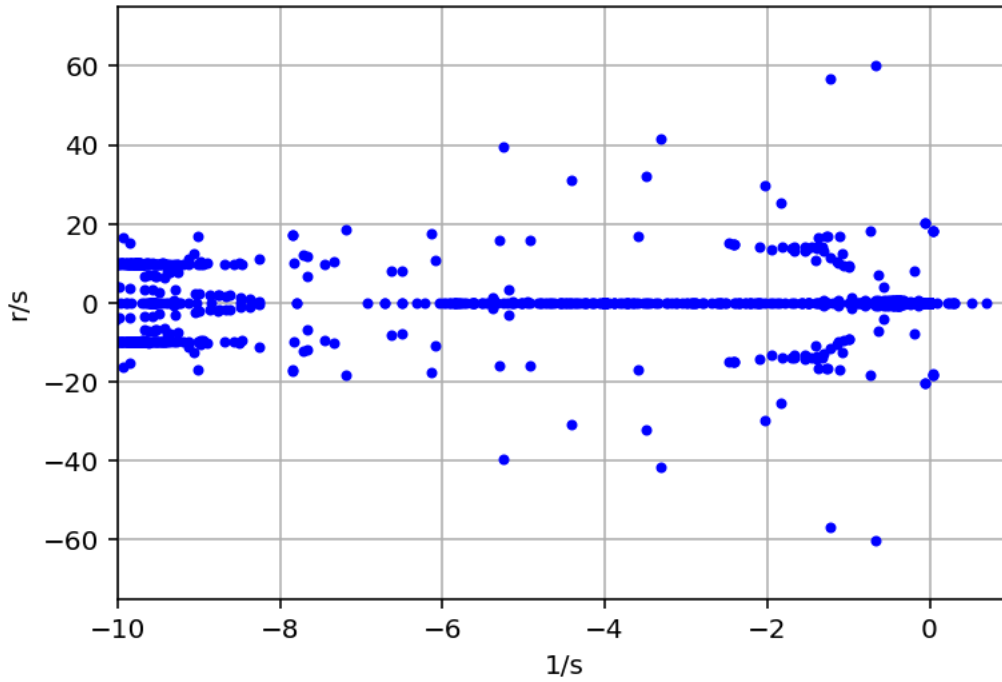


Figure 10 Closed Loop Poles with Blackbox GFM Models Integrated in the Synthetic NEM (r/s represents radians per second)

With the incorporation of the blackbox models in the small-signal model of the NEM system, no new low frequency instabilities were observed. The base case for comparison was the small-signal system model with only positive sequence models, which is examined in later sections. The only unstable poles observed are one of three alternatives.

- 1) Very high frequency and are usually cancelled by an associated zero.

These can be viewed as artifacts of the fitting process in the high frequency range. In addition, since the power system model does not incorporate network dynamics or generator stator dynamics, it cannot be used to assess stability at that frequency range, and instead, more detailed models, capturing those effects should be used for that purpose.

- 2) Real poles on the right half plane (RHP) which have participation only from black box GFM devices.

However, due to the errors observed at the lower frequency range, initially from the prediction and secondly from fitting the predicted admittances with state-space models, the most likely scenario is that errors were introduced that propagated in the closed loop dynamics. However, these poles are very low frequency and do not seem to affect the dominant generator and IBR dynamics.

- 3) Low damping poles that are accompanied by zeros (e.g. poles at 56 rad/s in Fig. 10).

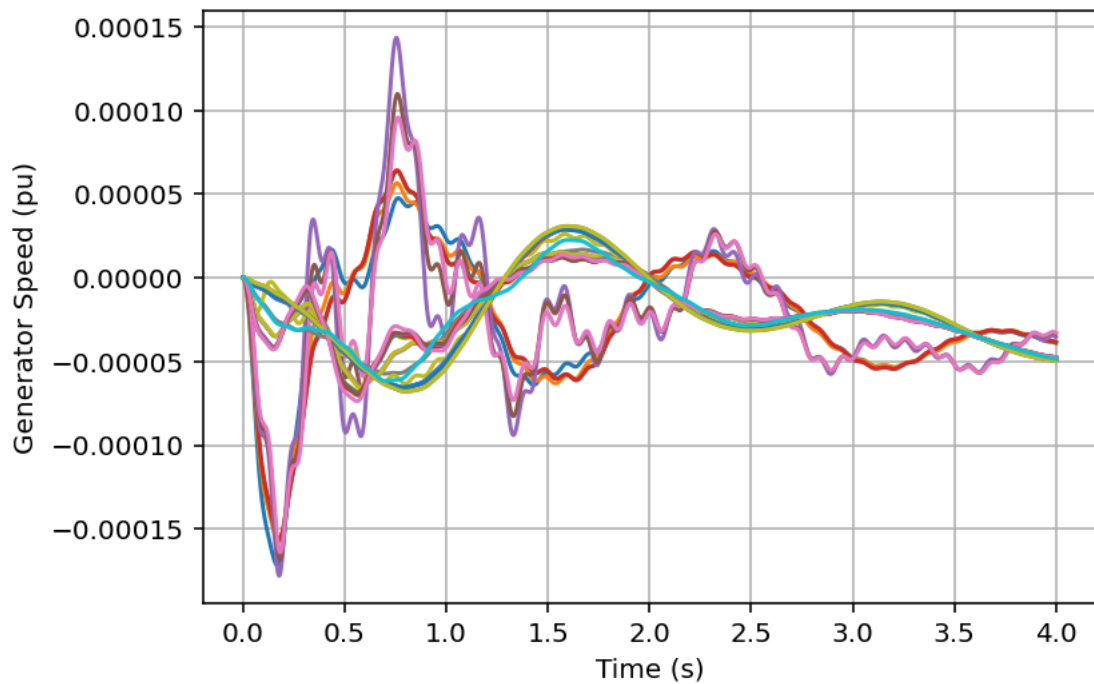


Figure 11 Generator Speed for System Impulse Response

3.3 Conclusions of Blackbox model identification and integration

In this section, the complete process of incorporation of OEM blackbox models, in a small-signal analysis framework was presented. Building upon previous work, the process of estimating the admittance from measurements, predicting it with the APM and then incorporating the models into an eigenvalue analysis framework was presented.

In particular, 3 OEM models were examined, 2 of the GFL type and 1 GFM. The results for the GFM and GFL 1 models, showed a good estimation and prediction of the equipment admittance by the APM, as verified by step response comparison of the models. The model GFL 2, presented some challenges in terms of prediction for some operating points. In addition, fitting of the model into a state-space model was also challenging. Future work can be geared towards addressing issues of successfully estimating linear models with the patterns examined in this report, in order to make the process more robust.

In the next step, the GFM blackbox models, were predicted for all the 35 grid forming models incorporated in the synthetic NEM system and then fitted in state-space objects. The closed loop dynamics did not exhibit any instabilities, with some low damping or unstable high-frequency poles, being artifacts of the fitting process which were not observable in the final time-domain responses of the small-signal model. Despite the process being successful, it will require future further refinement to address all those minor issues to yield a robust process that can be used for system-wide studies.

4 Utilizing positive sequence models for small signal analysis

In a small signal analysis of a network, devices such as IBRs can be represented using small signal state space models obtained from the frequency domain admittance (equivalently, impedance) characteristics of those devices. In the previous stage of the research (Stage 3 [3]) a systematic procedure was developed to form a small signal model of an IBR based on frequency domain admittance/impedance scans, and this was incorporated into small signal analysis of a power network. The same procedure as highlighted in the previous chapter is used for incorporating models based on frequency domain admittance scans of positive sequence IBR models in this chapter. Pictorially, these steps can be represented as given in Figure 12.

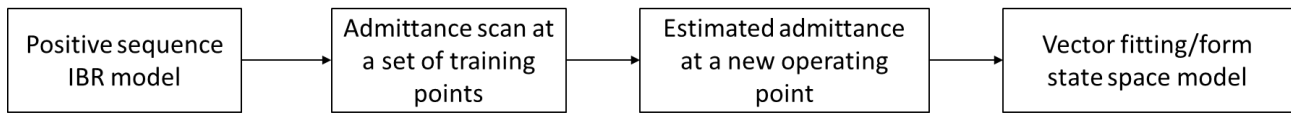


Figure 12 The procedure to use positive sequence models in a small signal assessment

Note, the above steps are reproduced from the previous stage report and are the same as the ones presented in the previous chapter. The admittance characteristics of IBRs depend on the operating point – typically, this has the largest variation impact on the lower frequency characteristics of the (frequency domain) admittance, i.e. lower than ~ 10 Hz. An example of this is shown from the previous stage of the research in Figure 1, where for the same IBR model the dq domain admittances are plotted for different operating points, in no specific order.

Traditionally, the frequency domain scans are performed on EMT domain IBR models (apart from physical hardware tests) to capture the frequency domain behaviour across a wide range of frequencies. This was the approach for the previous research stages (see [2], [3]) as well as other research, such as [12], [13], [14], [15] (this is a non-exhaustive list). Note, the majority of the operating point dependence is observed in the lower frequency region. Positive sequence IBR models (that is, quasi-steady state, dynamic RMS models) may be able to approximate the IBR behaviour in this range. Hence, a task was undertaken with the aim to evaluate the potential for using positive sequence IBR models to obtain frequency domain admittance/impedance characteristics, to be further utilized for small signal stability analysis. Another aim here was to compare the characteristics obtained from positive sequence models with those obtained from EMT models to highlight similarities and differences between using positive sequence and EMT IBR models.

Another benefit of using positive sequence models for obtaining the frequency domain admittance/impedance characteristics of IBRs is reduced computational burden. The previous stage of the research highlighted some of the computational challenges involved in performing the admittance scans. As the number of distinct frequencies to scan the model at is increased, and especially as the scans include lower frequencies, the computational burden of performing the admittance scans significantly increases. If this procedure is envisioned for a large number of devices connected to the network, this computational burden can be significant. This burden can

be alleviated to some extent, if positive sequence IBR models can be used for obtaining the IBR frequency domain characteristics.

4.1 Obtaining the small-signal models of IBRs based on positive sequence models

To test the procedure to take an IBR model and obtain frequency domain admittance characteristics that are in turn used to form a state space model for small signal analysis, a generic model based on one of the IBRs from the synthetic NEM model was selected. Here, the synthetic NEM model modified in Stage 2 work [2] and used in Stage 3 work [3] is used. This model is referred to as “generic IBR model A” in the report. The model parameters for this model are given in Appendix A. Similar to the analysis performed on the OEM model in the previous chapter, 19 training and 7 test points were selected, as shown in Figure 13. Note, these points are the same as the ones described earlier in Figure 2, the idea behind using the same training and test points was to try and identify if there are any general observations that are common to both models.

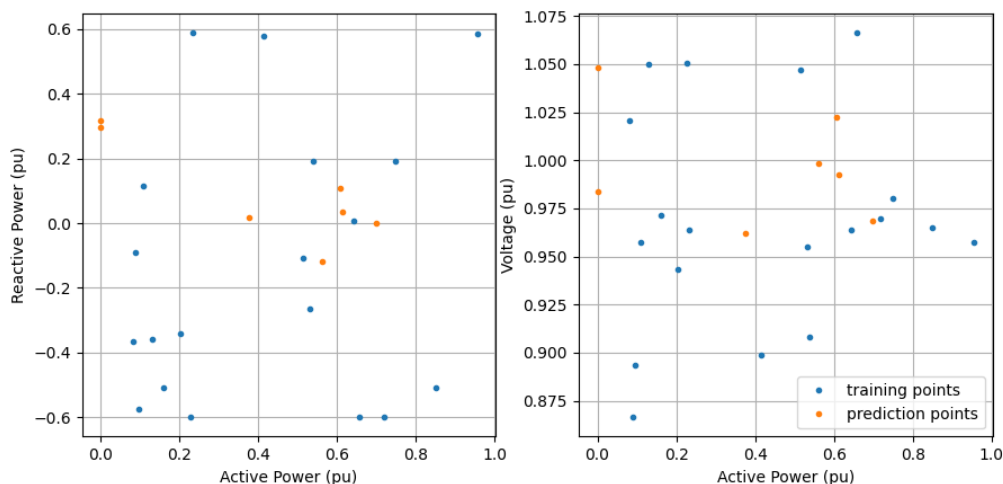


Figure 13 The training (blue) and test (orange) operating points selected for positive sequence IBR model

The first step was to apply and assess the performance of the analytical prediction algorithm (APM). When the APM algorithm was applied using these training and test points, the admittances at the test operating points obtained from the APM algorithm (denoted as the “predicted” admittances) were compared with the frequency domain admittances obtained at that test point (denoted by “expected” admittances). Figure 14 shows this comparison for two test points – it can be observed that in some cases the predicted and expected admittances match well (for example, the operating point 2 in the figure), while there are mismatches for other cases (operating point 4 in the figure). The cases with the mismatch also had large variations in the q phase term. Note, for the positive sequence models, a set of 24 frequencies spanning 0.1 to 15 Hz in a piecewise linear fashion, with steps of 0.1 Hz and 1 Hz for 0.1-1 Hz and 1-15 Hz regions.

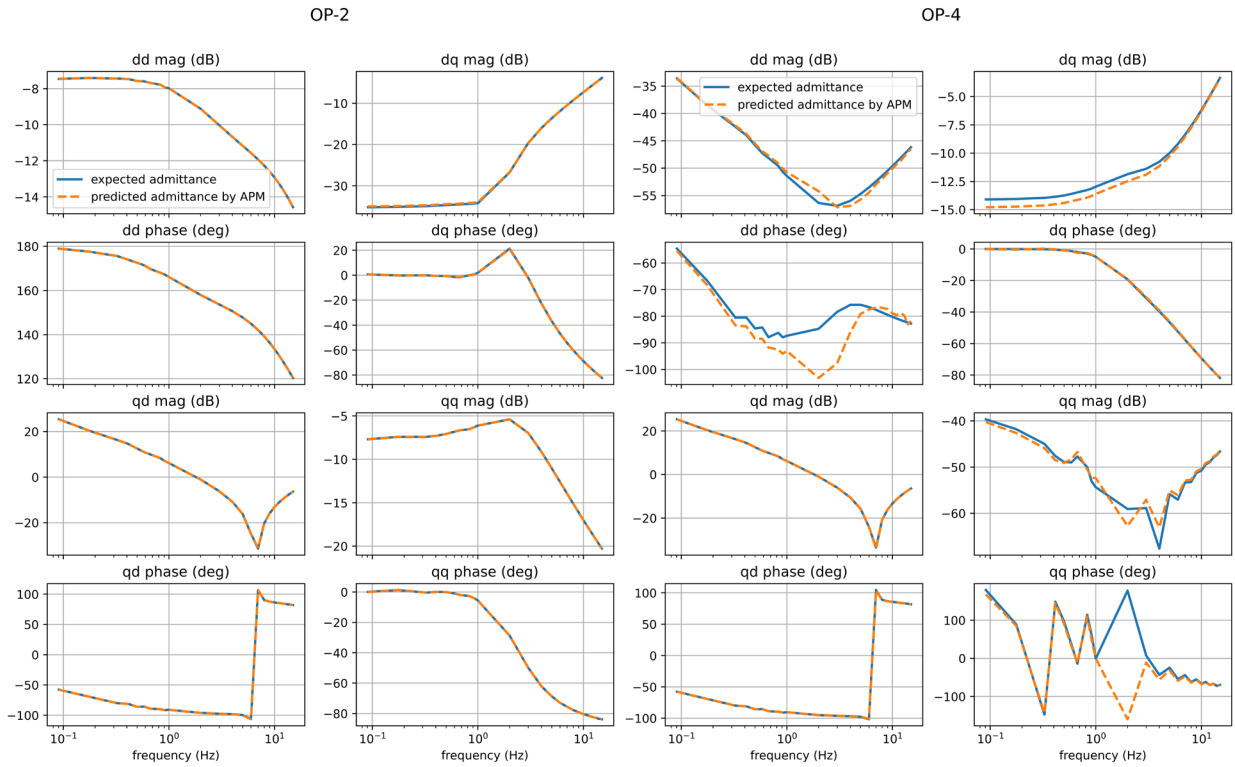


Figure 14 The expected frequency domain admittance characteristics (blue, solid) for a positive sequence IBR model compared with the predicted impedance characteristics (orange, dashed) at the same operating point using APM algorithm for two test operating points, OP-2 and OP-4.

The next step was applying vector fit to identify the poles and zeros for each term (that is Y_{dd} , Y_{dq} , Y_{qd} and Y_{qq}) – here, the same vector fitting algorithm as the one employed in the last stage of the project was utilized. More details of this algorithm are available in [16], [17] and [18] and the MATLAB version available from [19] was used here on the expected and predicted admittances. Note - here, the two terms with the same input are fitted together – i.e. Y_{dd} and Y_{qd} are fitted together and Y_{dq} and Y_{qq} are fitted together, ensuring that the terms with the same input have common poles. These two single input, multiple output (SIMO) models are combined to form the multi-input, multi-output model. For operating points where the predicted and expected admittances matched for APM, the vector fitting was successful in replicating the admittance. Other cases where APM algorithm had large mismatches between the expected and predicted admittances, there were challenges in successfully applying vector fitting to represent the admittance. The input data and vector fit are shown in Figure 15 for these two points (operating points from Figure 14).

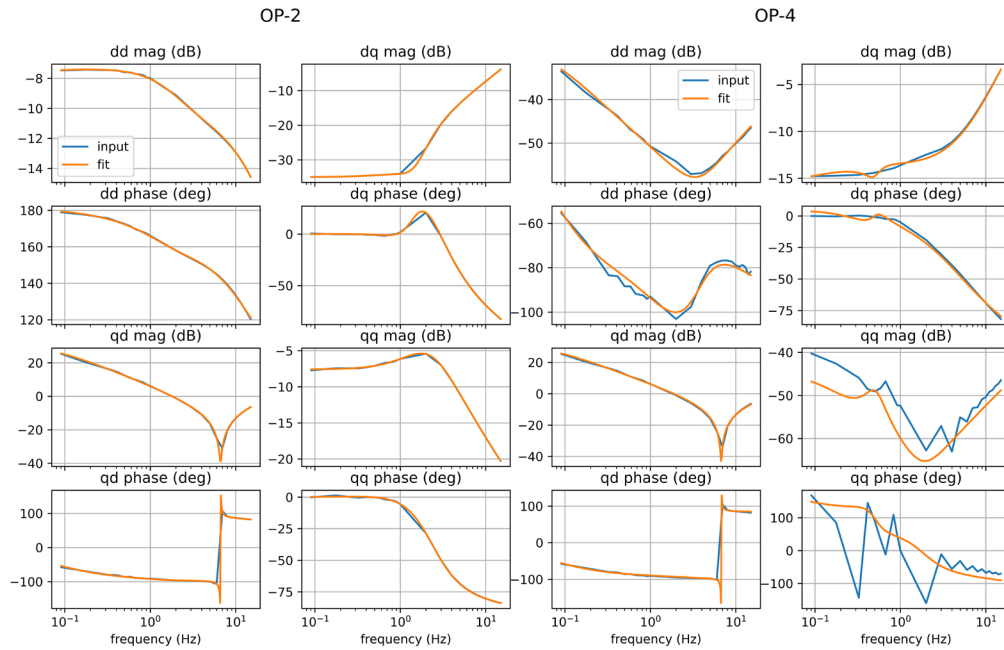


Figure 15 Vector fitted model compared with the input data supplied to the vector fitting block for the predicted admittances for two operating points, OP-2 and OP-4

4.2 Restricting the active power setpoint

In order to understand the relationship between the different qualitative trends (marked by presence or absence of large variations in phase angle for the qq term) observed in admittances observed for different operating points, the admittance scan is performed at a larger number of points (30), as shown in Figure 16. These points were selected to span active power setpoint of 0 to 1.0 p.u., reactive power setpoint of -0.66 p.u. to 0.66 p.u., and voltage magnitude of 0.95 p.u. to 1.05 p.u. The points are coloured orange or blue in the figure according to the qualitative trend of frequency domain admittance, and these two trends are shown in Figure 17, where the points coloured in blue exhibit the trend in Figure 17 (a), and the points coloured in orange exhibit the trend in Figure 17 (b). Hence, it was observed that at operating points with low active power reference, there is a different trend in terms of frequency domain admittance compared to other operating points. There are differences observed within the points coloured in blue and within the points coloured in orange, as the operating point changes, for example, from absorbing reactive power to injecting reactive power, but the overall smaller magnitude in the qq term as well as the large “jumps” in the phase seem to occur for operating points with active power equal to zero.

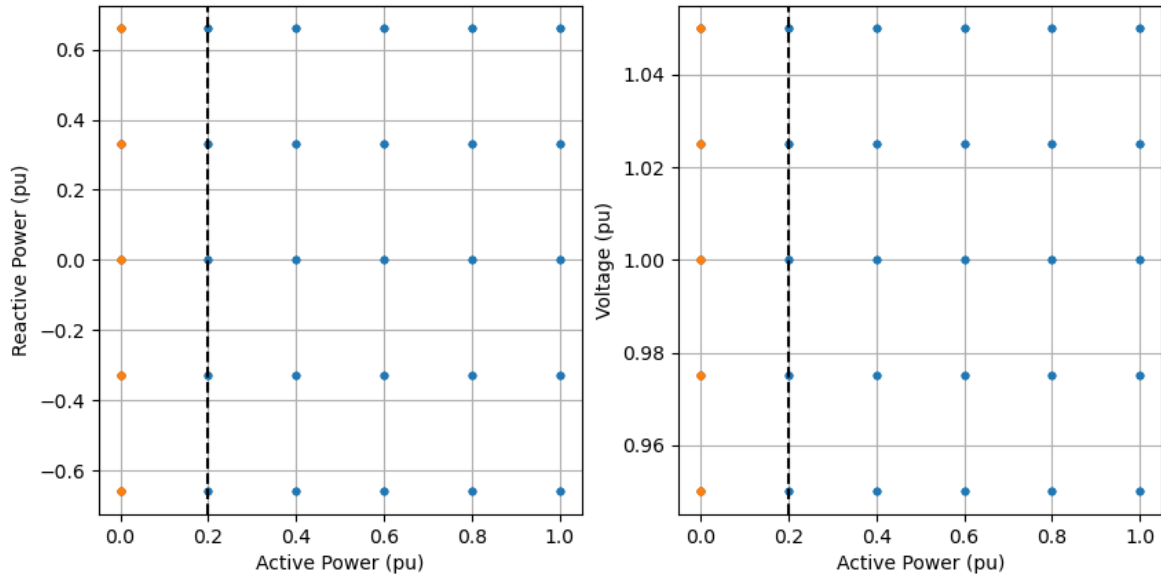


Figure 16 The different operating points chosen for testing the frequency domain admittance. The two colours of points indicate two distinct qualitative trends in the observed admittances

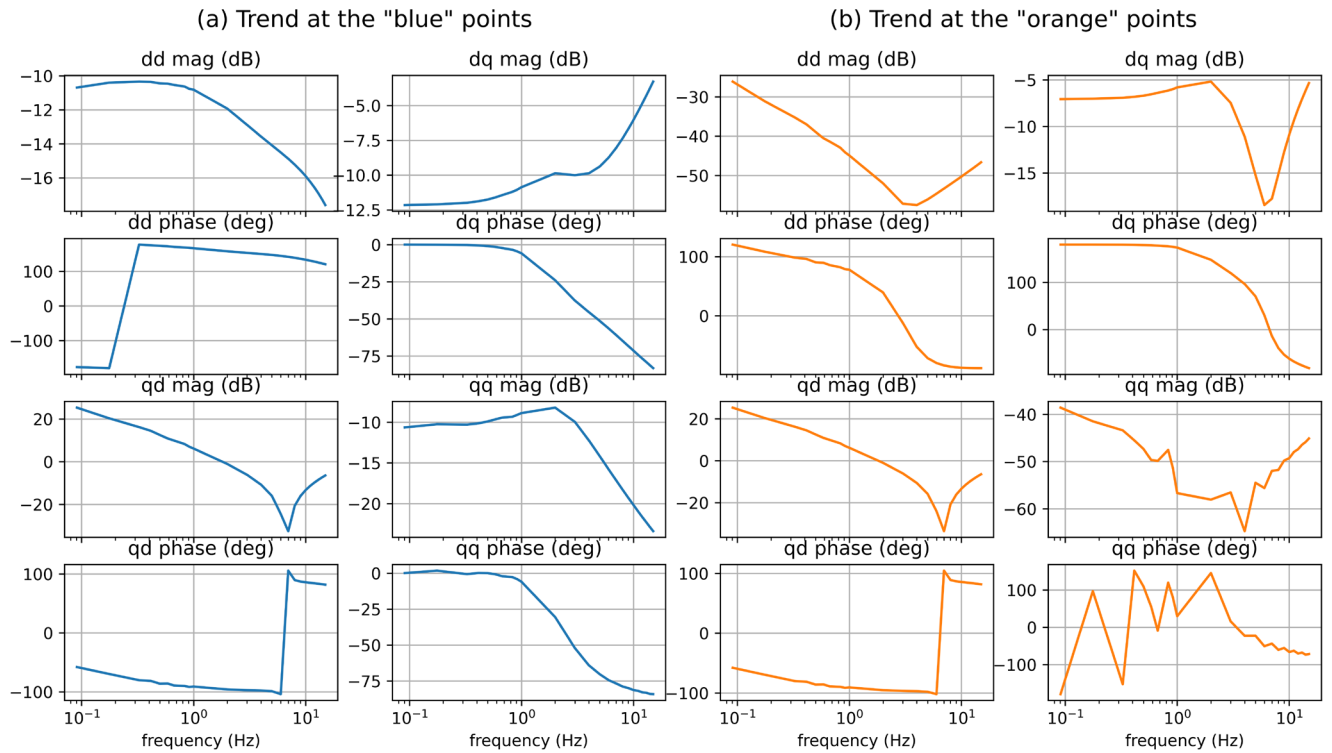


Figure 17 Two qualitative trends in the observed admittance at different operating points

Due to this difference, the training and test points were updated to restrict the region with active power equal to or greater than 0.2 p.u. Any training or test points with active power lower than that threshold were replaced with another point that had a larger active power – this replacement is shown in Figure 18.

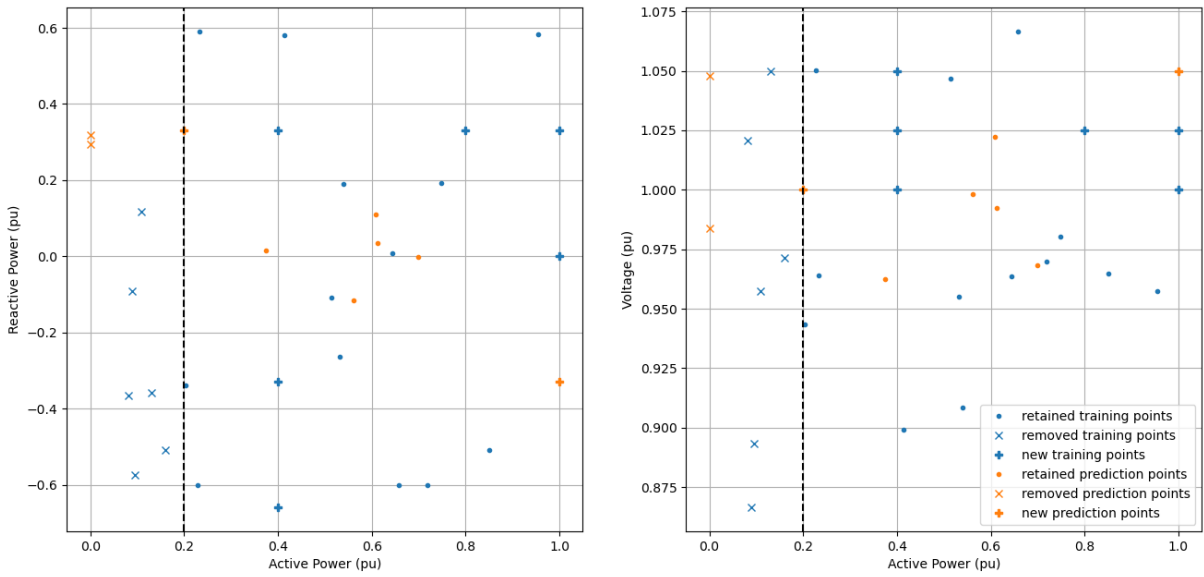


Figure 18 Updates to the training and test points to retain all the points above 0.2 p.u. active power setpoint

With this updated set of training points, the APM algorithm was again applied and the expected and predicted admittances at the updated test points were compared. For all seven test points, the predicted admittances were found to match the expected admittances well. For two of the test points, this comparison can be visually inspected, as shown in Figure 19.

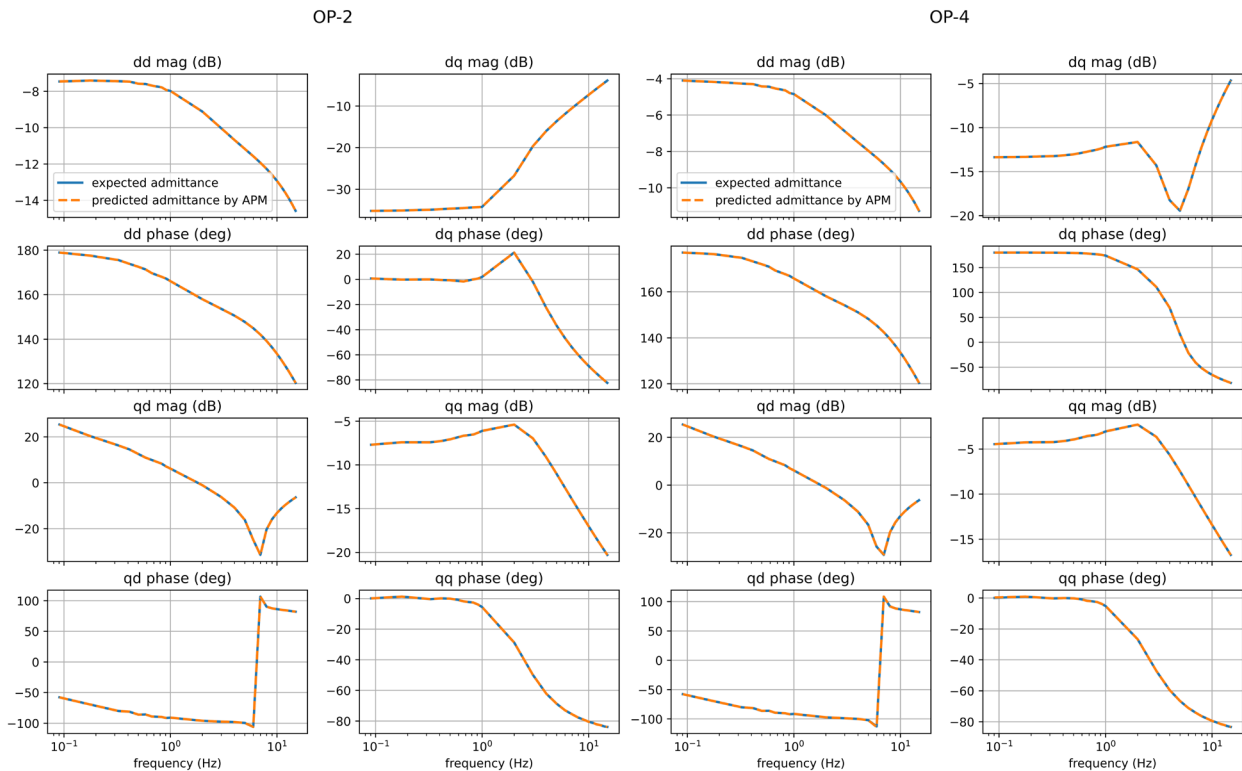


Figure 19 The expected (blue, solid) and predicted (orange, dashed) admittances at two test points (OP-2 and OP-4) with the updated data – the predicted and expected curves overlap, indicating a good match.

For all seven operating points, the goodness of fit between the expected and predicted operating points was calculated using the following formula (applied directly to the complex admittances), and is given in Table VI:

$$err_{fit} = \frac{\|x_{ref} - x\|}{\|x_{ref} - \text{mean}(x_{ref})\|} \quad (3)$$

Here x is any quantity for which the goodness of fit is calculated, i.e. test data. x_{ref} is the reference data array, i.e. expected data. $\|\alpha\|$ represents the 2-norm array of α . Note, this is the same formula used earlier in (2) in Section 3.1. Based on this formula, a smaller goodness of fit metric corresponds to a better fit with lower error. For each test operating points, the x and x_{ref} quantities are vectors consisting of values for the 24 frequencies spread over 0.1 Hz to 15 Hz for one operating point.

Table VI Goodness of fit metric comparing the expected and predicted admittances at the test points

OPERATING POINT	GFIT_DD	GFIT_DQ	GFIT_QD	GFIT_QQ
1	6.26E-05	1.01E-04	6.45E-04	3.67E-04
2	2.88E-04	2.19E-04	4.96E-04	1.22E-03
3	1.24E-03	4.88E-04	1.52E-04	2.70E-03
4	7.21E-04	4.10E-04	3.21E-03	4.28E-03
5	2.13E-04	1.40E-04	7.80E-04	3.40E-04
6	2.56E-03	1.42E-03	5.18E-04	4.12E-03
7	8.14E-04	1.91E-04	1.95E-04	8.78E-04

In each case, the vector fit process was able to identify a model, the open loop poles are plotted for the same two test points as Figure 19 in Figure 20. It can be observed that the poles fitted for the expected, and predicted models are very close for most of the poles.

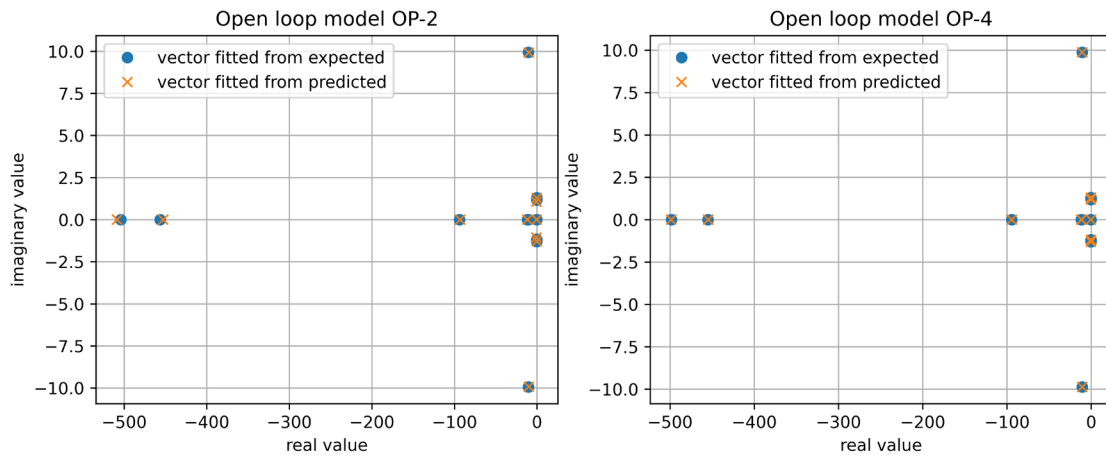


Figure 20 The open loop poles obtained for the fitted models based on the predicted and expected admittance at two test operating points, OP-2 and OP-4

To further test this model in a circuit, the admittance state space model formed using the vector fitted poles and zeros was interfaced with the state space model representing an infinite bus. Since the infinite bus model had an admittance form (where the dq domain voltages are inputs and dq domain currents are outputs), hence the IBR state space form in impedance form was desired in order to interface with it. Hence, IBR state space model in the admittance form was inverted to form a state space model in impedance form (where the dq domain currents are inputs

and dq domain voltages are outputs). For the same three test points as Figure 19 and Figure 20; Figure 21 shows the closed loop poles of the IBR interfaced with infinite bus. A SCR of 6.0 was used and an X/R ratio of 10.0 was used for the infinite bus for this figure. For each test IBR setpoint, there is one main chart that shows a zoomed-out view of the poles, as well as an inset chart showing a zoomed in view of the slower poles closer to the origin. It was again observed that the poles corresponding to the models based on expected and predicted admittances were close, and the overall closed loop system was stable (i.e. did not have any eigenvalues with positive real values), providing a sanity check.

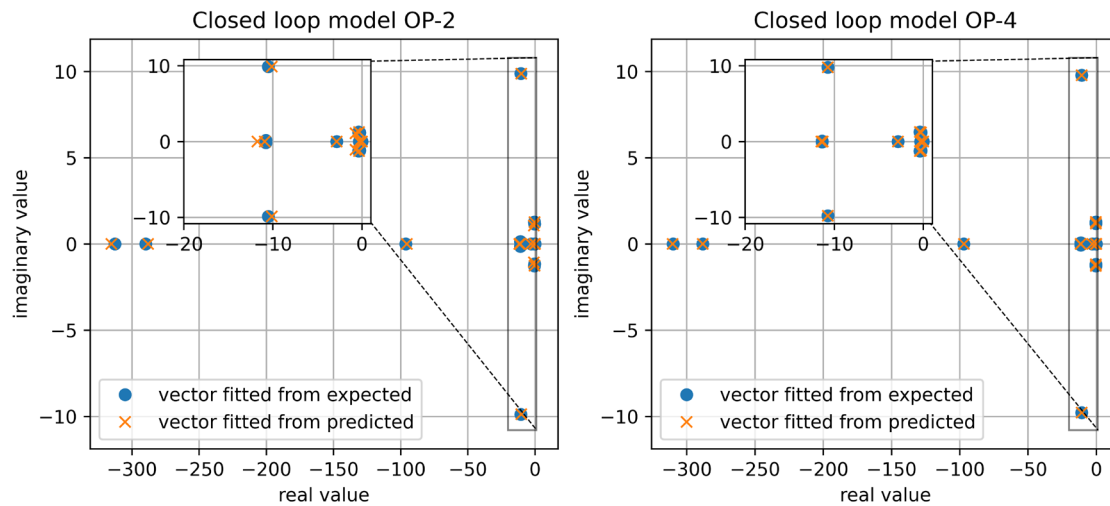


Figure 21 Closed loop poles when interfacing the fitted models based on expected and predicted models with an infinite bus model, OP-2 and OP-4

4.3 Validation against analytical models

As a next step, the frequency domain models of the positive sequence IBR based on admittance scans are compared with analytical models representing the inverter generator and electrical controls – since these are white box models it is possible to use the analytical equations of the models to represent them in small signal studies. The control structures used for the inverter generator and electrical controls are based on the standard models available for renewable generator and electrical control, which are currently available in most commercial positive sequence software packages. The generator controls may be indicated by “REGC_C” in the software (or some variant) while the electrical controls may be indicated by “REEC_C” in the software (or some variant). The control block diagrams for these would be available in software manual or model manual for these software, more details are also available in [20]. Figure 22 shows the comparison between the scanned admittances and the admittances based on the analytical small signal model for two of the 7 test operating points. A good match is observed, indicating that positive sequence domain admittance scans are successful in capturing the frequency domain admittances of these models. Other points also had a similarly good match. Note, there are some differences – for example – for OP-1 in the Figure 22, below 1 Hz there is some difference in the Y_{dq} term, however, the magnitude of this term in this frequency region is very small and these differences may not be very impactful. As a reminder, equation (1) describes the four terms in the 2x2 admittance.

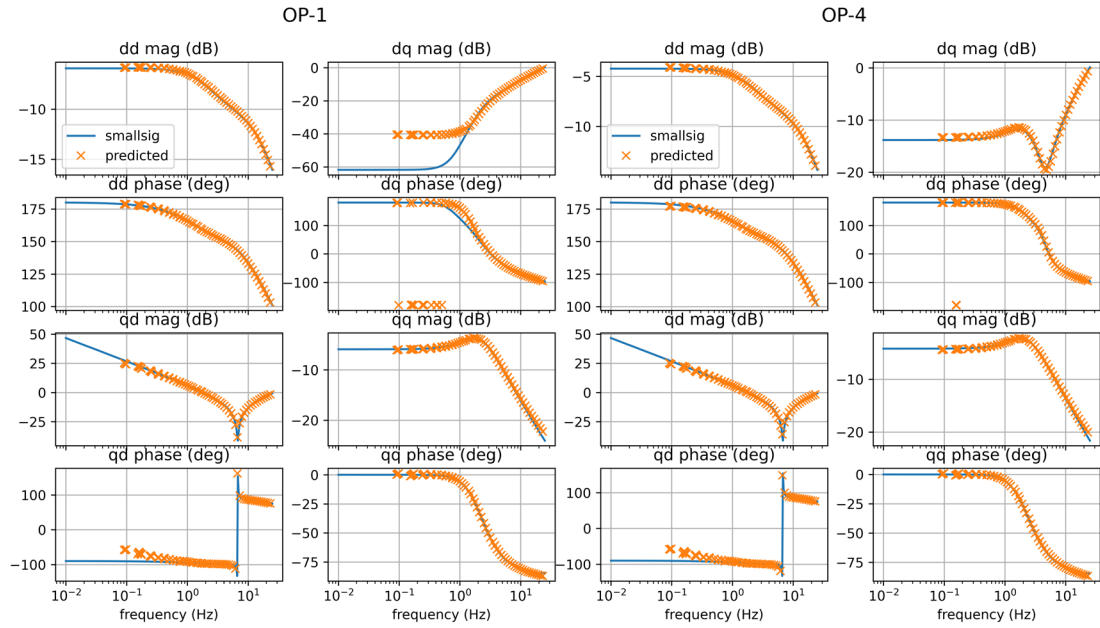


Figure 22 A comparison of the frequency domain admittance scans with the corresponding analytical small signal model admittances for two test operating points, OP-2 and OP-4

As a next step, frequency domain admittances are predicted for some of the operating points based on the operating points of IBRs from the synthetic NEM network. Here, the same operating conditions (power flow) as the model represented in Chapter 3 are used. After, vector fitting is applied to these predicted admittances to form small signal models to represent these IBRs. Figure 23 compares the predicted admittances from the vector fitted model, as well as the admittances predicted from analytical small signal model, to the expected admittances from the frequency scan, at this operating point. From comparing the predicted admittance values from the vector fitted model to the expected values from the frequency scan, it is apparent that the vector fitting process successfully represents the frequency domain admittances. Note, the difference between the analytical and scanned admittances for the Y_{dq} term in the lower frequency range that was observed for OP1 in Figure 22 is visible in this figure also. Further, by comparing across a larger frequency region than the frequencies used for fitting the model, it is observed that within the region with the frequency scans, the analytical and vector fitted models match well; however, outside these frequency regions (either at higher frequencies or lower frequencies) the model behaviour may differ. Now, the behaviour at frequencies higher than the frequencies included here in the scan and shown by 'x' in Figure 22, i.e. higher than 15 Hz may not be very important since positive sequence models may not be able to capture behaviour in this region successfully. More frequencies could be selected when performing the scans in the lower frequency region if this frequency region is considered critical (for example, due to historical oscillations observed in the field or in the time domain dynamic studies).

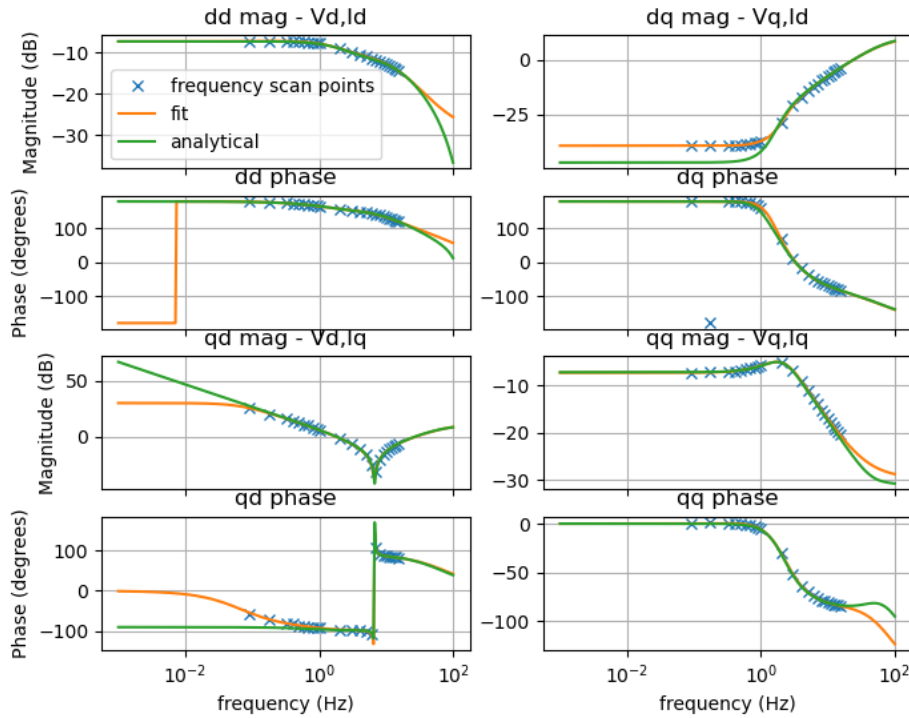


Figure 23 A comparison of the frequency domain admittance scans with the vector fitted model as well as the corresponding analytical small signal model admittances for a test point $V=0.95$ pu, $P=0.58$ pu, $Q=0$ pu

At this operating point, the open loop poles of the fitted model and the analytical small signal model are compared to each other in Figure 24, and the corresponding closed loop poles in a single machine infinite bus system ($SCR=3.0$ and $X/R=10.0$) are compared in Figure 25. It is observed that the poles observed in the analytical model that have a low (magnitude) negative real part are approximated in the vector fitted model, in both the open loop and closed loop models. There are a few poles that have large (magnitude) negative real parts, which have some more substantial differences between the two models in their imaginary parts, but these poles are very stable. There are also some (apparently) spurious poles added by the vector fit process that are close to the imaginary axis and that have a low imaginary value, but these do not seem to go unstable in the closed loop model.

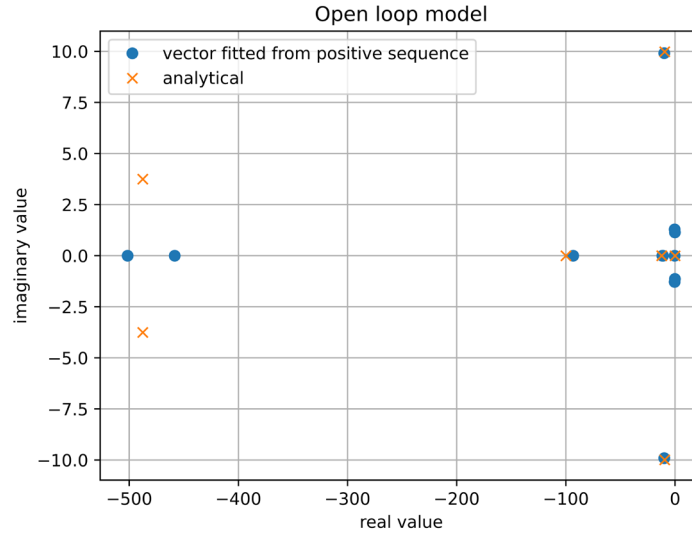


Figure 24 Open loop poles of the vector fitted model based on positive sequence IBR model and the corresponding analytical small signal model for a test point $V= 0.95$ pu, $P= 0.58$ pu, $Q= 0$ pu

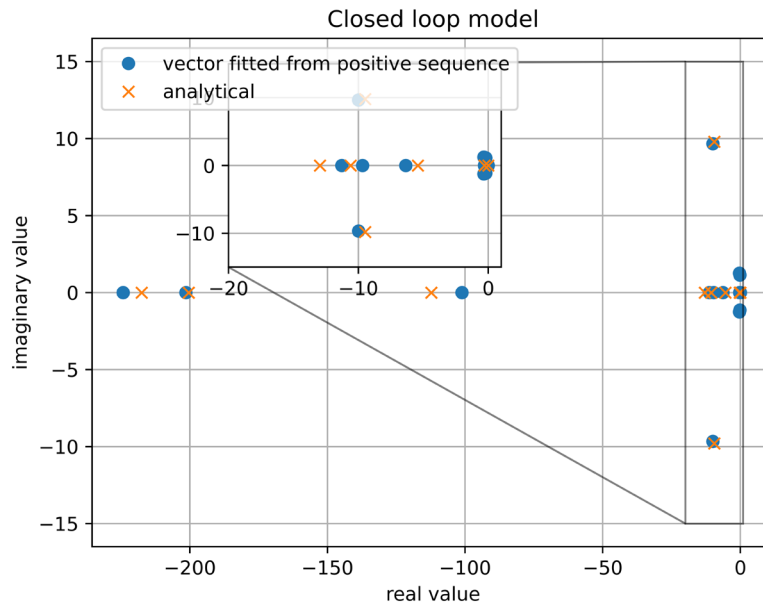


Figure 25 Closed loop poles in a single machine infinite bus system for the vector fitted model based on positive sequence IBR model and the corresponding analytical small signal model for a test point $V= 0.95$ pu, $P= 0.58$ pu, $Q= 0$ pu

Then, the procedure was repeated for 31 operating points from the synthetic NEM network at a single selected operating point for each, given in Table VII. These IBRs were selected from among the large (i.e. larger than 300 MVA) IBRs that are operating at active power more than 0.2 pu. The resultant vector fitted models were integrated into the small signal model of the network and compared with the small signal model using all analytical models.

Table VII Operating points from the synthetic NEM network where GFL IBR models are replaced by the fitted models

BUS NUMBER	BUS NAME		ID	TYPE	P MW	Q MVAR	V PU	MVABASE
6	BUS_1005	23.000	1	GFL	526.463	-5.5885	0.94839	915.05
18	BUS_1017	23.000	1	GFL	471.614	2.6859	0.95860	853.15
19	BUS_1018	23.000	1	GFL	553.485	3.0831	0.95805	828.59
20	BUS_1019	23.000	1	GFL	525.651	1.5669	0.95792	824.96
21	BUS_1020	23.000	1	GFL	550.676	1.7266	0.95672	815.54
34	BUS_1034	22.000	1	GFL	337.543	3.7196	0.92859	643.69
35	BUS_1036	22.000	1	GFL	339.813	3.9204	0.92734	645.29
36	BUS_1037	22.000	1	GFL	355.431	4.0095	0.92657	628.99
37	BUS_1038	15.400	1	GFL	205.304	2.6987	0.95957	343.07
38	BUS_1039	15.400	1	GFL	205.446	2.6684	0.96015	338.43
39	BUS_1040	15.400	1	GFL	207.055	2.7533	0.95921	341.42
40	BUS_1041	15.400	1	GFL	213.736	2.7655	0.95918	336.31
41	BUS_1042	15.400	1	GFL	204.470	2.7344	0.95939	333.51
42	BUS_1043	15.400	1	GFL	202.053	2.7290	0.95940	340.14
43	BUS_1044	23.000	1	GFL	534.340	-2.9764	0.99132	832.44
56	BUS_1058	21.000	1	GFL	341.628	-2.0584	0.94413	546.17
687	BUS_2043	24.000	1	GFL	289.126	-8.7523	0.99563	630.75
688	BUS_2044	21.000	1	GFL	454.669	-8.7690	0.99140	692.48
689	BUS_2045	21.000	1	GFL	438.952	-8.8174	0.99184	743.73
690	BUS_2046	20.000	1	GFL	426.573	-8.2485	0.96460	651.18
691	BUS_2047	20.000	1	GFL	441.467	-8.2148	0.96461	647.15
702	BUS_2063	20.000	1	GFL	216.485	-1.8642	0.94919	352.30
703	BUS_2064	20.000	1	GFL	206.563	-1.9920	0.95007	353.58
712	BUS_2073	24.000	1	GFL	394.479	-15.8130	0.91192	626.96
733	BUS_2095	20.000	1	GFL	320.252	-16.8768	0.96091	475.50
1558	BUS_3585	20.000	1	GFL	278.193	8.2864	0.99426	416.38
1559	BUS_3586	20.000	1	GFL	276.312	8.3814	0.99389	426.82
1560	BUS_3587	20.000	1	GFL	113.585	7.8577	0.99554	423.63
1561	BUS_3588	20.000	1	GFL	291.283	8.4146	0.99365	515.84
1628	BUS_3655	19.000	1	GFL	306.322	11.9022	0.96359	579.87
1629	BUS_3656	19.000	1	GFL	303.577	11.9422	0.96345	566.03

Two small signal representations of the synthetic NEM network are compared – in one case, all IBRs (233 – of varying sizes) are represented using analytical small signal models. In second case,

31 IBRs according to the Table VII are replaced by vector fitted models based on the frequency scans. In the second case, the remaining IBRs are still modelled using analytical small signal models. Figure 26 shows the comparison between these two alternatives, NEM scale, small signal models, and it is observed that most of the poles near the origin match between the two models, indicating that such models based on admittance scans of positive sequence models may be used in small signal stability assessment. As a further validation, Figure 27 shows the time domain response from these two small signal models (all-analytical models versus with vector fitted models based on the frequency scans from positive sequence IBR), and a good match in the trends is observed in the generator speeds for impulse response as well. The spurious poles do not seem to impact the single machine infinite bus (SMIB) as well as network-wide studies.

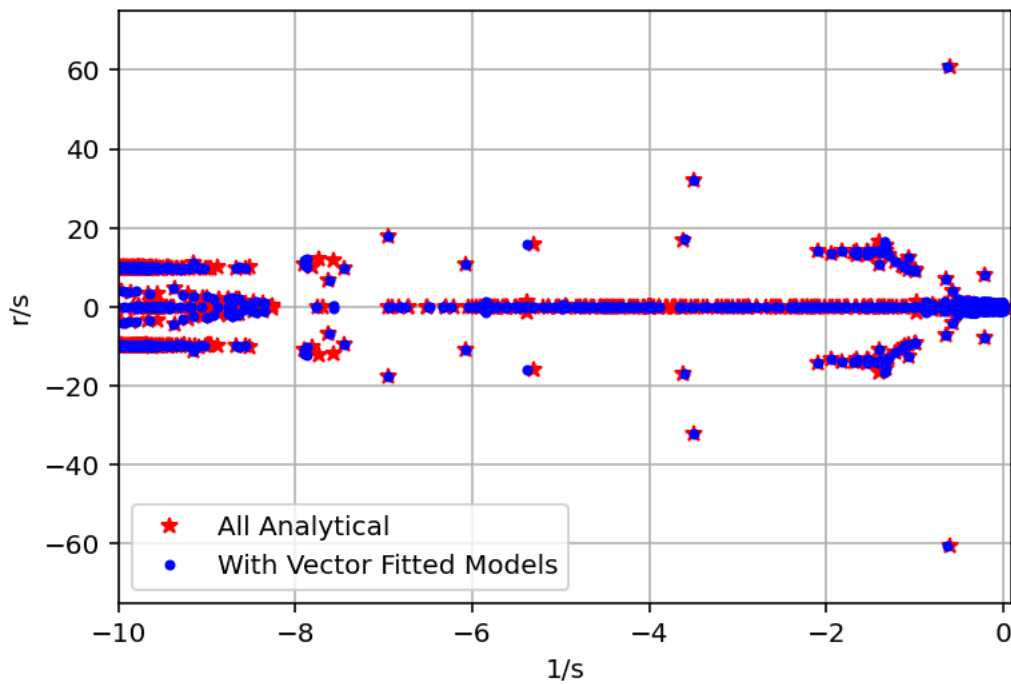


Figure 26 Comparison of the synthetic NEM network small signal models using analytical (red) or vector fitted (blue) models for 31 IBRs based on positive sequence IBR model (r/s represents radians per second)

As observed in the poles of the synthetic NEM system, incorporating generically tuned models, for all the analytical model and with the incorporation of their positive sequence vector fitted counterpart, the dominant dynamics are retained. The trend is also observable for the impulse response of both the small-signal systems, while perturbing the terminal of the generator on bus 3. Very small variation can be observed at the mode that occupies the 9.5 Hz range, with the vector-fitted models pushing it slightly in the left-hand plane. However, due to the location of the pole, the overall stability assessment is not affected. In particular, the vector fitters IBRs on buses 6, 18, 19, 20, 21, 34, 37, 38, 39, 40, 41, 42, 43 and 56 appear to participate (with various states) in this mode. In addition, the underdamped electromechanical mode, at the approximately 8 rad/s (1.27 Hz) also presents participation from IBRs on buses 688, 689, 690 and 691.

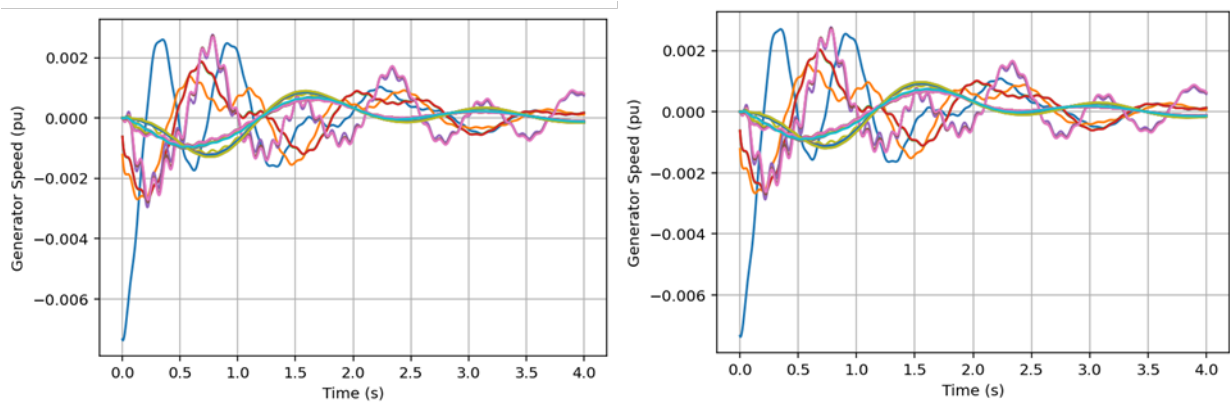


Figure 27 Comparison of the impulse response of the small signal model with all analytical models (left) and with fitted models for 31 IBRs

4.4 Comparing EMT and RMS models

While the previous sections in this chapter discuss the learnings from the efforts to incorporate and test small signal state space models based on positive sequence IBR models into network small signal analysis, this section describes efforts to compare frequency domain characterization from similar IBR models in EMT and RMS domains explicitly. For this purpose, the following models were selected:

- EMT domain: The IBR model utilized as a part of previous stage of the research (and described in [4]) was used as the EMT model. This EMT model represents a simple control, and it was used in the grid following mode for this comparison. In this chapter, this model is referred to by “Test model B_EMT” in this report.
- RMS domain: Generic renewable generator (REGC) and electric control (REEC) models were used to represent positive sequence grid following IBR. Specifically, REGC_C model from [21] was utilized as the generator model – in newer version of software (Siemens PTI PSS/E v34 was used here) this model is available as a standard library model. The electrical controls were represented using REEC_C model that was available as a standard library model. This model (combined representation of generic renewable generator and electrical controls for positive sequence IBR) is referred by “Test model B_PSeq” in this report.

The parameter values for these models are given in Appendix A.2. Note, these two models “Test model B_EMT” and “Test model B_PSeq” are not identical – due to the differences in EMT and positive sequence domains, the interfaces between the model and the rest of the network are significantly different between the two models. Further, the electrical controls also have differences, including different options available in the models to be selected using appropriate flags. However, they are intended to represent the same device keeping these limitations in mind. Such situation may arise when trying to approximately represent the response of a device in the positive sequence studies. Hence, a process of tuning the models to be as similar as possible was necessary. Step voltage response and step frequency response were used for this comparison to establish models exhibiting a similar behaviour. Then, frequency domain admittance scans were

performed on both Test model B_EMT and Test model B_PSeq to assess the similarities and differences between the admittance scans. Further, the vector fitting procedure was applied to these scanned admittances for both models. For the fitted small signal models based in Test model B_EMT and Test model B_PSeq, the open loop poles as well as the closed loop poles in a single machine infinite bus setup were compared to assess the similarities and differences in small signal behaviours. The model parameters used for these tests for both Test model B_EMT and Test model B_PSeq are given in Appendix A.

Figure 28 and Figure 29 show the voltage step and frequency step responses of the two models for the same operating point ($V = 1.0175$ pu, $P = 27.1$ MW and $Q = 6.775$ MVar, for a 67.75 MVA IBR). The disturbances applied were a drop in source voltage of 0.05 pu, and a drop in source frequency of 0.5 Hz. Both disturbances were applied at the infinite bus source and these tests were conducted at SCR=10.0 and X/R=15.0. It is observed that the overall behaviour of the two models, especially in the slower regions (lower frequencies) matches well, with similar active and reactive powers, voltage and current magnitudes in response to the disturbances. Despite the tuning/matching efforts, some differences in the models remain, especially in terms of the faster time scale (higher frequency) dynamics. However, given the differences in model structures and simulation domains a perfect match may not be expected.

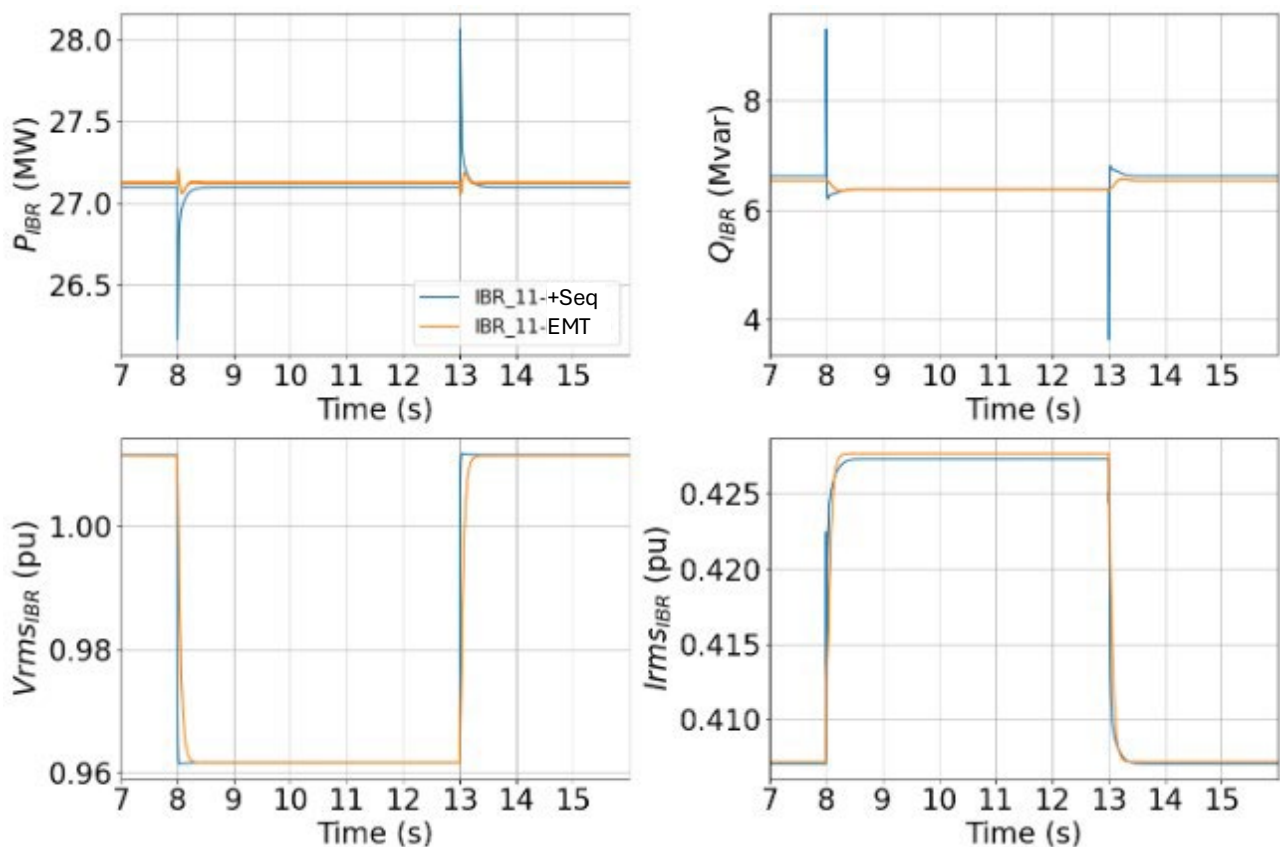


Figure 28 Frequency step response of Test model B_EMT and Test model B_PSeq

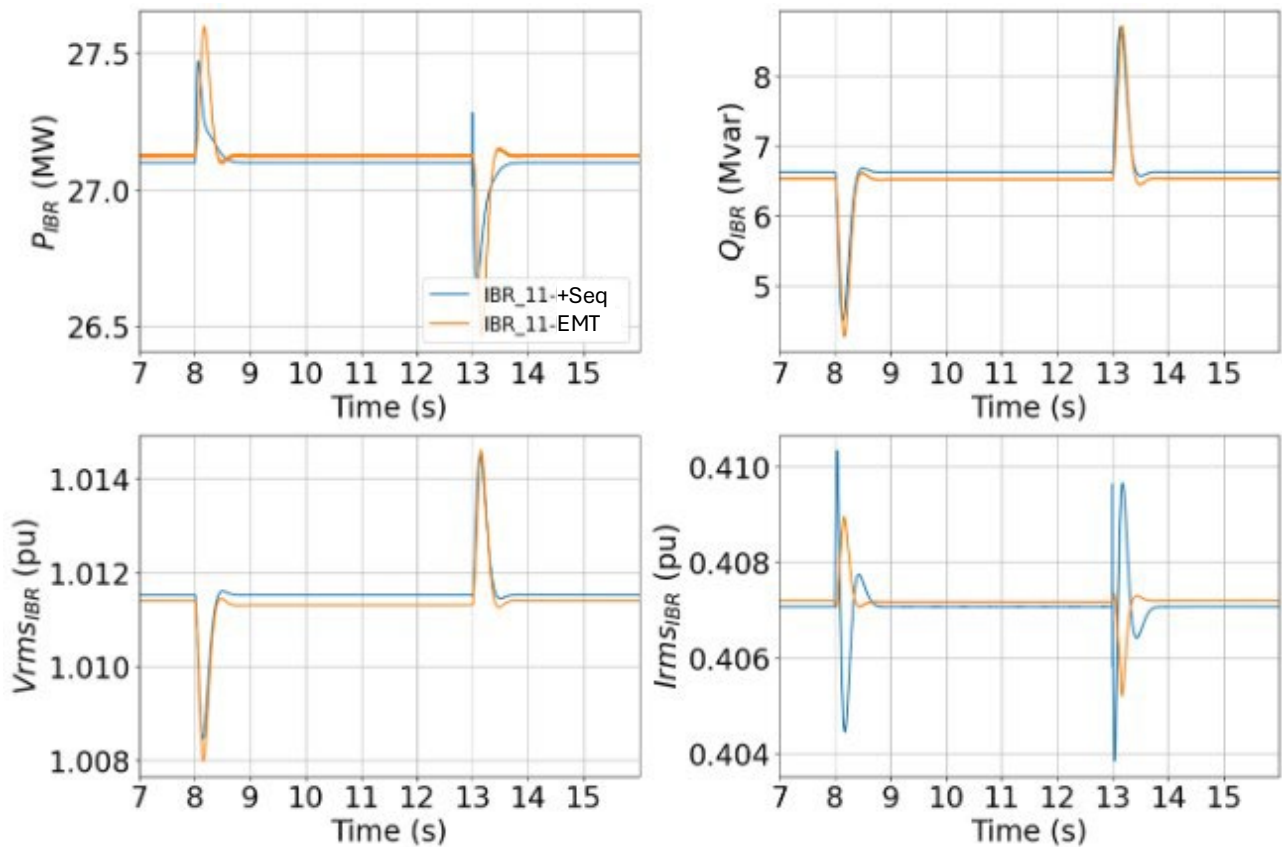


Figure 29 Voltage step response of Test model B_EMT and Test model B_PSeq

Having established the parameters for both Test model B_EMT and Test model B_PSeq, small signal admittance scans are performed for both the models at this operating point. Figure 30 shows the comparison of the scanned admittances. The same set of frequencies is used to scan both models. It is observed that the self terms (Y_{xx} and Y_{yy}) match well in the lower frequency regions, with some mismatches above ~ 5 Hz. While the cross terms have more differences – with some similarities in the behaviour up to ~ 1 Hz. Note, however, the cross terms are much smaller than the self terms. These differences may be due to the difference in model structure including generator interface, measurements and the different representations of filter used as well as the control structures of both models not being exactly the same. Here, in the time domain, the Test model B_PSeq was found to approximate the behaviour exhibited by Test model B_EMT in both the voltage and frequency step tests – yet large differences were observed in the frequency domain comparison, highlighting the desirability of utilizing multiple types of tests when comparing the behaviour of two different models.

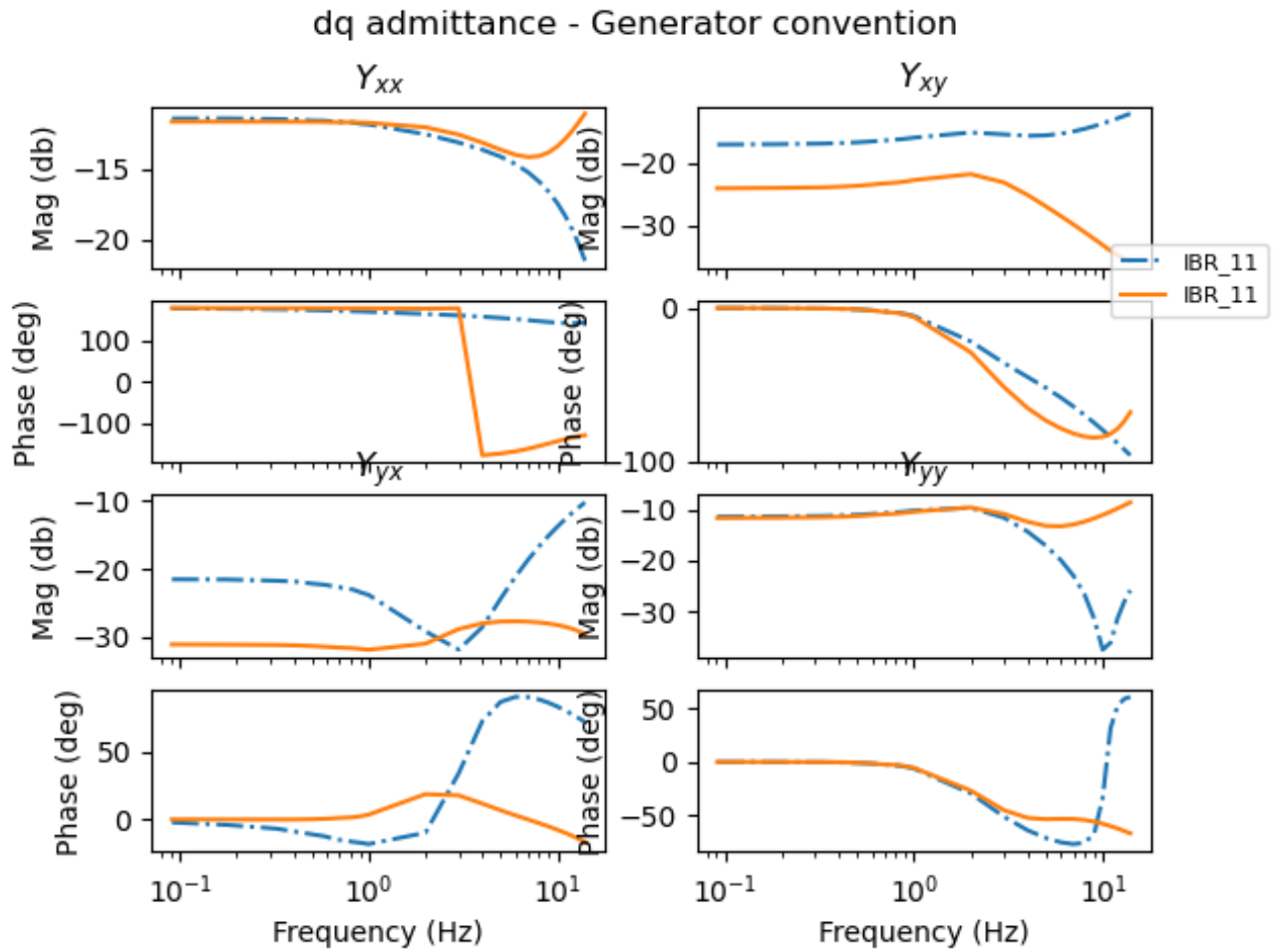


Figure 30 Comparing frequency domain admittances - Test model B_EMT (orange) and Test model B_PSeq (blue)

Despite these differences, the vector fitting method was applied to both these Test models. The intention here is to check the similarities and differences between the fitted models and find whether the differences observed in the frequency domain lead to significantly different fitted models or whether, despite the differences, are there commonalities between them. Vector fitting is successful for both the models, and the frequency scans from Figure 30 are compared with the fitted model for Test model B_EMT in Figure 31 and for Test model B_PSeq in Figure 32.

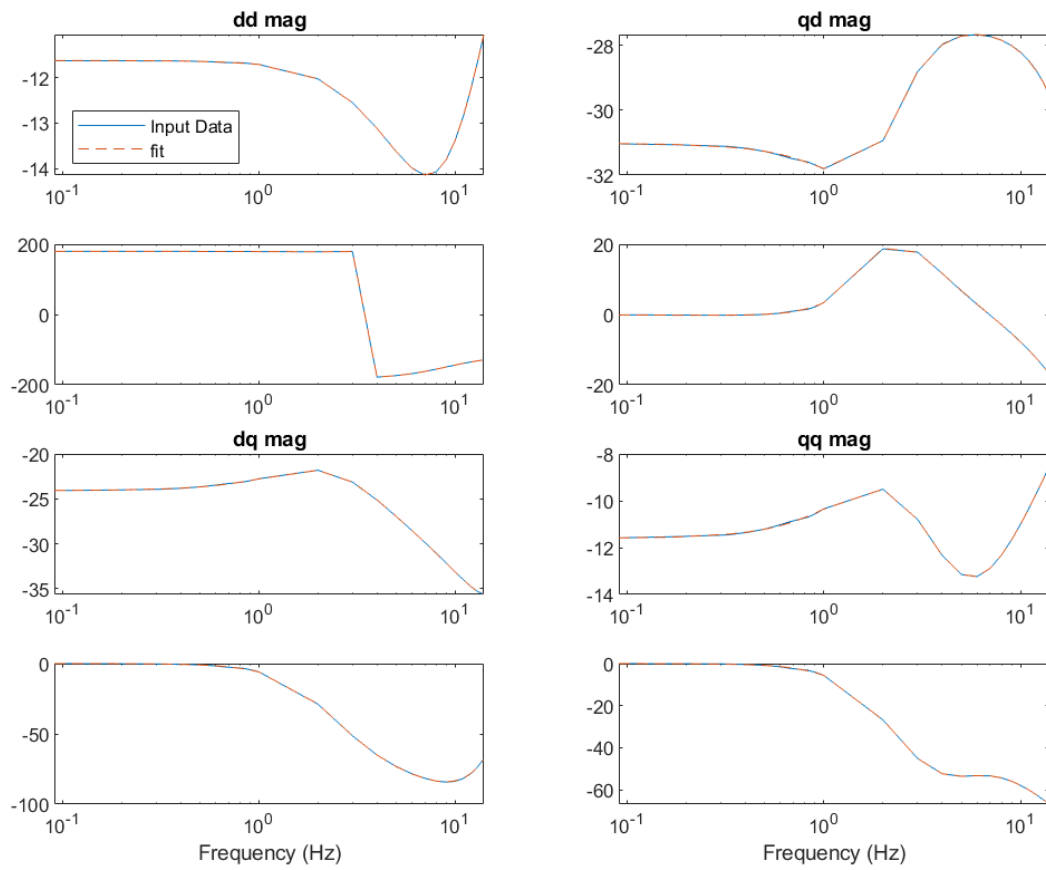


Figure 31 Frequency domain admittance scans and the vector fitted model for Test model B_EMT – close match of the curves resulting in overlap at many frequencies shows a successful fit

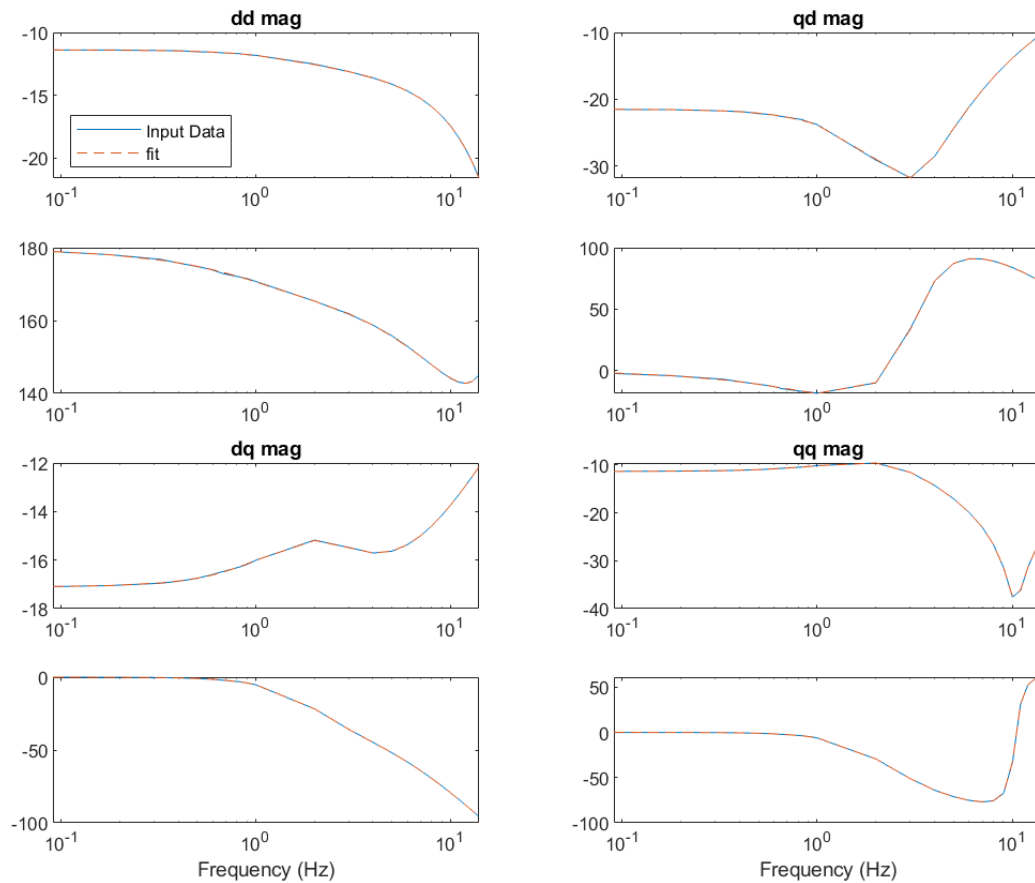


Figure 32 Frequency domain admittance scans and the vector fitted model for Test model B_PSeq – close match of the curves resulting in overlap at many frequencies shows a successful fit

Finally, the open loop poles of both the fitted models are compared in Figure 33. It is observed that some of the poles are similar between the two models, though there are differences as well. Some of the differences are in terms of poles with large (magnitude) negative real values – these are stable poles, and dynamics corresponding to these poles are expected to damp out relatively fast. There are a couple of additional open loop poles for the Test model B_EMT that have imaginary values close to 300 rad/s. These are not relevant for the positive sequence analysis, since the positive sequence domain modelling is at rms time scales and usually considered appropriate only up to ~ 10 Hz around the nominal frequency (which corresponds to ~ 63 r/s). For poles closer to the imaginary axis, the similarities and differences may be more critical from a standpoint of the lower frequency region and eigenvalues that may potentially become unstable (have positive real values) under certain network conditions/circumstances. In this region, some of the eigenvalues do match between the Test model B_EMT and Test model B_PSeq. However, there are additional poles for the model fitted based on the frequency response of Test model B_PSeq that are not present in the Test Model B_EMT.

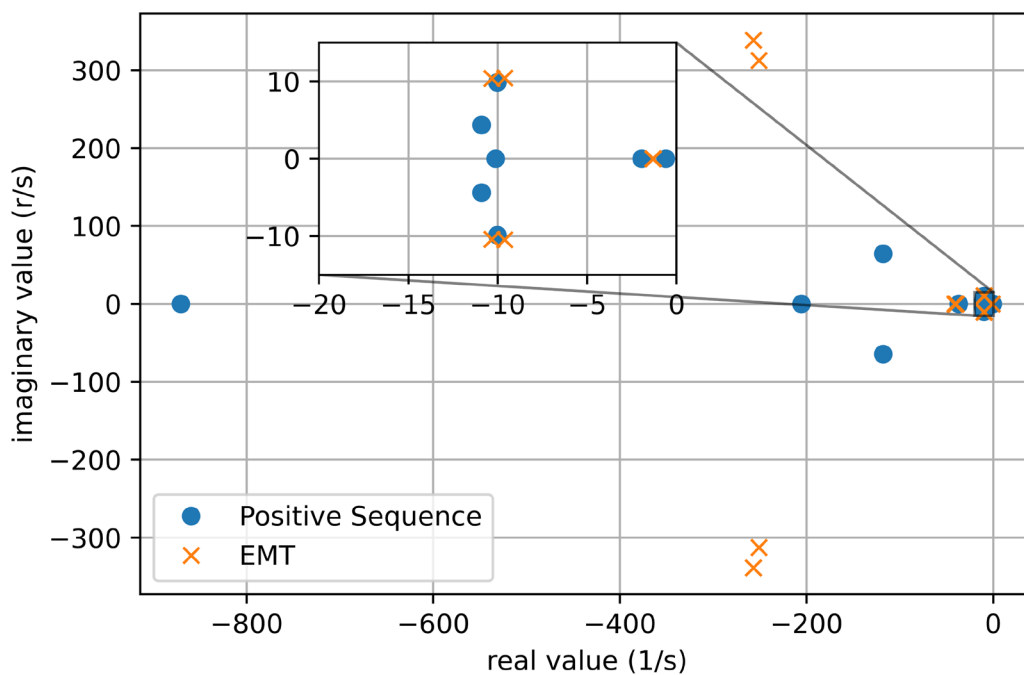


Figure 33 Comparing open loop poles of the models fitted based on frequency responses of Test model B_EMT and Test model B_PSeq (r/s represents radians per second)

To further compare the two fitted models, they are interfaced with an analytical small signal model representing an infinite source. Note, in positive sequence this impedance is represented using algebraic equations, while the EMT representation of the infinite source includes modelling the network dynamics corresponding to this impedance. This comparison is performed at multiple network conditions – and plotted for SCR=6.0 and X/R=10.0 in Figure 34 and for another much weaker grid corresponding to SCR=1.5 and X/R=10.0 in Figure 35. The observations are similar to the open loop model here. In lower frequency region closer to the imaginary axis (or, the region close to the origin), some poles are represented for both positive sequence and EMT models, and there are a few additional poles for the fitted positive sequence model that do not appear in the fitted EMT model. However, even when the network SCR is varied in the closed loop configuration, the closed loop poles corresponding to the additional open loop poles in the positive sequence model do not seem to move a lot. The poles for the fitted model for the EMT domain Test model B_EMT with high imaginary values do move closer to the imaginary axis as the network becomes weaker, but such high frequency dynamics are not expected to be represented by the positive sequence models.

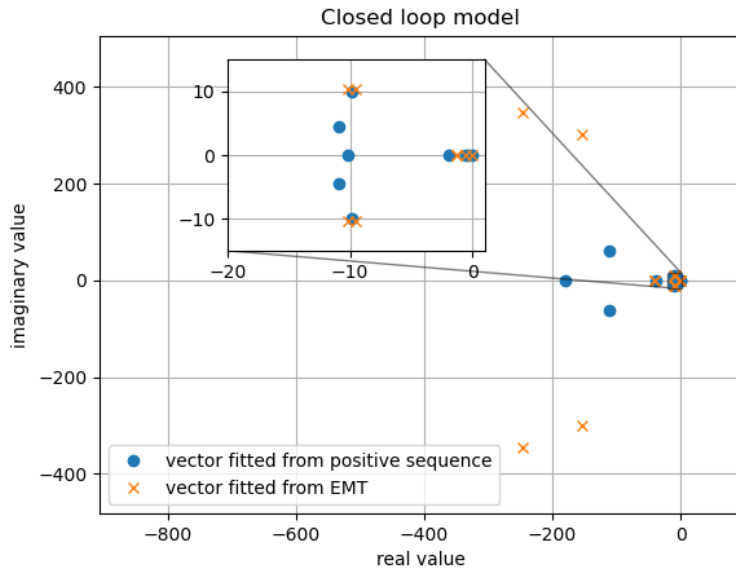


Figure 34 Comparison of the poles for the closed loop model in a single machine infinite bus system for vector fitted models based on Test model B_EMT and Test model B_PSeq. This plot corresponds to network conditions of SCR=6.0 and X/R=10.0

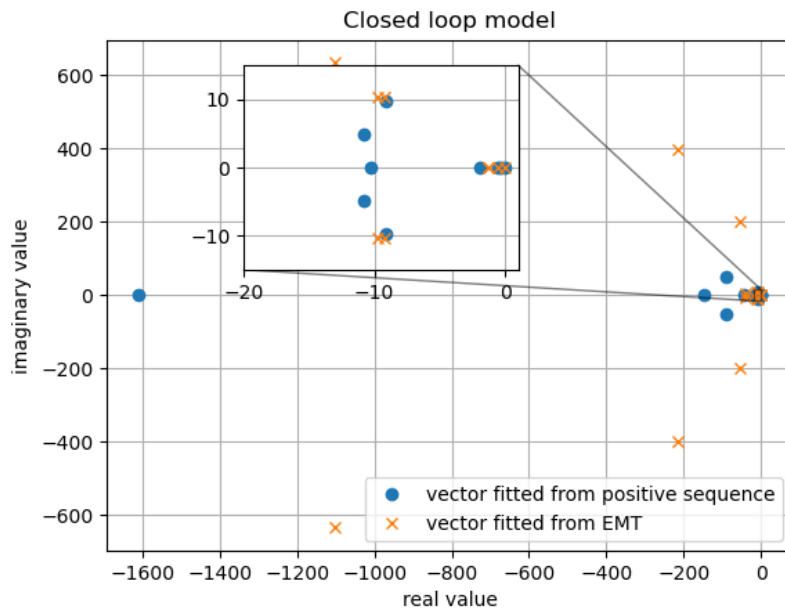


Figure 35 Comparison of the poles for the closed loop model in a single machine infinite bus system for vector fitted models based on Test model B_EMT and Test model B_PSeq. This plot corresponds to network conditions of SCR=1.5 and X/R=10.0

This overall exercise of comparing positive sequence and EMT models and trying to incorporate admittance-scan based models based on positive sequence models led to the following key observations:

- Frequency domain admittance scans may be performed on positive sequence models and these can successfully approximate the small signal behaviour of these positive sequence models.
- Even when a positive sequence model can be considered to approximate the time domain response of an EMT model in the form of voltage and frequency step tests, the frequency domain characteristics of these models may reveal additional differences in these models. However, despite these differences, some aspects of small signal stability behaviour of these models may still be captured.

Part III Services from IBRs and small signal stability

5 Impact of obtaining services from IBRs on small signal stability

IBRs can be used to obtain various grid services such as reactive power/voltage support, active power/frequency support and fault current. One aspect in being able to obtain these services from IBRs includes having physical hardware capability in terms of factors such as device MVA ratings or energy storage, or operational capacity such as power headroom. However, even with appropriate hardware capabilities, obtaining these services from IBRs involves selecting appropriate control configuration and parameters. The aim in this task is to assess the IBR small signal models, for a few of these services, in order to determine whether there are trade-offs and synergies in terms of improvements or deterioration of small signal stability characteristics when IBR controls provide/do not provide these services. Three modes of IBR controller operation are considered all three IBR modes considered here are represented only in the positive sequence domain, as they are tested in a positive sequence small signal model of the synthetic NEM system used previously in Chapter 3. These models use small signal models based on standard inverter generator (REGC_C), electrical (REEC_C) and higher level controls such as plant controls (REPC_A) models. These models are available in standard libraries in most positive sequence domain software, and more details can also be found in [20].

For this task, three IBR controller modes were selected:

- IBR_ConstPQ – this parameterization aims to control the active and reactive power of the IBR to preset values (obtained from the power flow, in case of positive sequence models). Hence, this IBR mode does not provide any frequency or voltage support. This IBR mode uses REGC_C and REEC_C models together to represent the IBR.
- IBR_slow_resp – this parameterization includes REGC_C, REEC_C and REPC_C models used together to represent the IBR, and includes slower plant level frequency and voltage support. The plant model REPC_C contains the control loops that change the active and reactive power references when subjected to frequency and voltage magnitude disturbances, whereas the electrical controls follow those references.
- IBR_fast_resp – this parameterization includes REGC_C, REEC_C and REPC_A models, and includes faster frequency and voltage response, that is achieved (for the most part) within the first second of operation. Here, the voltage control objective is also modelled in the electrical control (REEC_C), and while the electrical control REEC_C model does not have provision for frequency control directly, the frequency control in the REPC_A model is made faster to simulate an IBR that may be providing a unit-level faster voltage and frequency support.

In order to illustrate the difference/s between these three IBR control modes, the voltage step response of these three modes operating at the same operating point is plotted in Figure 36, and the frequency step response is plotted in Figure 37. For the voltage step, a dip of 0.05 pu is applied, while for the frequency step, a dip of 0.5 Hz is applied. Note, in terms of voltage support, IBR_slow_resp and IBR_fast_resp modes are closer (IBR_fast_resp provides most of the change in

reactive power within the first second of operation, while in IBR_slow_resp most of the change is achieved in 2 seconds of operation. In terms of frequency support, these are much farther spaced – for IBR_fast_resp most of the change is still achieved in the first second of operation, while the IBR_slow_resp control is much slower. Note, both for the voltage and frequency support, for the IBR_slow_resp and IBR_fast_resp modes, the droop parameters are the same so that the final reactive/active power levels after the disturbances are applied are also the same. For IBR_ConstPQ mode, since it tries to follow the active and reactive power setpoints, the final active and reactive power does not change compared to the initial value.

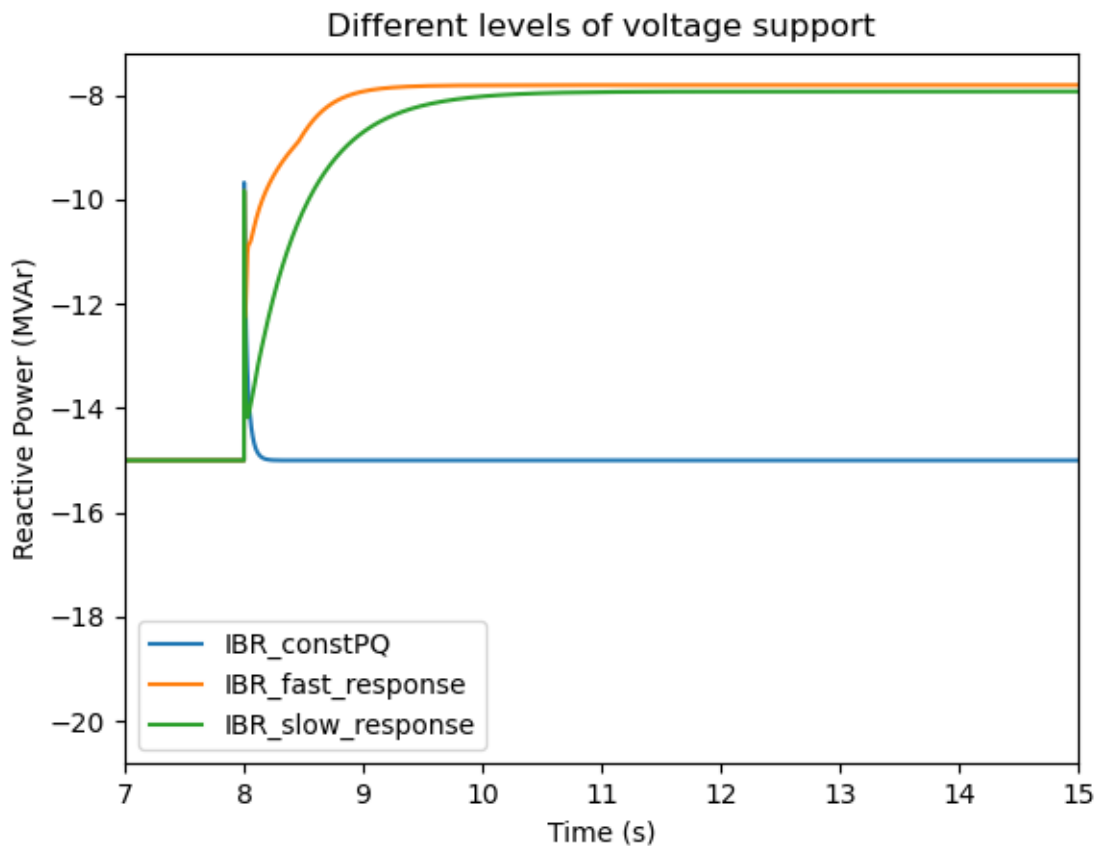


Figure 36 Comparison of the voltage step response for the three IBR modes, a voltage dip of 0.05 pu applied at 8s

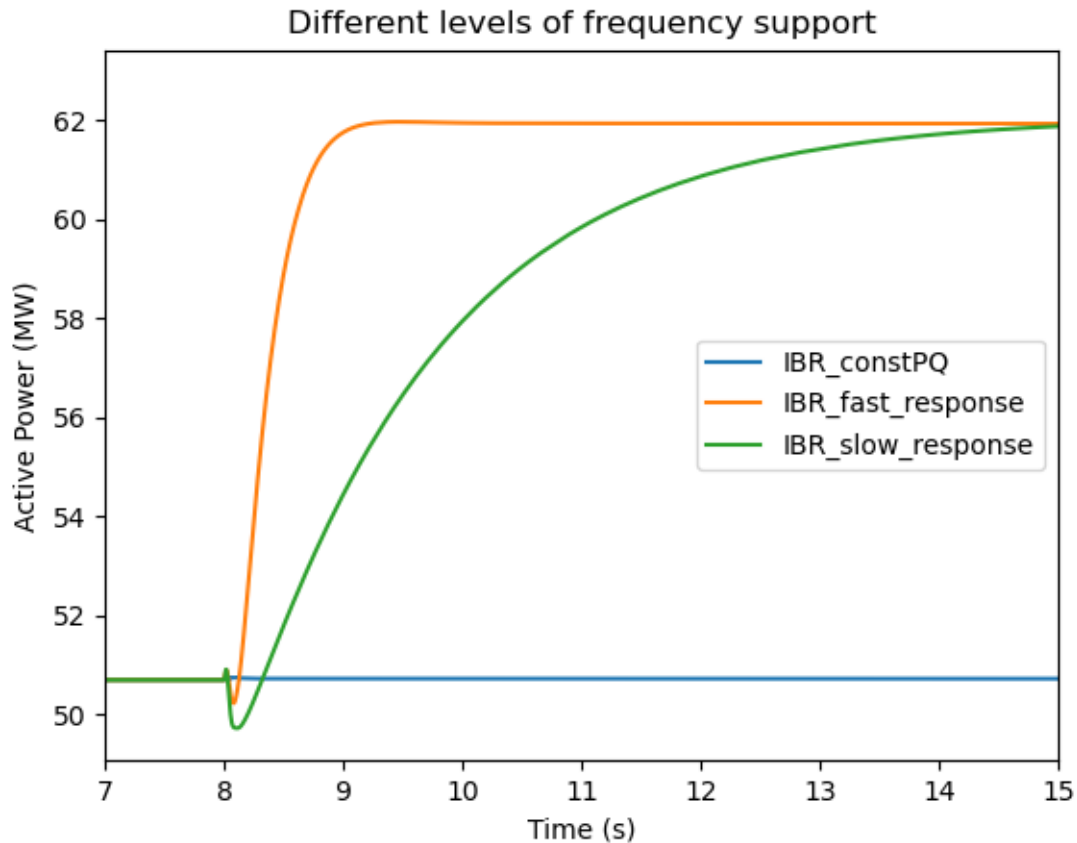


Figure 37 Comparison of the frequency step response for the three IBR modes, a frequency dip of 0.5 Hz is applied at 8s.

Now, the frequency domain admittances of these IBR modes are compared for three operating points – these were selected to be across different reactive power and voltage ranges. Operating point 1 corresponds to $V=0.97$ pu, $P=47.33$ MW, $Q=-0.08$ MVar ; operating point 2 corresponds to $V=1.02$ pu, $P=50.7$ MW, $Q=10.0$ MVar ; and operating point 3 corresponds to $V=1.035$ pu, $P=50.7$ MW, $Q=-15.0$ MVar (for 67.75 MVA IBR). These comparisons are plotted in Figure 38, Figure 39 and Figure 40. Across the three figures, it is observed that there are differences between the frequency domain admittances of the three IBR modes. In these plots, IBR_PQ is more different from each of IBR_fast and IBR_slow than the differences between IBR_fast and IBR_slow.. For the IBR_fast_resp and IBR_slow_resp modes, the differences between them are larger at higher frequencies, greater than ~ 1 Hz, than at lower frequencies where the admittances match better (that is, in the slower time scales). Between these two IBR modes, larger differences in the faster dynamics are also observed in the step response plots earlier. Note, admittances are not directly related to active power/frequency and reactive power/voltage dynamic response. By “not directly related” here it means without algebraic manipulation. Although it is true that all these responses are related in the sense that they can be derived from the current and voltage measurements at the IBR terminal, the equations used to compute admittance are different from those used to compute active/reactive power, and the input/output signals for these relationships are also different. In the future, other transfer functions such as those for frequency/active power or voltage magnitude/reactive power could be explored, in order to better understand how the properties of IBRs vary when designed to provide various frequency and voltage support functions.

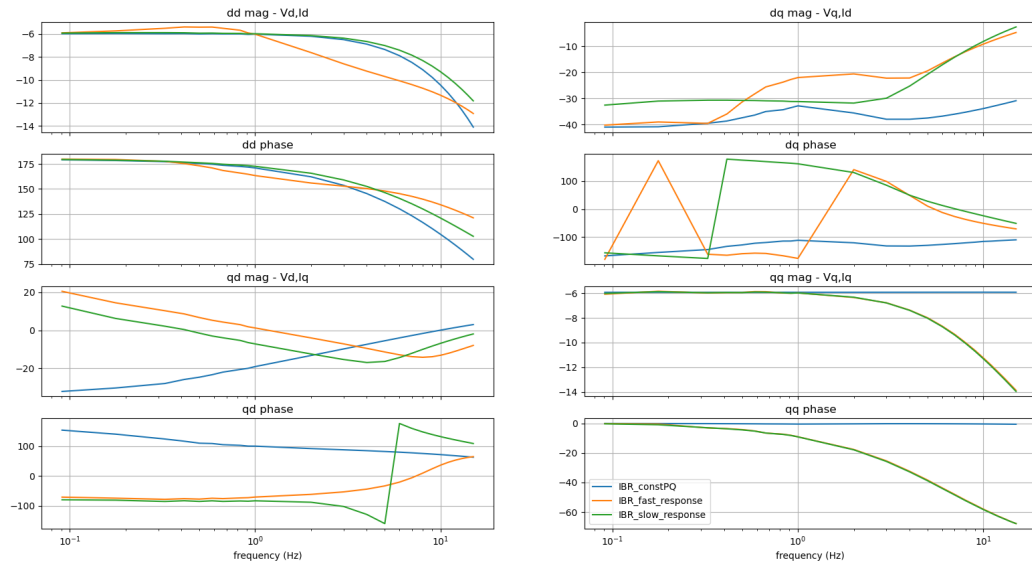


Figure 38 Comparison of the frequency domain admittances of the three IBR modes for the first operating point - $V=0.97$ pu, $P=47.33$ MW, $Q=-0.08$ MVar

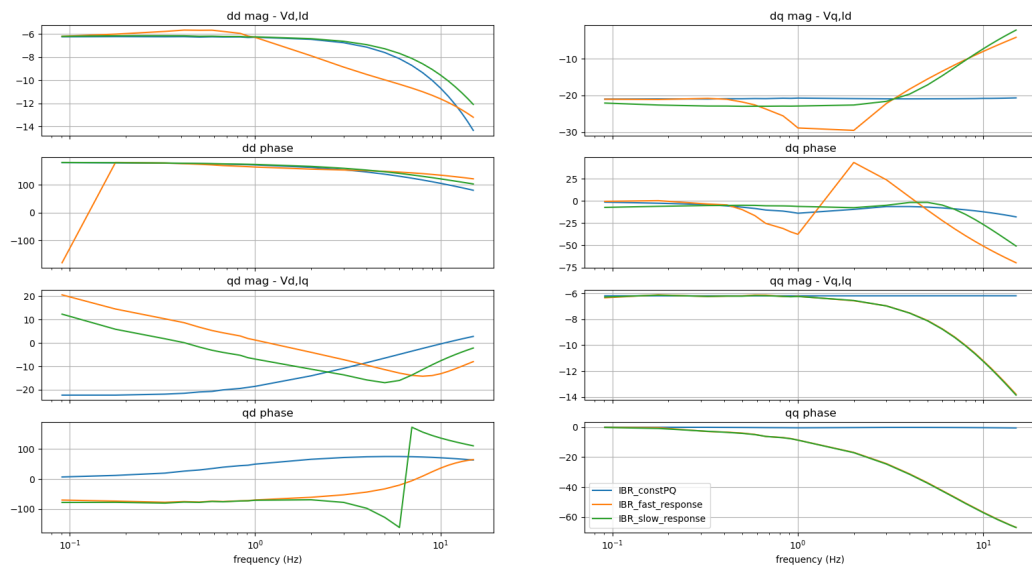


Figure 39 Comparison of the frequency domain admittances of the three IBR modes for the second operating point - $V=1.02$ pu, $P=50.7$ MW, $Q=10.0$ MVar

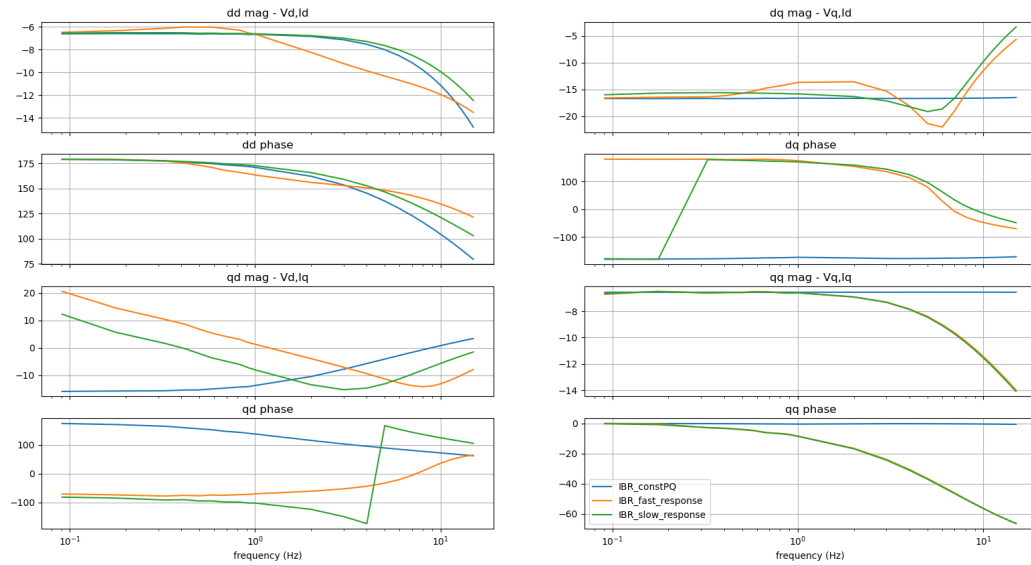


Figure 40 Comparison of the frequency domain admittances of the three IBR modes for the third operating point - $V=1.035$ pu, $P=50.7$ MW, $Q=-15.0$ MVar

Finally, the impact of these three alternative IBR controller modes on small signal stability is tested using the synthetic NEM model described earlier in Chapter 3. Here, all the GFL IBRs in the small signal model of the synthetic NEM network are replaced with the small signal model corresponding to one of the three IBR control modes – IBR_ConstPQ, IBR_slow_resp, and IBR_fast_resp. The eigenvalues of the system for each of these three cases are plotted in Figure 41, Figure 42 and Figure 43. It is observed that there are a few eigenvalues with positive real values with the IBR_ConstPQ and IBR_slow_resp modes, while the small signal model is stable for the IBR_fast_resp case. These differences showcase the impact that varying levels of service provisions from IBRs can have on small signal stability characteristics, and establish the need for studying these aspects more in the future. Note, the small signal formulations used for the synthetic NEM model do not include the impact of deadbands and assume that the oscillations induced are larger than the deadband thresholds. Assessing the impact of deadbands (and other non-linear control elements such as current limits) on small signal stability may be a future effort.

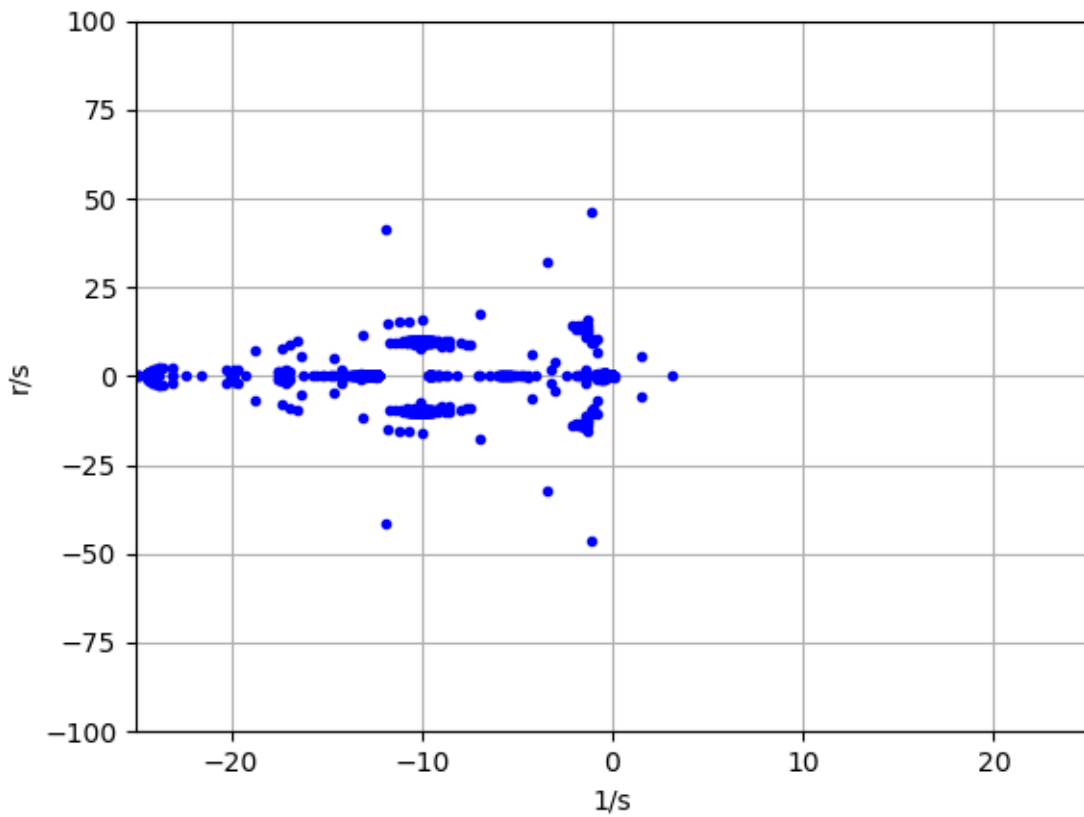


Figure 41 Poles of the synthetic NEM network small signal model where the GFL IBRs use the parameterization of IBR_ConstPQ mode (r/s represents radians per second)

For this figure, the unstable eigenvalues include interactions between synchronous machine and IBR PLL parameters based on the participation factors for these poles from the small signal analysis leading to oscillations with a frequency of ~ 0.87 Hz (imaginary value ~ 5.47), another mode with a much smaller oscillation between some of the GFM phase angles (frequency ~ 0.05 Hz – this eigenvalue is much closer to the origin, with real value of 0.138), as well as a non-oscillatory mode, again involving the angles of the synchronous generators and IBRs in the network. Further, the power system stabilizer models are also not represented. Including the power system stabilizer models may have a beneficial damping effect (that is greater damping) on some of the modes involving synchronous generators.

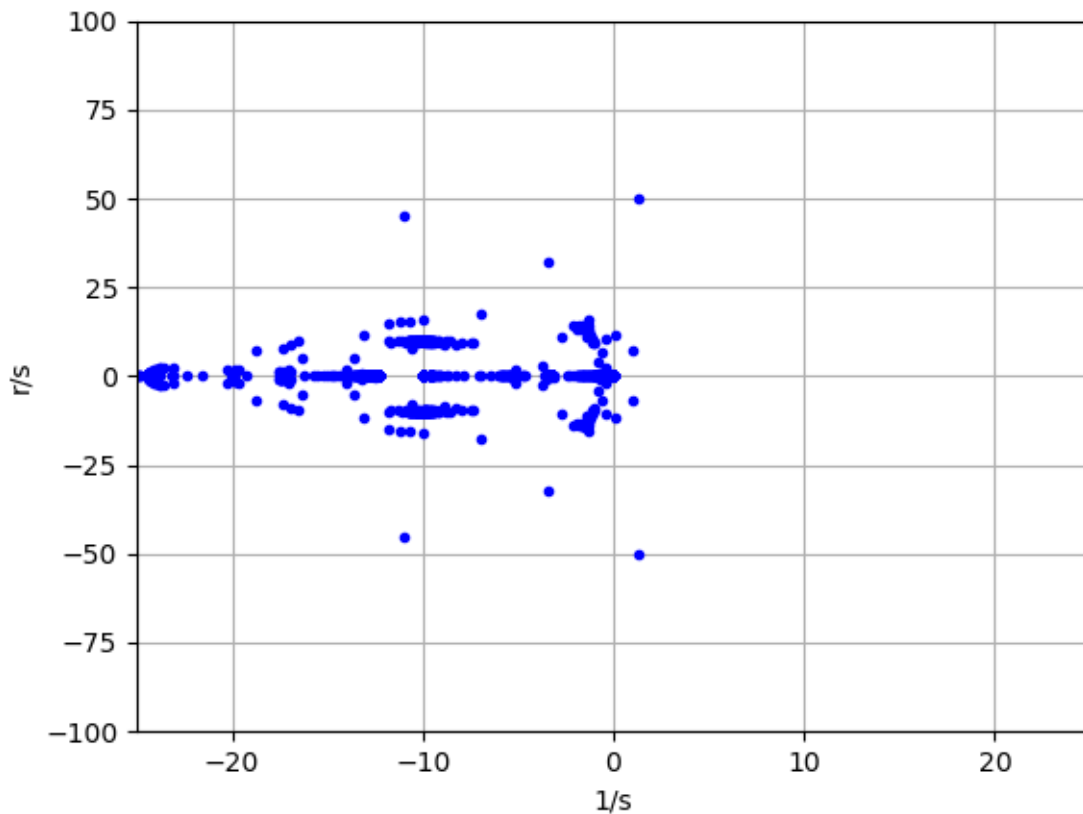


Figure 42 Poles of the synthetic NEM network small signal model where the GFL IBRs use the parameterization of IBR_slow_resp mode (r/s represents radians per second)

This model exhibits a ~7.95 Hz unstable mode (imaginary value ~50) that involves primarily the states from IBR generator model (including current controls) and some of the IBR angles (both from the REGC_C model), a 1.84 Hz unstable mode (imaginary value ~11.58) with some synchronous generators that are close-by oscillating against each other, and a ~1.12 Hz oscillation (imaginary value ~7) with participation from synchronous generators speeds and phase angles, and IBR phase angles and frequencies. There are also some non-oscillatory unstable modes that have very small positive eigenvalues (less than 0.05) that could be a result of minor initialization errors for some of the IBR models. For small signal stability model of such a large system, small initialization errors may sometimes be present and require increased efforts to remove. Note, the power system stabilizer models are also not represented. Including the power system stabilizer models may have a beneficial damping effect on some of the modes involving synchronous generators.

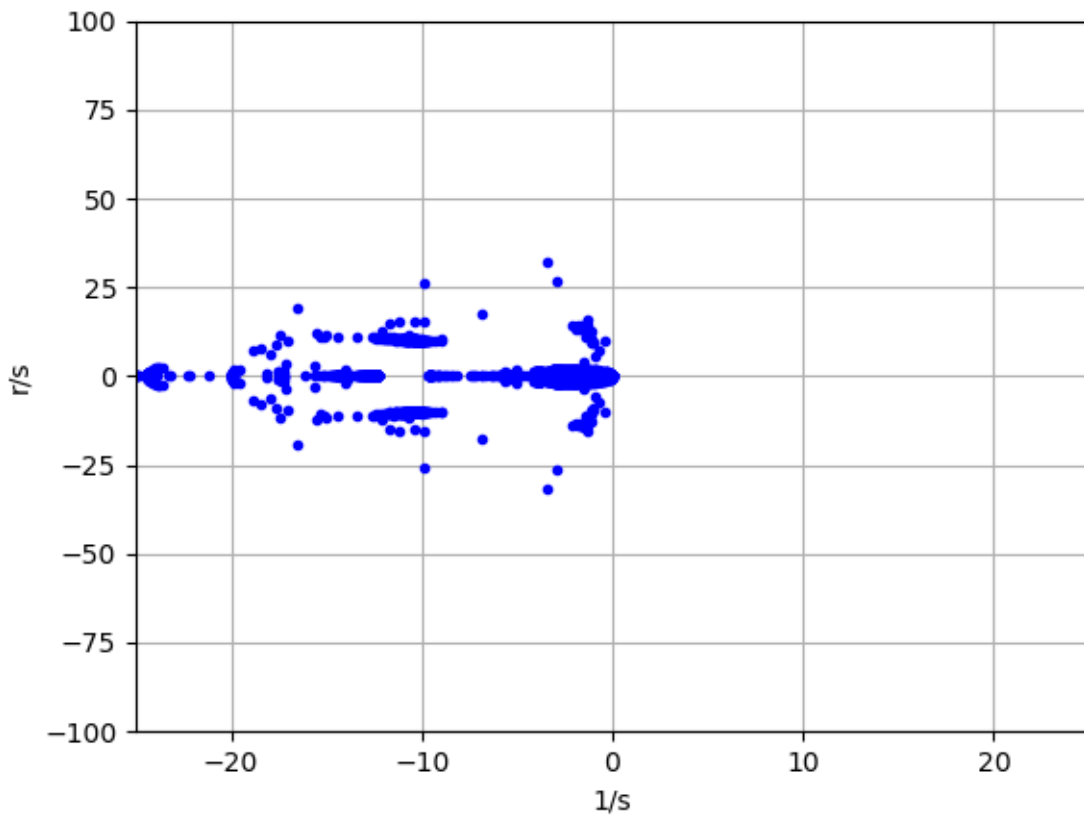


Figure 43 Poles of the synthetic NEM network small signal model where the GFL IBRs use the parameterization of IBR_fast_resp model (r/s represents radians per second)

In this model, all the eigenvalues have negative real values (are stable).

Part IV Conclusions and future work

6 Conclusion and future work

Few of the key learnings from the different efforts in this project are as follows:

- Admittance prediction of OEM models has been successfully completed for most operating points tested, with APM followed by state-space identification methods, and vector fitting methods, being utilized for different models.
- Some difficulties were observed for the prediction of OEM GFL model 2, where discrepancies were observed for some operating points. These discrepancies manifested in the low and (for some cases) the mid frequency range.
- The operating point dependence of IBR frequency domain admittance characteristics is well-established in the existing and previous stages of research. However, the investigation conducted in this stage of the project demonstrated that there can also be a qualitative change in the observed admittance characteristics in certain regions among the operating set points. This was especially the case near an active power setpoint of 0 p.u. for one IBR resource investigated, a positive sequence RMS generic IBR model with known controller structure. In particular, the frequency domain admittance characteristics of the positive sequence model tested was significantly different, when compared to the rest of the operating points
- Once restricted to the region of active power above a certain threshold, the procedure to obtain a small signal model for a new testing point within that region by using APM to predict the admittance and vector fitting to fit a model for the predicted admittance was successfully applied on the positive sequence IBR model. Further, the vector fitted model was found to successfully approximate the small signal behaviour when compared to the corresponding analytical small signal formulation.
- Obtaining various alternative levels of frequency support (no/slow/fast) from an IBR model led to differences in terms of the frequency domain admittance characteristics as well as the small signal stability behaviour of such IBRs.

Some avenues of future work based on this research can be:

- Admittance characteristics of additional OEM device models could be tested. Various alternative vector fit methods might also be used to obtain small signal models of each OEM device and the accuracy of these alternative methods compared.
- One future area of work could be to apply the procedure of incorporating blackbox IBR models to a real network. In the previous stage of the project, the small signal model was developed for a large synthetic network with 35 blackbox IBRs that were created by the project team. Applying the procedure to an actual network is likely to uncover additional potential challenges and practical lessons in applying the developed procedure.

- The positive sequence models utilized here so far were generic models, and applying the procedure of forming small signal models to the positive sequence behaviour of black box OEM models could be a next step. OEM positive sequence models may come with a unique set of challenges particular to each model, similar to some of the challenges observed in this research stage for the OEM models in the EMT domain.
- In addition to IBR generator models, other devices such as loads (both inverter based or non-inverter-based) can also play a role in terms of large and small signal stability – hence a possible extension can look at the modelling of loads in more detail in the small signal framework to identify potential for load-IBR interactions.
- The relationship between the services provided by the IBRs and the small signal characteristics could be studied further to establish, for each service, the impact on small signal stability that might be expected (whether either improving or deteriorating the small signal stability of the IBR from which this service is provided).
- The small signal model obtained for each IBR is valid at and near the operating point used. Through the procedure described and utilized in this project, such small signal models can be obtained at new operating points. A future effort can examine the extent to which the small signal model of an IBR at a single operating point or at multiple operating points can be used to infer/estimate the response (or at least, whether the response would be stable) for some large signal disturbances.

The developed small signal evaluation method is largely robust and allows for comparison across positive sequence RMS and EMT domain. However, its application in a variety of scenarios and situations are yet to be tested more completely. Further testing will allow identification of limitations that may exist in the technique developed so far and would also allow for identification of improvements that are to be made. Further, the application scenarios must be carefully considered to allow for accommodation of various operating points and scenarios that are likely to occur in the power system. A few scenarios that can be considered include weak grid situations brought upon by reduced system strength, inertia, or a combination of both, and black start and system restoration conditions. Additionally, a transmission system planner/operator is increasingly having to consider connected distributed energy resources and various types of emerging loads. The impact that they may have on the stability of the bulk power system, both positive (providing services) and negative impact (impact on oscillation/damping) is to be evaluated. With many of these technologies also being blackboxed, this makes stability analysis of the interactions all the more challenging, and suggests that frequency domain techniques may become even more applicable.

Appendix A IBR model parameters

This appendix presents the model parameters used for some of the IBR models utilized in this research. All the positive sequence models use the following models:

- REGC_C model as the generator model
- REEC_C model to represent the electrical controls
- REPC_A model to represent the higher level controls (which could be plant controls)

Note, these models are available as library models in most of the commercial positive sequence softwares. The block diagrams of these are also available in the user manual/model manual for each software. More details are also available in [20]. For REGC_C, a model version was also released in [21] for older versions of PSS/E software, that version is used in this project.

A.1 Positive sequence IBR model used in Section 4.1-4. 3 (generic IBR model A)

The following models and parameters are used for the model used in Section 4.1-4.3. These are given in Apx Table I for the REGC model, and Apx Table II for the REEC model. Here, REPC model was not used.

Apx Table I REGC_C model parameters for positive sequence model used in Sections 4.1-4.3

PARAMETER	VALUE	PARAMETER	VALUE	PARAMETER	VALUE
mva	67.72	iqrmax	99990.5	kii	30
tfltr	0.017	iqrmin	-99990.5	kpll	20
te	0.005	rateflg	0	kipll	200
rrpwr	100	imax	1.7	wmax	75
re	0.0015	dqflag	0	wmin	-75
xe	0.2	kip	1.5	vdip	0.005

Apx Table II REEC_C model parameters for positive sequence model used in Sections 4.1-4.3

PARAMETER	VALUE	PARAMETER	VALUE	PARAMETER	VALUE	PARAMETER	VALUE
vdip	0.8	tp	0.02	pmin	-1	vq4	1.1
vup	1.5	qmax	1	imax	1.7	iq4	1.7
trv	0.01	qmin	-1	tpord	0.02	vp1	0.01
dbd1	-0.05	vmax	1.2	pfflag	0	ip1	1.7
dbd2	0.05	vmin	0.9	vflag	0	vp2	0.5

PARAMETER	VALUE	PARAMETER	VALUE	PARAMETER	VALUE	PARAMETER	VALUE
kqv	5	kqp	0	qflag	1	ip2	1.7
iqh1	1	kqi	0	pqflag	0	vp3	1
iq11	-1	kvp	0.5	vq1	0.01	ip3	1.7
vref0	0	kvi	20	iq1	1.7	vp4	1.1
SOCini	0.5	tiq	0.02	vq2	0.5	ip4	1.7
SOCmax	0.8	dpmax	99	iq2	1.7		
SOCmin	0.1	dpmin	-99	vq3	1		
T	999	pmax	1	iq3	1.7		

A.2 Models used in Section 4.4 (Test model B_EMT and Test model B_PSeq)

For the EMT model, the parameters are given in Apx Table III.

Apx Table III Model parameters for the Test model B_EMT

PARAMETER	VALUE	PARAMETER	VALUE	PARAMETER	VALUE	PARAMETER	VALUE
P_Vbase	0.65	P_Pmin	0	P_cflag	0	P_Kil	20
P_Sbase	0.25	P_Qmax	1	P_Vdip	0.8	P_KpPLL	20
P_Vdcbase	1.5	P_Qmin	-1	P_Vup	1.2	P_KiPLL	200
P_del_f_limit	2	P_PQflag	0	P_KpV	10	P_Tr	0.001
P_lmax	1.2	P_KfDroop	20	P_KiV	20		
P_Pmax	1	P_KvDroop	30	P_Kpl	10		

For the positive sequence model, REGC_C model parameters are given in Apx Table IV and REEC_C model parameters are given in Apx Table V. REPC model was not used.

Apx Table IV REGC_C model parameters for positive sequence model used in Section 4.4

PARAMETER	VALUE	PARAMETER	VALUE	PARAMETER	VALUE	PARAMETER	VALUE
mva	67.75	xe	0.2	dqflag	0	wmax	75
tfltr	0.017	iqrmax	99990.5	kip	4	wmin	-75
te	0.005	iqrmin	-99990.5	kii	50	vdip	0.005
rrpwr	100	rateflg	0	kppll	20		
re	0.0015	imax	1.7	kipll	200		

Apx Table V REEC_C model parameters for positive sequence model used in Section 4.4

PARAMETER	VALUE	PARAMETER	VALUE	PARAMETER	VALUE	PARAMETER	VALUE
vdip	0.8	tp	0.02	pmin	-1	vq4	1.1
vup	1.2	qmax	1	imax	1.7	iq4	1.7
trv	0.01	qmin	-1	tpord	0.02	vp1	0.01
dbd1	-0.05	vmax	1.2	pf flag	0	ip1	1.7
dbd2	0.05	vmin	0.9	vflag	0	vp2	0.5
kqv	5	kqp	0	qflag	0	ip2	1.7
iqh1	1	kqi	0	pqflag	0	vp3	1
iq1	-1	kvp	0.5	vq1	0.01	ip3	1.7
vref0	0	kvi	20	iq1	1.7	vp4	1.1
SOCini	0.5	tiq	0.02	vq2	0.5	ip4	1.7
SOCmax	0.8	dpmax	99	iq2	1.7		
SOCmin	0.1	dpmin	-99	vq3	1		
T	999	pmax	1	iq3	1.7		

A.3 Model parameters for the three IBR parameterizations from Chapter 5

For the IBR_ConstPQ mode, the parameters for the REGC_C and REEC_C models are given in Apx Table VI and Apx Table VII, respectively.

Apx Table VI REGC_C model parameters for IBR_ConstPQ model

RateFlag	0
PQ-priority Flag	0
Tg	0.0033
Tfltr	0
Iqrmax	100
Iqrmin,	-100
Rrpwr	10
Te (s)	0.005
I _{max}	1.1

Apx Table VII REEC_C model parameters for IBR_ConstPQ model

PFFLAG	0	Tp	0.02	PMIN	-1	Vp2	0.5
VFLAG	0	QMax	1	Imax	1.1	Ip2	1
QFLAG	0	QMin	-1	Tpord	0.02	Vp3	1
PQFLAG	0	VMAX	1.1	Vq1	0.01	Ip3	1
Vdip	0.85	VMIN	0.09	Iq1	1	Vp4	1.1
Vup	1.15	Kqp	0	Vq2	0.5	Ip4	1
Trv	0.017	Kqi	1	Iq2	1	T	999
dbd1	-0.15	Kvp	0	Vq3	1	SOCini	0.5
dbd2	0.15	Kvi	1	Iq3	1	SOCmax	0.8
Kqv	4	Tiq	0.005	Vq4	1.1	SOCmin	0.1
Iqhl	1	dPmax	999	Iq4	1		
Iqll	-1	dPmin	-999	Vp1	0.01		
Vref0	0	PMAX	1	Ip1	1		

For the IBR_slow_resp mode, the parameters for the REGC_C, REEC_C and REPC_A models are given in Apx Table VIII, Apx Table IX and Apx Table X, respectively.

Apx Table VIII REGC_C model parameters for IBR_slow_resp

KPQ	0.9	KIP	100	KIPLL	4	IMAX	1.1
KIQ	100	TE	0.005	DWMAX	100		
KPP	0.9	KPPLL	40	DWMIN	-100		
PQFLAG	0	PLLFLG	1	RRCUR	10		

Apx Table IX REEC_C model parameters for IBR_slow_resp

PFFLAG	0	Tp	0.01	PMIN	0	Vp2	2
VFLAG	0	QMax	1	Imax	1.1	Ip2	1.2
QFLAG	0	QMin	-1	Tpord	0.02	Vp3	2.01
PQFLAG	0	VMAX	1.1	Vq1	0.01	Ip3	1.2
Vdip	0.85	VMIN	0.09	Iq1	1.2	Vp4	2.02
Vup	1.2	Kqp	0	Vq2	2	Ip4	1.2
Trv	0.01	Kqi	0.01	Iq2	1.2	T	100
dbd1	-0.05	Kvp	2.5	Vq3	2.01	SOCini	0.5
dbd2	0.05	Kvi	20	Iq3	1.2	SOCmax	1
Kqv	0	Tiq	0.01	Vq4	2.02	SOCmin	0
Iqhl	1	dPmax	100	Iq4	1.2		
Iqll	-1	dPmin	-100	Vp1	0.01		
Vref0	0	PMAX	1	Ip1	1.2		

Apx Table X REPC_A model parameters for IBR_slow_resp

Remote	0	Ki	3.75	dbd1	0	femax	99
Monitored	0	Tft	0.02	dbd2	0	femin	-99
Monitored	0	Tfv	0.02	Qmax	1.1	Pmax	1
Monitored	'0'	Vfrz	0.2	Qmin	-1.1	Pmin	-1
VCFlag	0	Rc	0	Kpg	0.05	Tg	0.1
RefFlag	1	Xc	0	Kig	0.5	Ddn	20
Fflag	1	Kc	0.01	Tp	0.25	Dup	20
Tfltr	0.02	emax	0.1	fdbd1	0		
Kp	0.25	emin	-0.1	fdbd2	0		

For the IBR_fast_resp mode, the parameters for the REGC_C, REEC_C and REPC_A models are given in Apx Table XI, Apx Table XII and Apx Table XIII, respectively.

Apx Table XI REGC_C model parameters for IBR_fast_resp

PQFLAG	0	KPP	1.5	KIPLL	4	IMAX	1.1
PLLFLG	1	KIP	30	DWMAX	100		
KPQ	1.5	TE	0.005	DWMIN	-100		
KIQ	30	KPPLL	40	RRCUR	1000		

Apx Table XII REEC_C model parameters for IBR_fast_resp

PFFLAG	0	Vref0	0	dPmin	-999	Iq4	1
VFLAG	0	Tp	0.02	PMAX	1	Vp1	0.1
QFLAG	1	QMax	1.38	PMIN	-1	Ip1	1
PQFLAG	0	QMin	-1.38	Imax	1.1	Vp2	0.2
Vdip	0.85	VMAX	1.1	Tpord	0.02	Ip2	1
Vup	1.15	VMIN	0.9	Vq1	0.1	Vp3	0.3
Trv	0.01	Kqp	0	Iq1	1	Ip3	1
dbd1	-0.01	Kqi	0	Vq2	0.2	Vp4	0.4
dbd2	0.01	Kvp	1	Iq2	1	Ip4	1
Kqv	2	Kvi	10	Vq3	0.3	T	100
Iqhl	1	Tiq	0.02	Iq3	1	SOCini	0.5
Iqll	-1	dPmax	999	Vq4	0.4	SOCmax	1
						SOCmin	0

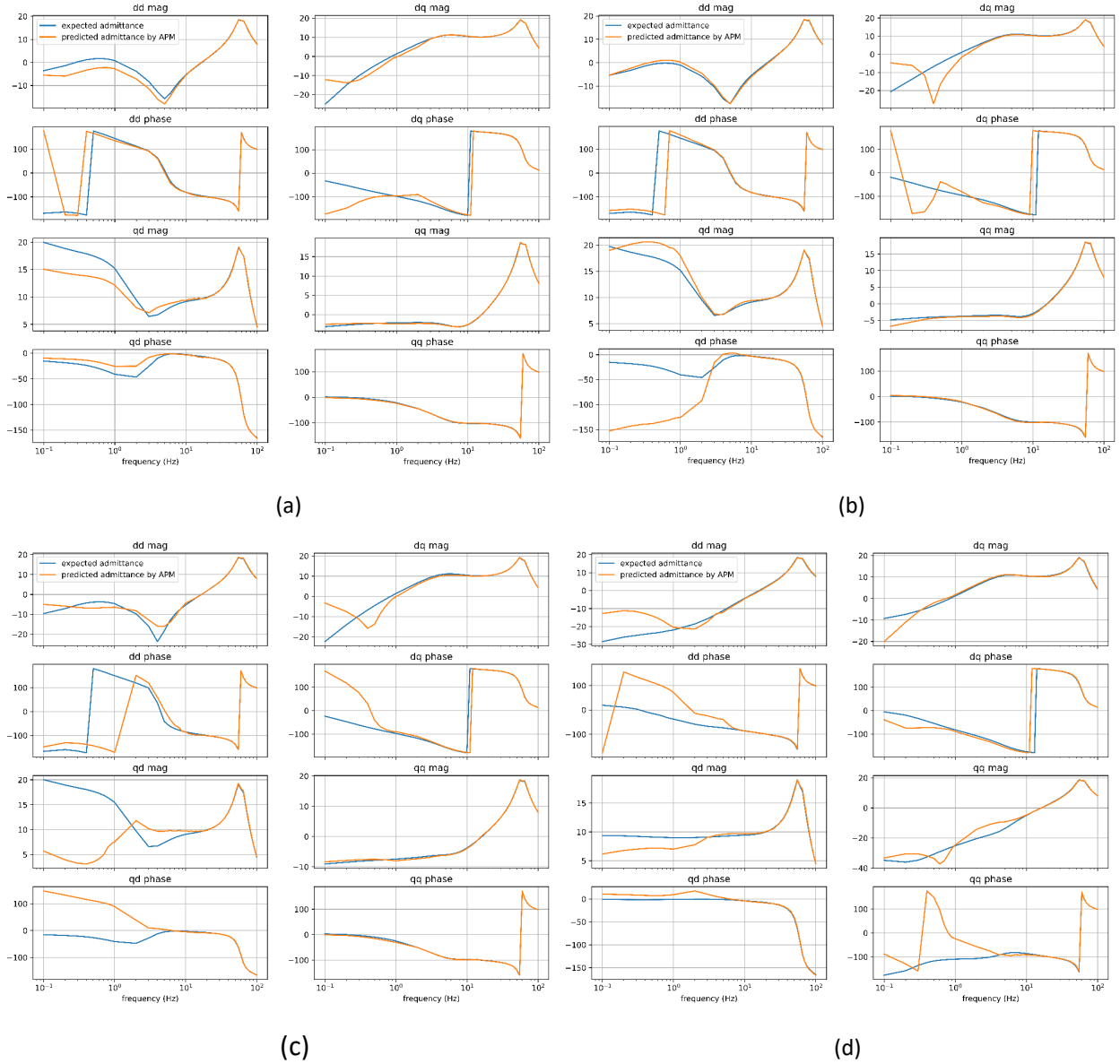
Apx Table XIII REPC_A model parameters for IBR_fast_resp

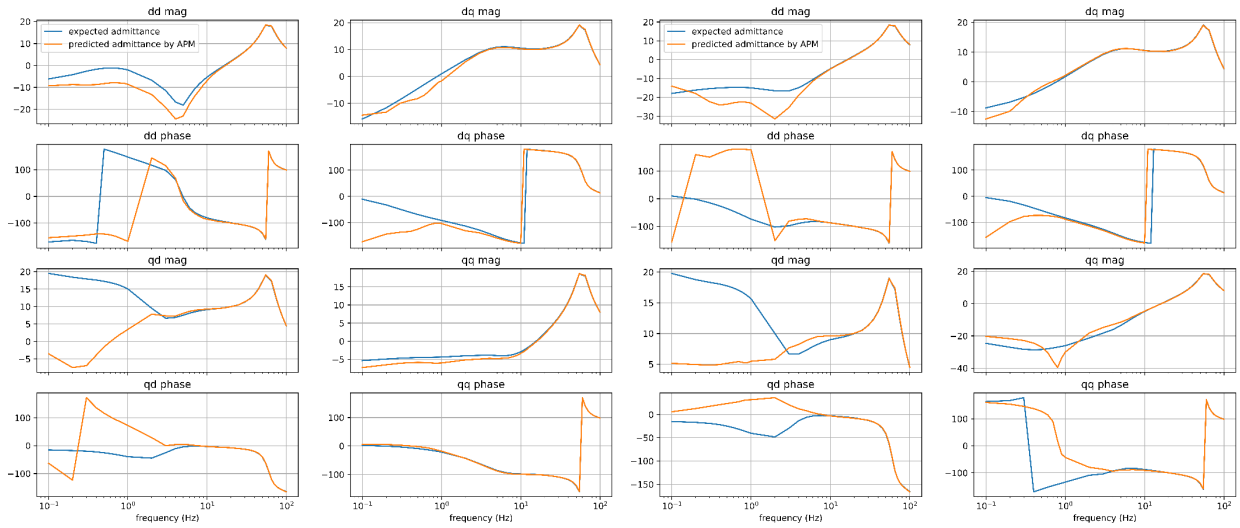
Remote	0	Ki	20	dbd1	-0.1	femax	1
Monitored	0	Tft	0.1	dbd2	0.1	femin	-1
Monitored	0	Tfv	0.05	Qmax	1.1	Pmax	1
Monitored	'0'	Vfrz	0.9	Qmin	-1.1	Pmin	0
VCFlag	0	Rc	0	Kpg	0.5	Tg	0.1
RefFlag	1	Xc	0	Kig	2	Ddn	20
Fflag	1	Kc	0	Tp	0.25	Dup	20
Tftr	0.02	emax	0.5	fdbd1	-0.0001		
Kp	2	emin	-0.5	fdbd2	0.0001		

Appendix B APM results for OEMs

This appendix shows the APM results and the comparison of time response between actual model and estimated model of different OEMs for all the test operating points.

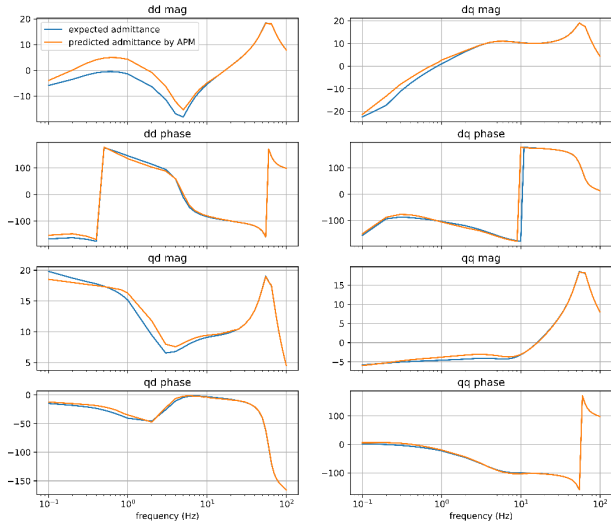
B.1 APM results for grid forming model (GFM)





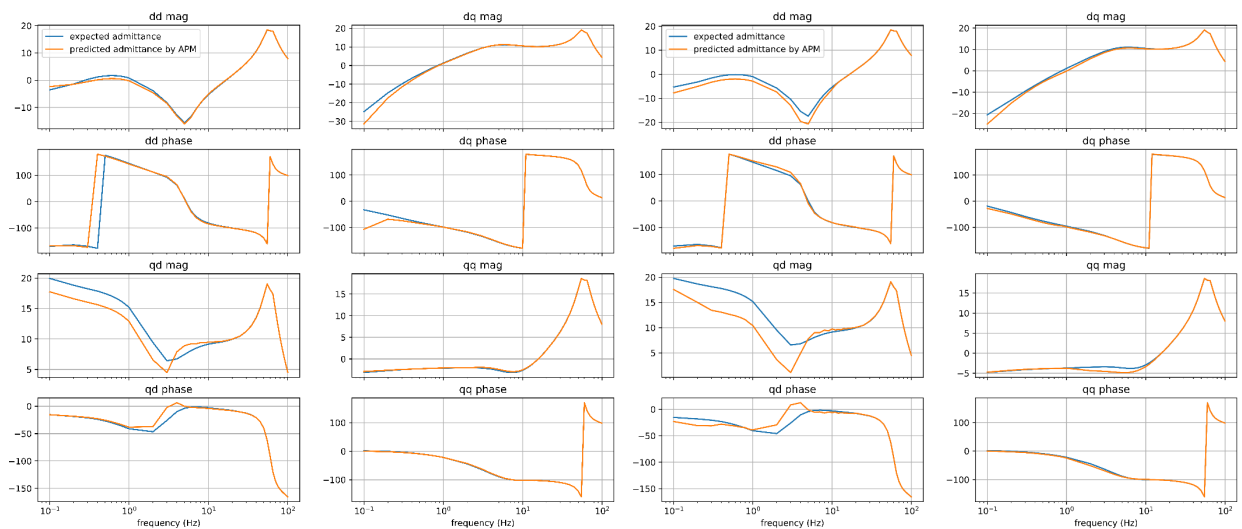
(e)

(f)



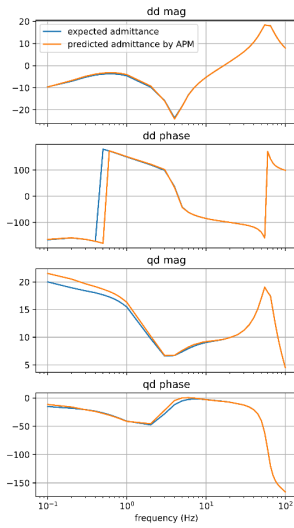
(g)

Apx Figure 1 Qualitative trends in the observed admittance before addition of additional training points at test operating points OP-1 to OP-7 a) - g)

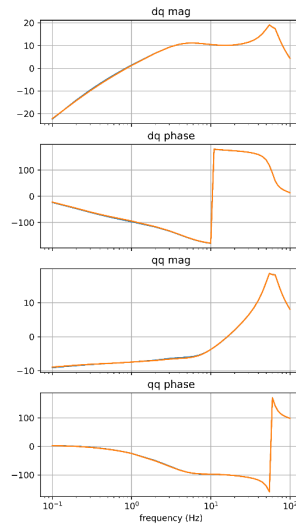


(a)

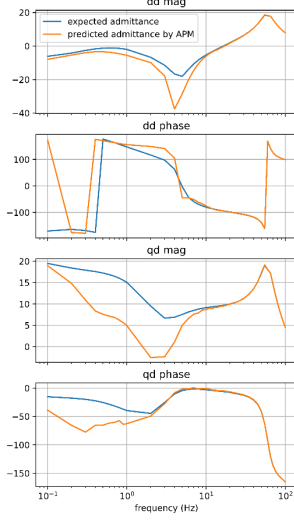
(b)



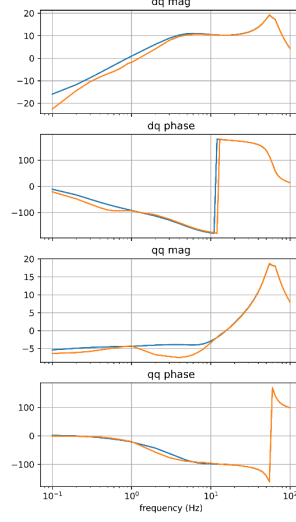
(c)



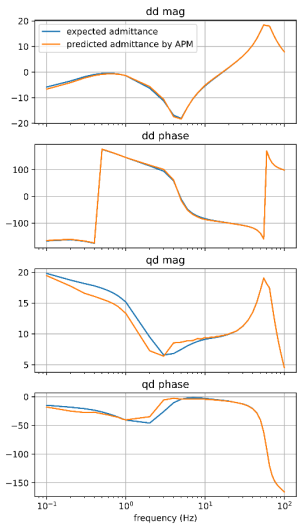
(d)



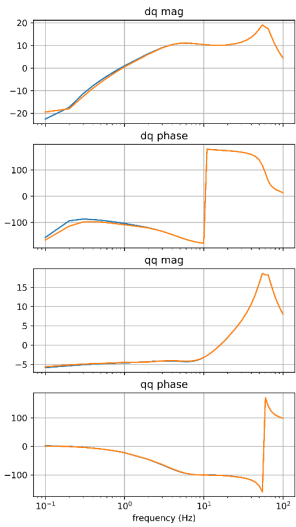
(e)



(f)

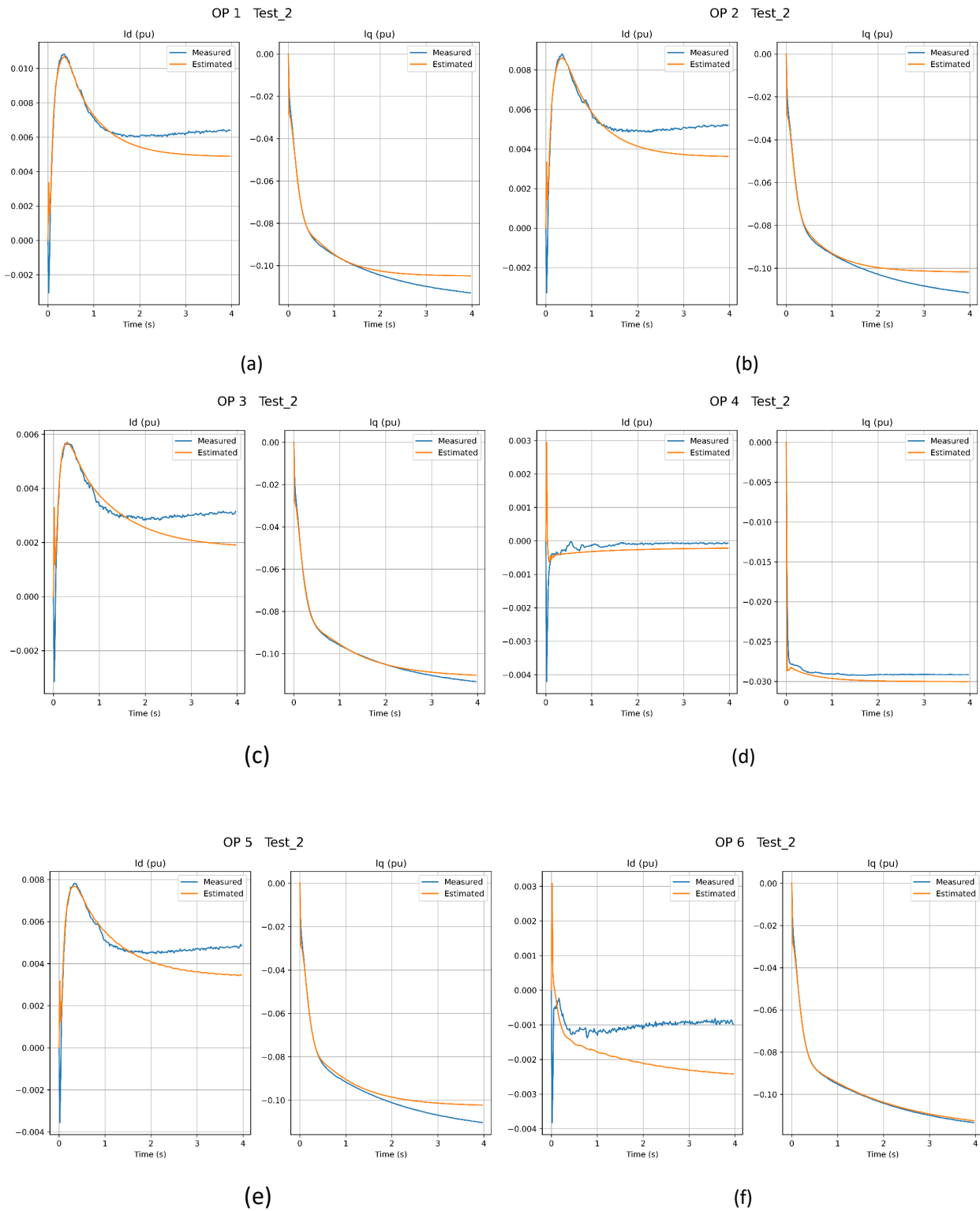


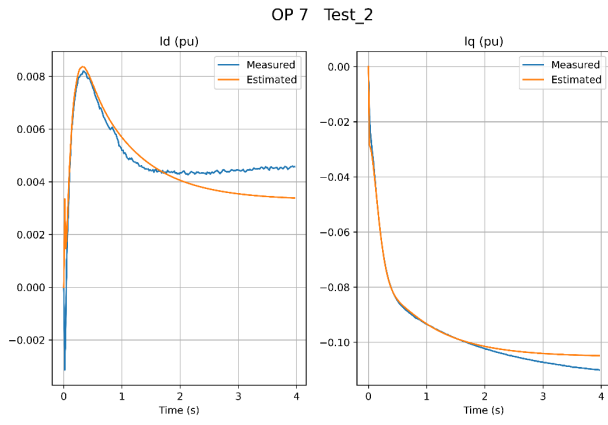
(g)



Apx Figure 2 Qualitative trends in the observed admittance after addition of additional training points at test operating points OP-1 to OP-7 a) - g)

B.2 Measured and estimated time response for GFM

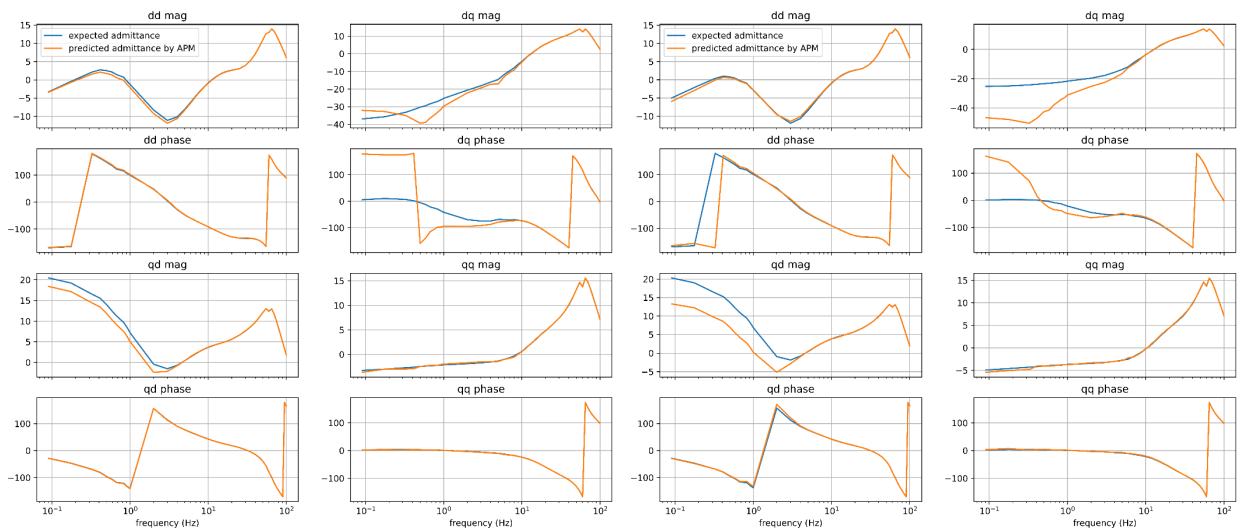




(g)

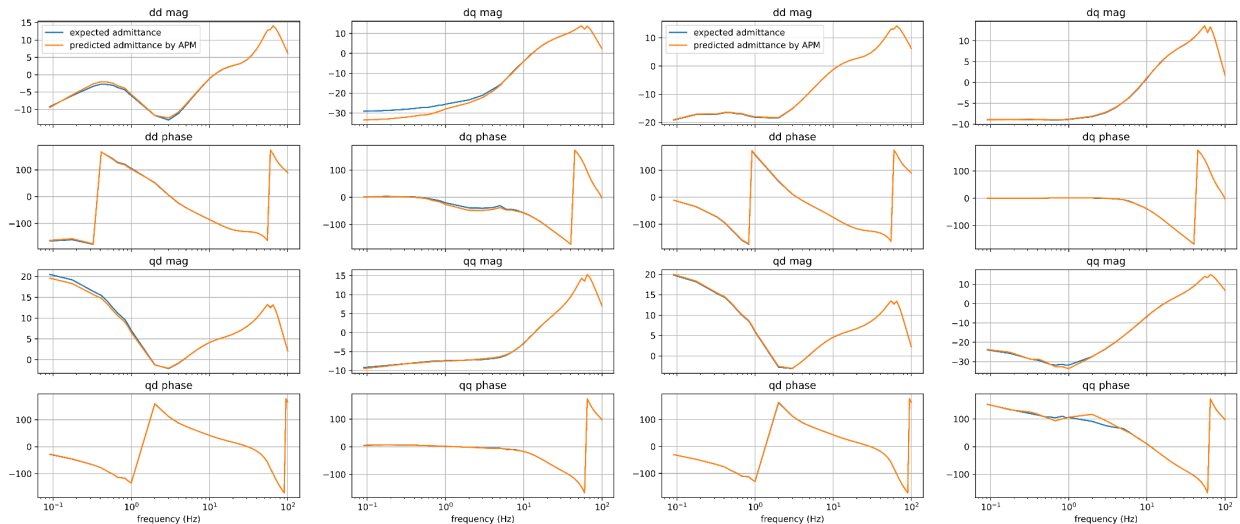
Apx Figure 3 Comparison of measured and estimated time response at different test operating points OP-1 to OP-7
a) - g)

B.3 APM results for grid following model (GFL) 1

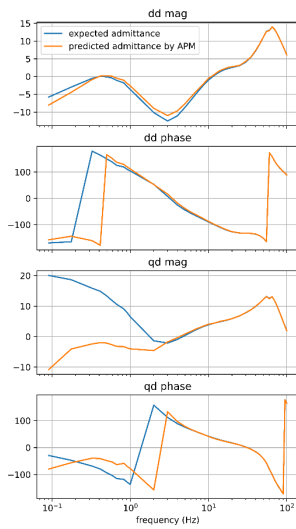


(a)

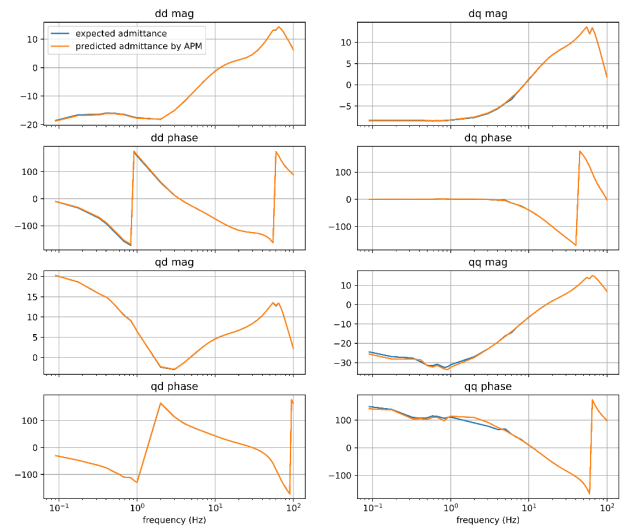
(b)



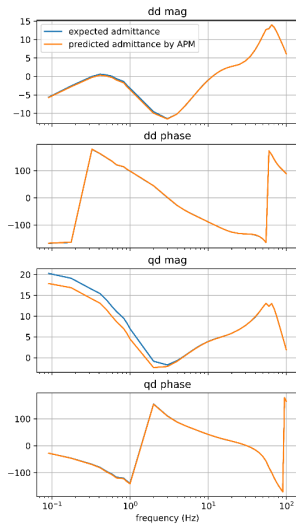
(c)



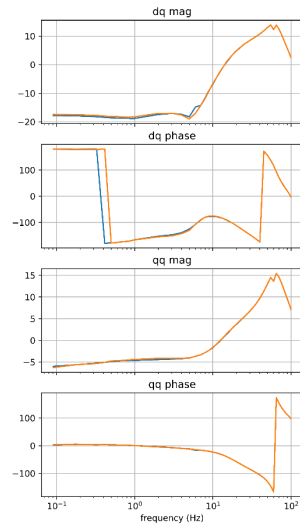
(d)



(e)



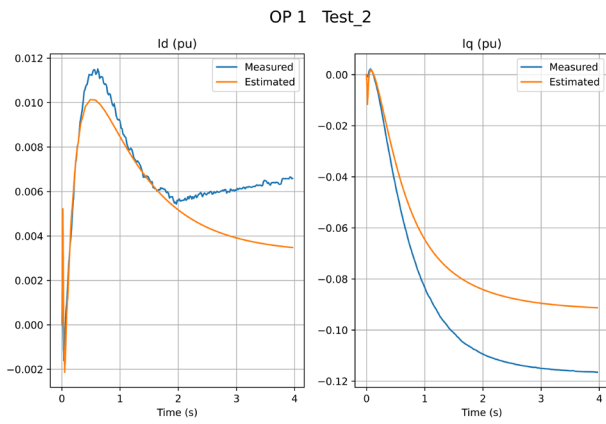
(f)



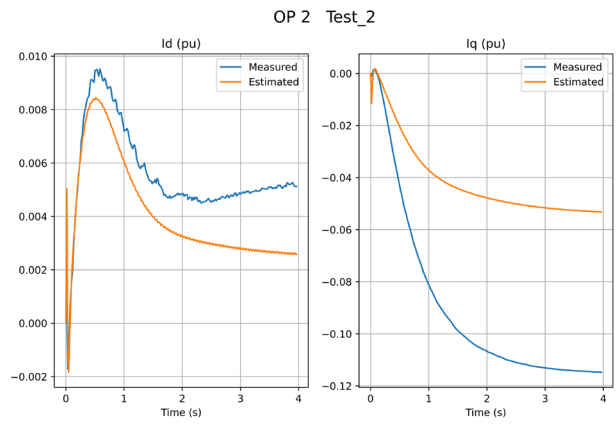
(g)

Apx Figure 4 Qualitative trends in the observed admittance at test operating points OP-1 to OP-7 a) - g)

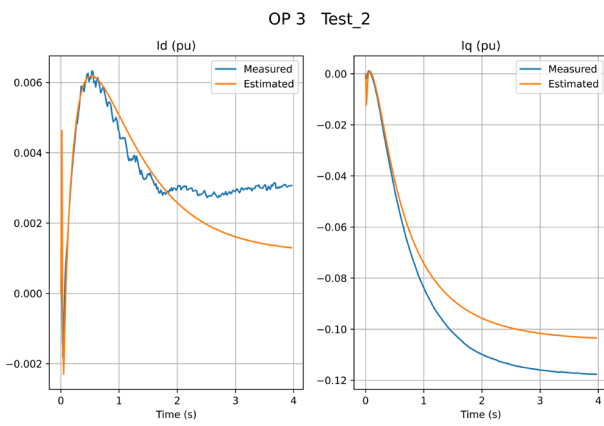
B.4 Measured and estimated time response for GFL1



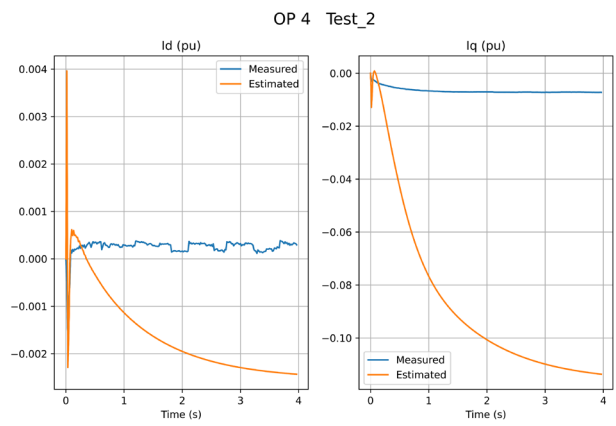
(a)



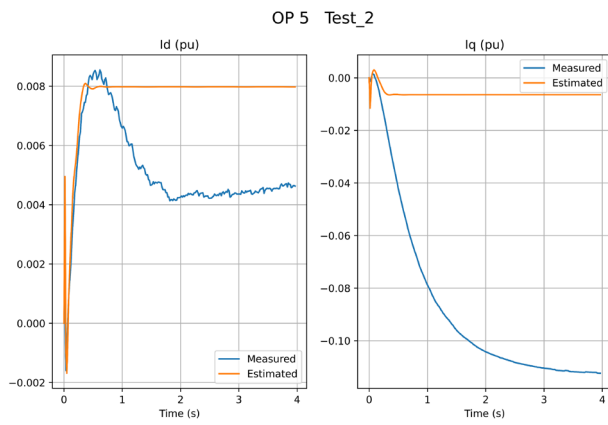
(b)



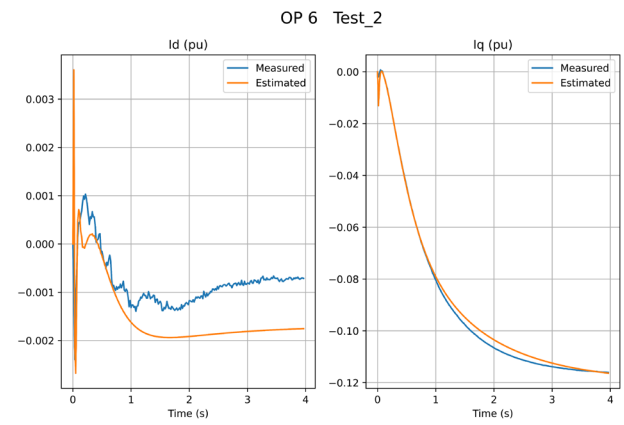
(c)



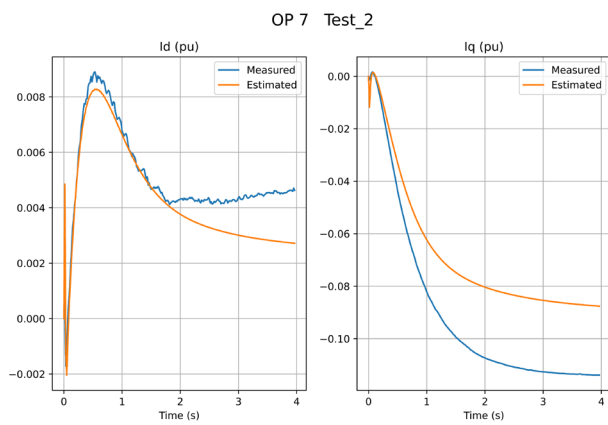
(d)



(e)



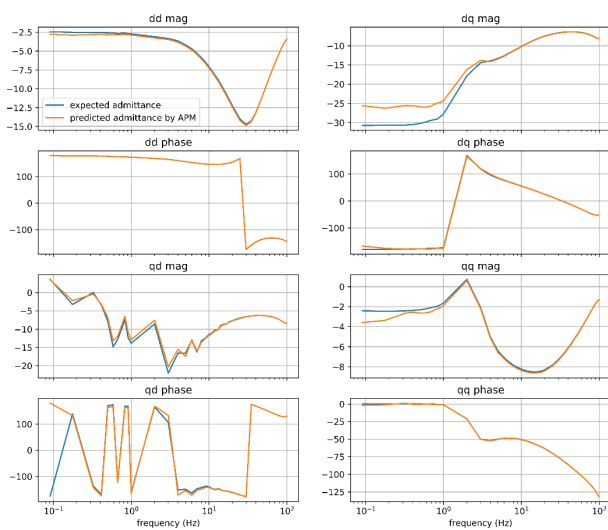
(f)



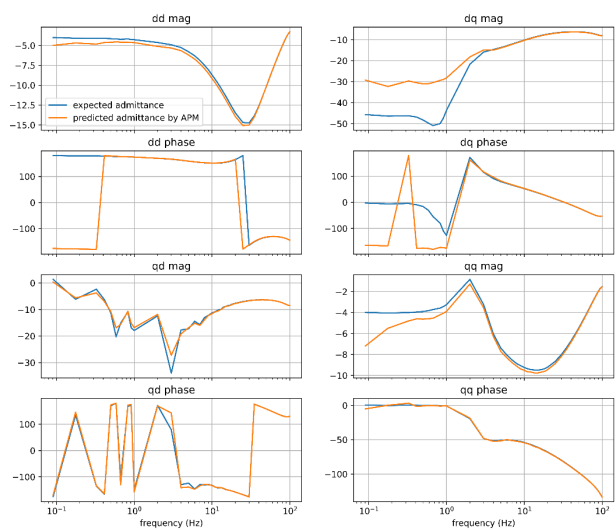
(g)

Apx Figure 5 Comparison of measured and estimated time response at different test operating points OP-1 to OP-7
a) - g)

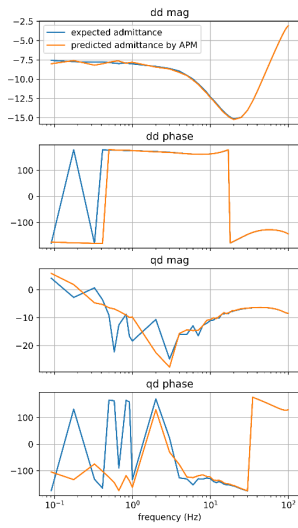
B.5 APM results for grid following model (GFL) 2



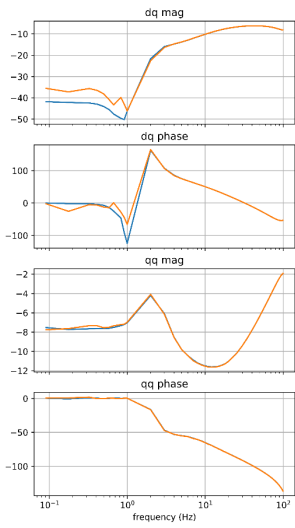
(a)



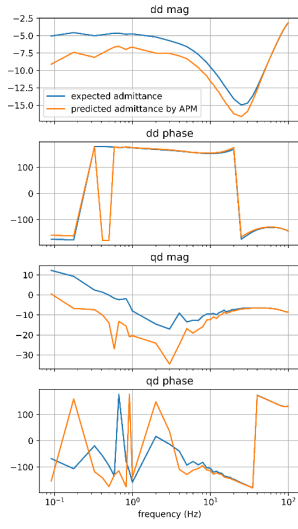
(b)



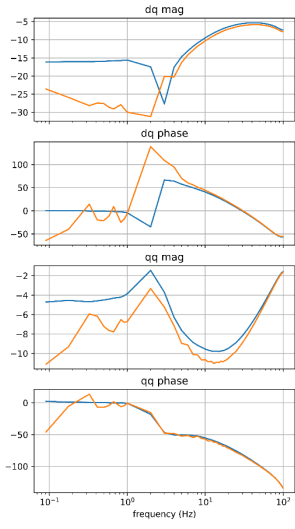
(c)



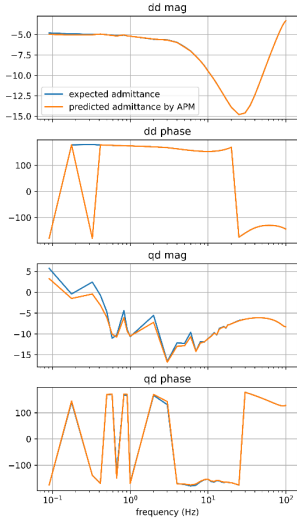
(d)



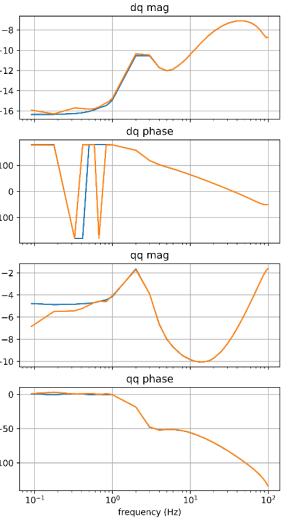
(e)



(f)



(g)

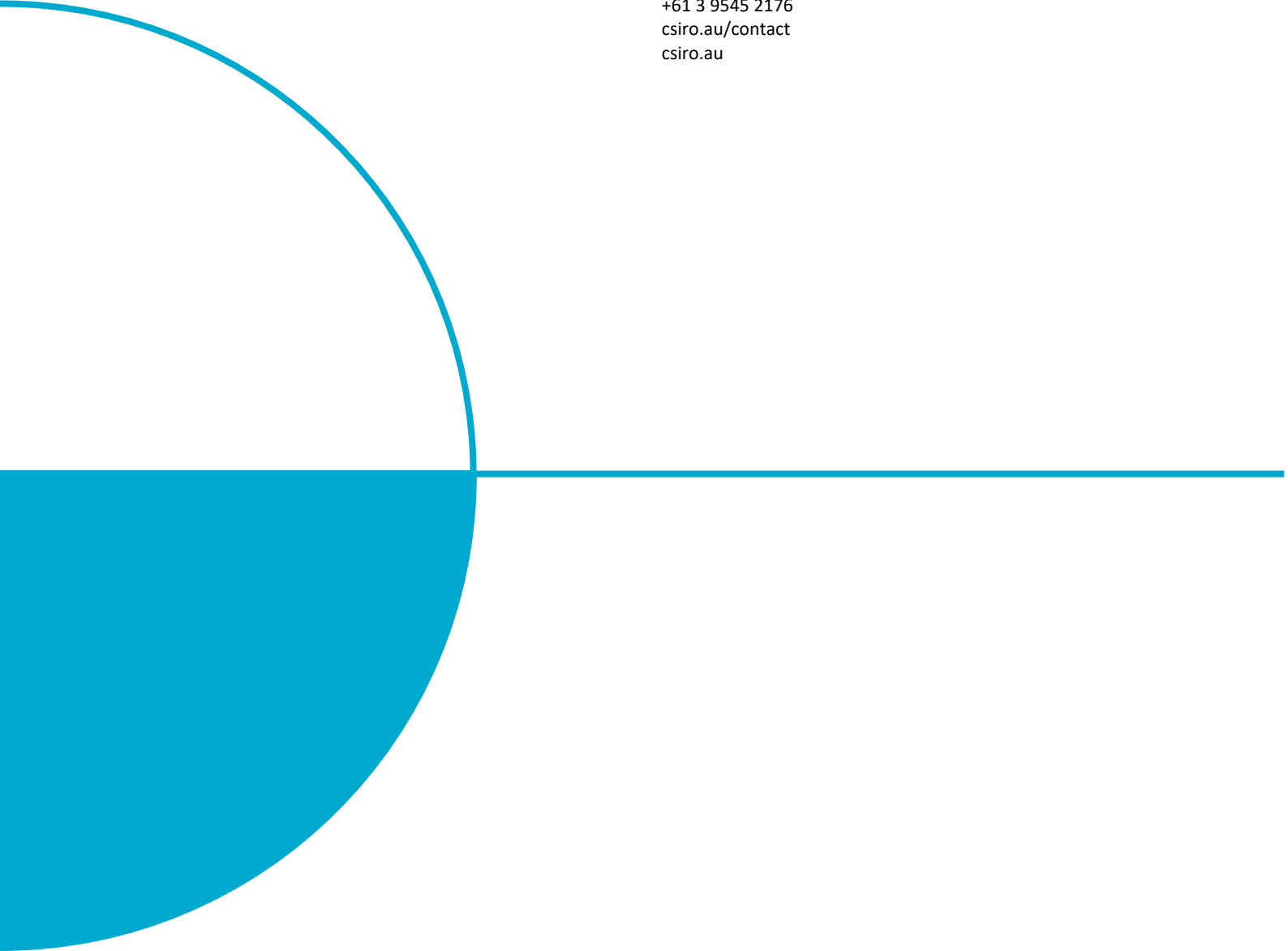


Apx Figure 6 Qualitative trends in the observed admittance at test operating points OP-1 to OP-7 a) - g)

References

- [1] EPRI, “CSIRO Australian Research for the GPST: Topic 2 - Stability Tools and Methods,” CSIRO, 2021.
- [2] S. Dutta, W. Zhou, N. Mohammed, B. Bahrani, M. Bello and D. Ramasubramanian, “Topic 2 – Analytical methods for determination of stable operation of IBRs in a future power system,” CSIRO, Australia, 2023.
- [3] S. Thakar, S. Konstantinopoulos, V. Verma, D. Ramasubramanian, M. Bello, J. Xu, J. Mesbah, W. Zhou and B. Bahrani, “Topic 2 – Analytical methods for determination of stable operation of IBRs in a future power system,” Commonwealth Scientific and Industrial Research Organization, Australia, 2024.
- [4] EPRI, “Code Based Generic Inverter Based Resource Model,” EPRI, Palo Alto, CA. 3002028322, 2023.
- [5] EPRI, “Small-Signal Stability of 100% IBR Dominated Power Systems During Blackstart: Eigenvalue Analysis and Stability Properties of Grid-Forming IBR-based Blackstart,” EPRI, Palo Alto, CA, 3002026981, 2023.
- [6] F. Arraño-Vargas and G. Konstantinou, “Synthetic Grid Modeling for Real-Time Simulations,” in *2021 IEEE PES Innovative Smart Grid Technologies - Asia (ISGT Asia)*, Brisbane, Australia, 2021.
- [7] R. Heidari, M. Amos and F. Geth, “An Open Optimal Power Flow Model for the Australian National Electricity Market,” in *2023 IEEE PES Innovative Smart Grid Technologies - Asia (ISGT Asia)*, Auckland, New Zealand, 2023.
- [8] T. Philpott, A. P. Agalgaonkar, K. M. Muttaqi, T. Brinsmead and H. Ergun, “Development of High Renewable Penetration Test Cases for Dynamic Network Simulations using a Synthetic Model of South-East Australia,” in *2023 IEEE International Conference on Energy Technologies for Future Grids (ETFG)*, Wollongong, Australia, 2023.
- [9] EPRI, “Grid Forming Inverters for Increase in Inverter Based Resource Percentage,” EPRI, Palo Alto, CA, 2002020786, 2021.
- [10] S. Thakar and D. Ramasubramanian, “Intricacies of formulating measurement-based small signal models of inverter based resources,” in *1th Bulk Power Systems Dynamics and Control Symposium (IREP 2022)*, Banff, Canada, 2022.
- [11] The MathWorks Inc, “System Identification Toolbox: Version 24.2 (R2024b),” 2024. [Online]. Available: <https://www.mathworks.com>. [Accessed 20 May 2025].
- [12] L. Fan, Z. Miao, L. Bao, S. Shah and R. H. Ramakrishna, “DQ Admittance Model Extraction for IBRs via Gaussian Pulse Excitation,” *IEEE Transactions on Power Systems*, vol. 38, no. 3, pp. 2966 - 2969, 2023.
- [13] M. Zhang, L. Bao, Z. Miao, L. Fan and P. Gomez, “Measured Admittance Model for Dynamic Simulation of Inverter-Based Resources Using Numerical Laplace Transform,” in *2021 North American Power Symposium (NAPS)*, College Station, TX, USA, 2021.
- [14] W. Zhou, B. Liu, N. Mohammed and B. Bahrani, “An Efficient Method to Estimate Admittance of Black-boxed Inverter-based Resources for Varying Operating Points,” *CSEE Journal of Power and Energy Systems*, vol. 10, no. 1, pp. 421 - 426, 2023 .

- [15] D. Sun, H. Liu and M. Gong, "A Stability Analysis Tool for Bulk Power Systems Using Black-Box Models of Inverter-based Resources," in *2022 IEEE Industry Applications Society Annual Meeting (IAS)*, Detroit, MI, USA, 2022.
- [16] B. Gustavsen and A. Semlyen, "Rational approximation of frequency domain responses by vector fitting," *IEEE Transactions on Power Delivery*, vol. 14, no. 3, pp. 1052-1061, 1999.
- [17] B. Gustavsen, "Improving the pole relocating properties of vector fitting," *IEEE Trans. Power Delivery*, vol. 21, no. 3, pp. 1587-1592, 2006.
- [18] D. Deschrijver, M. Mrozowski, T. Dhaene and D. De Zutter, "Macromodeling of Multiport Systems Using a Fast Implementation of the Vector Fitting Method," *IEEE Microwave and Wireless Components Letters*, vol. 18, no. 6, pp. 383-385, 2008.
- [19] B. Gustavsen, "Vector Fitting - SINTEF," SINTEF, [Online]. Available: <https://www.sintef.no/en/software/vector-fitting/>. [Accessed 26 February 2025].
- [20] EPRI, "Model User Guide for Generic Renewable Energy System Models," EPRI, Palo Alto, CA: 3002027129., 2023.
- [21] EPRI, "REGC_C Implementation in PSS/E (REGC_C (PSS/E)) v1.3," EPRI, Palo Alto, CA. 3002027337, 2023.



As Australia's national science agency and innovation catalyst, CSIRO is solving the greatest challenges through innovative science and technology.

CSIRO. Unlocking a better future for everyone.

Contact us

1300 363 400
+61 3 9545 2176
csiro.au/contact
csiro.au